TRANSFERRED MONOLAYER AND AB STACKED BILAYER (0001) SiC EPITAXIAL GRAPHENE

A Dissertation

Presented to the Faculty of the Graduate School Of

Cornell University

In Partial Fulfillment of the Requirements for the Degree of

Doctor of Philosophy

by

Hussain Alsalman

February 2016

TRANSFERRED MONOLAYER AND AB STACKED BILAYER (0001) SiC EPITAXIAL GRAPHENE

Hussain Alsalman, Ph. D.

Cornell University 2016

Graphene is a leading two dimensional (2D) material with good technological potential. Currently, it is being scaled up in synthesis methods in order to meet future demands in technology markets. In this dissertation, a study of transferred epitaxial graphene (TEG) as a synthesis method, for large area monolayer and AB stacked bilayer Graphene, is presented. Monolayer epitaxial graphene (EG) is grown on the (0001) face of silicon carbide (SiC) in an argon atmosphere at a temperature of 1600 ^{o}C. Bilayer graphene can thereafter be synthesized if needed by intercalating the monolayer in a 100% hydrogen flow at 1050 ^{o}C to release what is known as the "buffer layer" into another graphene layer forming a bilayer. Either form of graphene can subsequently be transferred off the SiC substrate to mitigate the negative effects of the substrate. We develop a transfer process based on a gold adhesion layer and demonstrate for the first time, the transfer of high quality monolayer transferred epitaxial graphene (MTEG) and AB stacked bilayer transferred epitaxial graphene (BTEG). We use Raman characterization methods to determine the number and quality of graphene layers as well as orientation for bilayers which was made possible by contrast enhancement upon substrate transfer. We report these characteristics for the first time. Extensive structural characterization that have never been done before and were made possible by the successful transfer procedure, are presented in the Transmission Electron Microscopy (TEM) section. We successfully show suspended

MTEG and BTEG samples which was never shown in literature before. We fabricate Transmission Line Measurement (TLM) structures to study the quality of the contact resistance for MTEG and BTEG. We report values in the range of 600 $\Omega.\mu m$ for MTEG and 2400 $\Omega.\mu m$ for BTEG. We also fabricate Field Effect Transistors (FETs) to study the field effect mobility and carrier concentration of MTEG and BTEG. We report average room temperature field effect mobility values of around 1700 $cm^2/V.s$ with best value of 2800 $cm^2/V.s$ for MTEG. This is over two times gain in mobility before transfer and is competitive with current leading synthesis methods. We measured the room temperature field effect mobility of BTEG to be 250 $cm^2/V.s$ on average and with a best value of 335 $cm^2/V.s$. To the knowledge of the author, there are no reports in literature on the measured mobility of BTEG. We carry out annealing studies at argon ambient of 300 ^oC for TEG and show unique properties for BTEG in which a demonstrated ten orders of magnitude, higher moisture absorption than MTEG is shown.

A section in this dissertation will be dedicated to related work on chemical vapor deposition (CVD) hexagonal boron nitride (h-BN) which is a complimentary 2D material to graphene. Improvements on CVD growth by electropolishing the copper substrate will be demonstrated where root mean square (RMS) surface roughness of starting material is reduced from 177 *nm* to 12 *nm*, considerably improving subsequent h-BN CVD growth. A procedure for the transfer of CVD graphene onto CVD h-BN as well as fabrication of Van der Paw structures will be presented. We show initial results of improvements in mobility when CVD h-BN is used as a substrate for CVD graphene.

BIOGRAPHICAL SKETCH

Hussain Alsalman was born in Saudi Arabia and earned his bachelorettes degree in electrical engineering from King Fahd University of Petroleum and Minerals (KFUPM). He worked as an assistant research engineer at King Abdulaziz City for Science and Technology (KFUPM) and earned a fellowship for pursing higher studies. He joined Cornell University Electrical Engineering Ph.D. program and is conducting research in transferred epitaxial graphene.

ACKNOWLEDGMENTS

I would like to thank Cornell University, the Graduate Program, and the ECE department for providing the opportunity to pursue research at a scientifically advance institute with many collaborators and instructors that are world class, very competitive, insightful and helpful.

I express my dearest appreciation for my committee chair Prof. Michael Spencer for supporting me throughout my program and guiding me in my research. I greatly thank Prof. Paul McEuen for being on my committee and for being an excellent professor in general that goes way beyond the call of duty for the support of graduate student education as well as providing valuable feedback on both research and academic life. It was a great honor.

I greatly thank Prof. Abdulrahman Al-Muhanna for being my mentor since my undergraduate degree as well as being a big brother figure that words fail to acknowledge his impact.

I would like to dearly thank Prof. Roald Hoffmann for saving moments of his busy schedule to chat with me and advise me on my career as a researcher. I would like to dearly thank Prof. David Muller for being a great professor and giving me a lot of advice all throughout my stay at Cornell University.

I thank Prof. Khlil Najafi and Prof. Wei Lu of the University of Michigan Ann Arbor for advising me for my Masters.

I would like to thank my group members, Dr. Jeonghyun Hwang for the endless support given in both research as well as personal copping with the stress of being a graduate student. I would like to thank Dr. Moon Kim for his invaluable training and advice in device fabrication. I thank Dr. Virgil Shields for being a good friend and for developing the SiC epitaxy process. I would very dearly like to thank Dr. Nini Munoz

for being a friend as well as being a research partner in work that yielded excellent results. I dearly thank Dr. Lori Lepak for being an amazing friend as well as a chemist that will answer any question with enthusiasm. I thank Dr. Dorr Cambell for his work on SiC Epitaxial Growth, Dr. Joon Kwak for various collaboration efforts throughout my PhD, Brian Calderon for h-BN related collaborations as well as characterizations and a lot of fun scientific discussions, Yanxin Ji for h-BN growth collaborations, Brian Schutter for useful discussion on material growth, Gina Howard for being a dear friend and for collaborations on CVD graphene electrical characterization, Conrad Blash for electropolishing copper.

I thank my various Collaborators throughout my PhD including, and not limited to, Linas Ardaravicicus, Prof. Mark Rummeli, Dr. Sandeep Gorantla, and Dr. Alicja Bachmatiuk, who worked on various fruitful projects.

I thank Dr. Marcos Guimaraes for his indispensable and deep knowledge of graphene transport. I thank Dr. Melina Bless for her suggestions on graphene transfer, Haining Wang for help on CVD graphene transfer, Roberto de Alba for being a friend and his insight on PMMA contaminations, Jared Strait and Parinita Nene for IR characterization, Dr. Jay Vandelden for various processing tips, Dr. Samantha Roberts for being a good friend and for her various tips on processing and general life as an academic and Dr. Kwame Amponsah his friendship and for help on four point probing.

I greatly thank Scott Coldren for being an older brother figure that listened to ECE graduate student problems and provided sound and understanding personal advice.

I thank Karen Heinselman, Dr. Laura Fegely, and Jer Lin Pu for being close friends as well as the endless useful discussions on materials and processing.

I thank Prof. James Shealy and all my students of the 2013 Electron Device class I was TA for the endless good memories and to have had the privilege of teaching such well

accomplished and motivated students.

I thank all members of Cornell CNF, especially Michale Skvarla for the endless processing advice as well as the stories of the electronics industry, John Treichler for his endless help on AFM and being the kindest man, Aaron Windsor for tolerating me breaking his e-beam evaporator, Vincent Genova for breaking his Oxford 100 deep etcher, and Dr. Robert Ilic for motivating me to be a better process engineer that only sleeps 3 hours a day and publishes 10 papers a year. I thank CCMR and its members for their help and facilitations throughout my PhD. I thank KACST for providing their generous fellowship that allowed me to pursue this PhD.

I thank Steve and Susan Hesses, and John and Kathy Ludders for their tremendous support for me at my stay in the US. I also thank the Sunday hiker's club for their support.

Last but not least, I greatly thank my family for providing tremendous support while writing this dissertation.

TABLE OF CONTENTS

Bibliographic Sketch…… v

Acknowledgment…… vi
Table of Content……..... ix
List of Figures……..... xi
List of Tables…….. xiv
List of Abbreviations…….. xv

1. Introduction……... 1
   1.1. Two Dimensional Materials…… 1
   1.2. Graphene……..... 4
   1.3. Bilayer Graphene…… 6
   1.4. 2D hexagonal Boron Nitride and Other Materials……..... 8
   1.5. Current Graphene Synthesis Methods…… 9
      1.5.1. Exfoliation……..... 9
      1.5.2. Chemical Vapor Deposition……. 10
      1.5.3. SiC Epitaxial Graphene……... 12
   1.6. Motivation for Pursuing Transferred Epitaxial Graphene ……..... 13

2. Growth and Characterization of Epitaxial Graphene……..... 15
   2.1. Cold Wall High Temperature Furnace Growth……..…. 15
   2.2. Silicon Carbide Epitaxial Graphene……..…. 17
   2.3. Monolayer Growth Procedure……..... 21
   2.4. Pre-Transfer Raman and Atomic Force Microscopy Characterization….. 28
   2.5. Intercalation and Bilayer Graphene Synthesis …… 32

3. Epitaxial Graphene Transfer ……. 34
   3.1. Overview of Transfer Methods for 2D materials ……..…. 34
   3.2. Literature on Epitaxial Graphene Transfer ……..... 36
   3.3. Attempts in Transferring High Quality Epitaxial Graphene ……..... 38
   3.4. The Au/PVA Transfer Method……..……. 40
   3.5. Adhesion Energy ……..…. 46

4. Transferred Epitaxial Graphene Structural Characterization ……..... 49
   4.1. Optical Characterization……...…….. 49
   4.2. Raman Characterization……..... 52
   4.3. Transmission Electron Microscopy Characterization ……...…. 59

5. Transferred Epitaxial Graphene Electrical Characterization …… 64
5.1. Fabrication…….. 65
5.2. Contact Resistance ……. 67
5.2.1. 2p-4p Method……... 68
5.2.2. TLM Method…… 69
5.3. MTEG FET Characterization ……...…… 73
5.4. BTEG FET Characterization …….……...…… 81
5.5. BTEG Gas Absorption Properties ……...……. 86

6. Boron Nitride Related Work……. 91
6.1. Boron Nitride Chemical Vapor Deposition Growth…….. 91
6.2. Copper Template Electropolishing…… 91
6.3. CVD Graphene on CVD Boron Nitride Electric Transport ……..….. 97

7. Summary and Future Prospective ……..……. 102

LIST OF FIGURES

Figure 1.1: The carbon family of directional materials…… 2

Figure 1.2: Numerous Families of 2D materials and applications……... 3

Figure 1.3: Graphene honeycomb lattice……. 4

Figure 1.4: Suspended graphene……... 5

Figure 1.5: AB stacked bilayer Graphene……. 6

Figure 1.6: Bilayer graphene bolometer illustration……. 7

Figure 1.7: h-BN Substrate…… 8

Figure 1.8: Graphene contrast as a function of wavelength and SiO_2 thickness… 10

Figure 1.9: Grain boundaries of CVD graphene…… 11

Figure 1.10: SiC EG illustration…… 12

Figure 2.1: Purpose built SiC epitaxial graphene chamber ……... 16

Figure 2.2: Illustration of step bunching……. 19

Figure 2.3: Illustration of SiC EG formation…….. 20

Figure 2.4: Heating cycle for monolayer EG growth……. 21

Figure 2.5: Number of graphene layers grown as a function of time and temp… 23

Figure 2.6: Overlay of XPS for 15 minute growth…… 25

Figure 2.7: Average number of graphene layers as a function of time…… 26

Figure 2.8: Hall measurement of carrier mobility versus carrier density…… 27

Figure 2.9: Typical Raman signal graphene…… 28

Figure 2.10: Typical Raman of EG before transfer…….. 30

Figure 2.11: AFM image of SiC surface steps before growth…….. 30

Figure 2.12: AFM phase image of non-ideal growth…… 31

Figure 2.13: Intercalation releasing the buffer layer forming bilayers…… 33

Figure 3.1: Exfoliated monolayer graphene we isolate…… 35

Figure 3.2: Early carbon nanotube research relying on gold adhesion layers…. 37

Figure 3.3: Schematic of PMMA transfer method…… 38

Figure 3.4: Illustration of the Au/PMMA method…… 39

Figure 3.5: Illustration of the Au/PVA method…… 40

Figure 3.6: 6 X 6 mm MTEG on SiO_2/Si substrate…… 41

Figure 3.7: Microscope image of MTEG…… 42

Figure 3.8: Adhesion problem to various substrates…… 43

Figure 3.9: Microscope image of cracked film problem……. 44

Figure 3.10: Schematic overview of PVA/Au transfer method…….. 45

Figure 4.1: Illustration of SiO_2 interference effect……. 50

Figure 4.2: 6 X 6 mm MTEG BTEG visible contrast……. 51

Figure 4.3: 2D peak of exfoliated bilayer graphene verification…… 53

Figure 4.4: Original Ferrari et al. work explaining 2D peak……. 54

Figure 4.5: Raman EG before transfer, MTEG, BTEG……. 55

Figure 4.6: Raman of AB stack, rotated, monolayer……. 56

Figure 4.7: Two dimensional Raman mapping of BTEG…… 57

Figure 4.8: Raman of transferred CVD graphene and MTEG……. 58

Figure 4.9: TEM images of MTEG……. 60

Figure 4.10: TEM images of BTEG…… 60

Figure 4.11: Intensity plot obtained from BTEG SAED…… 61

Figure 4.12: TEM etching of BTEG…….. 62

Figure 4.13: Visualization of graphene moiré pattern…… 63

Figure 4.14: TEM images of rotated BTEG……... 63

Figure 5.1: Fabricated TEG FETs and TLMs……. 66

Figure 5.2: Schematic of contact resistance measurement…… 68

Figure 5.3: Illustration of TLM theory…… 69
Figure 5.4: TLM measurements for MTEG and BTEG……. 71
Figure 5.5: Probing setup for two point probe and four point probe…….. 74
Figure 5.6: micro-crack issue with TEG with Raman overlay…….. 74
Figure 5.7: Conductivity curve for MTEG……. 75
Figure 5.8: MTEG field effect mobility Vs. carrier concentration…… 76
Figure 5.9: MTEG hole universal mobility curves……. 77
Figure 5.10: Density independent mobility fitted to MTEG…….. 80
Figure 5.11: BTEG conductivity plot showing Dirac point shift with annealing.. 82
Figure 5.12: BTEG voltage plots with annealing…… 83
Figure 5.13: BTEG field effect mobility Vs. carrier concentration…… 84
Figure 5.14: MTEG field effect mobility over time…… 87
Figure 5.15: BTEG field effect mobility over time …… 87
Figure 5.16: MTEG Dirac point shift with time……. 88
Figure 5.16: BTEG Dirac point shift with time……. 89
Figure 6.1: Coalesced h-BN films with growth imperfections……. 92
Figure 6.2: Rolling lines in unpolished copper foils……. 93
Figure 6.3: Electropolishing setup……. 94
Figure 6.4: Etching in surface kinetics controlled region…….. 95
Figure 6.5: Microscope and AFM copper foil before and after electropolishing.. 96
Figure 6.6: CVD h-BN nucleation triangles on electropolished copper foils…... 97
Figure 6.7: Early attempts CVD graphene devices on h-BN flakes……... 98
Figure 6.8: Transfer procedure for CVD graphene on CVD h-BN……. 99
Figure 6.9: Thick CVD h-BN wrinkling and subsequent delamination……. 99
Figure 6.10: Van der Paw structures formed from CVD graphene on CVD h-Bn.. 100
Figure 6.11: Hall mobility Vs. carrier concertation for CVD graphene on h-BN.. 101

LIST OF TABLES

TABLE 3.1 Adhesion Energy and Experimental Notes……... 48

TABLE 4.1 Raman Characteristics of Graphene Layers…….. 59

TABLE 5.1 Transport Characteristics of Large Area Graphene Synthesis…….. 86

TABLE 5.2 List of Cornell Nano Fabrication Facility Tools used for Fabrication.. 90

LIST OF ABBREVIATIONS

0D:	Zero Dimensional
1D:	One Dimensional
2D:	Two Dimensional
3D:	Three Dimensional
TEM:	Transmission Electron Microscopy
h-BN:	Hexagonal Boron Nitride
CVD:	Chemical Vapor Deposition
EG:	Epitaxial Graphene
TEG:	Transferred Epitaxial Graphene
XPS:	X-ray Photo-electron Spectroscopy
AFM:	Atomic Force Microscopy
FWHM:	Full Width at Half Maximum
MTEG:	Monolayer Transferred Epitaxial Graphene
BTEG:	Bilayer Transferred Epitaxial Graphene
PMMA:	Poly(methyl methacrylate)
PDMS:	Polydimethylsiloxane
PVA:	Poly(vinyl alcohol)
SAED:	Scanning Area Electron Diffraction
TLM:	Transmission Line Measurement
FET:	Field Effect Transistor
RIE:	Reactive Ion Etch

CHAPTER 1

INTRODUCTION

1.1 Two Dimensional Materials

Humanity has come a long way since the initial speculations of ancient Greeks on the atomic composition of matter. Dalton's work provided the first experimental evidence that started the whole world of precision material science and, at the turn of our century, it would seem the horizon is pivoted on exotic structures of materials. This is more so driven by the overall nanotechnology efforts and a very large and lucrative electronics industry that stands to benefit greatly in finances.

One can say that the earliest form of these exotic material structures to capture the interest of the sciences is the buckminsterfullerene (figure 1.1), first discovered by Smalley et al. back in 1985 [1]. Such material is deemed zero dimension (0D) since it cannot be reduced beyond its physical structure. Carbon nanotubes were the second exotic material structure to be discovered. Carbon nanotubes came to the spotlight through Sumio Iijima's work back in 1991 [2][3]. Carbon nanotubes represented the one dimensional (1D) material world and soon were followed by a large family of other 1D materials with very exotic properties. Although the field is comparatively old by now, it is still a very rich field to explore scientifically. These materials are being used in industry but to a limited extent considering their exotic material properties.

Surprisingly, from an intuitive point of view, two dimensional (2D) materials were the last to come to the spotlight of exotic material structures.

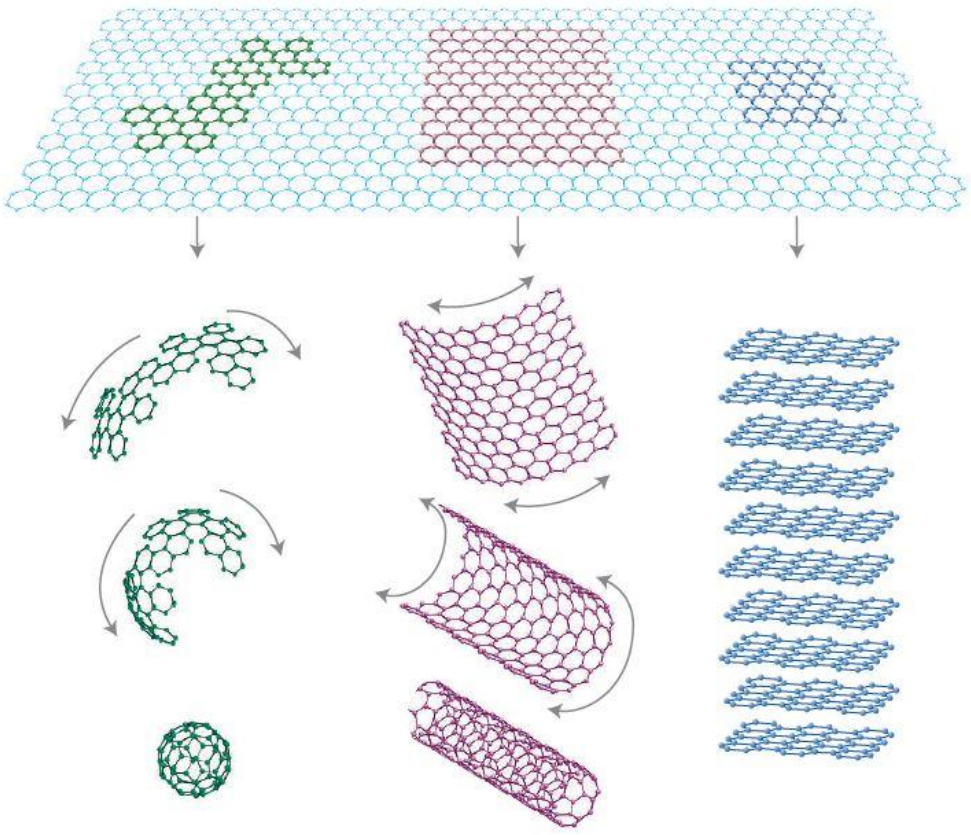

Figure 1.1: The carbon family of dimensional materials which includes buckminsterfullerene, nanotubes, and graphene (Adopted from [4]).

It is less surprising from a scientific point of view though, considering there were studies showing that strict 2D structures are unstable [5]. The pioneering work of Geim and Novoselov back in 2004 [6][7] on isolating monolayers of graphite was the first demonstration of 2D materials. A very large family of other 2D materials followed which will be covered in section 1.4. The whole family of 2D materials have given the science community truly exotic properties that are subject of intense research today [4].

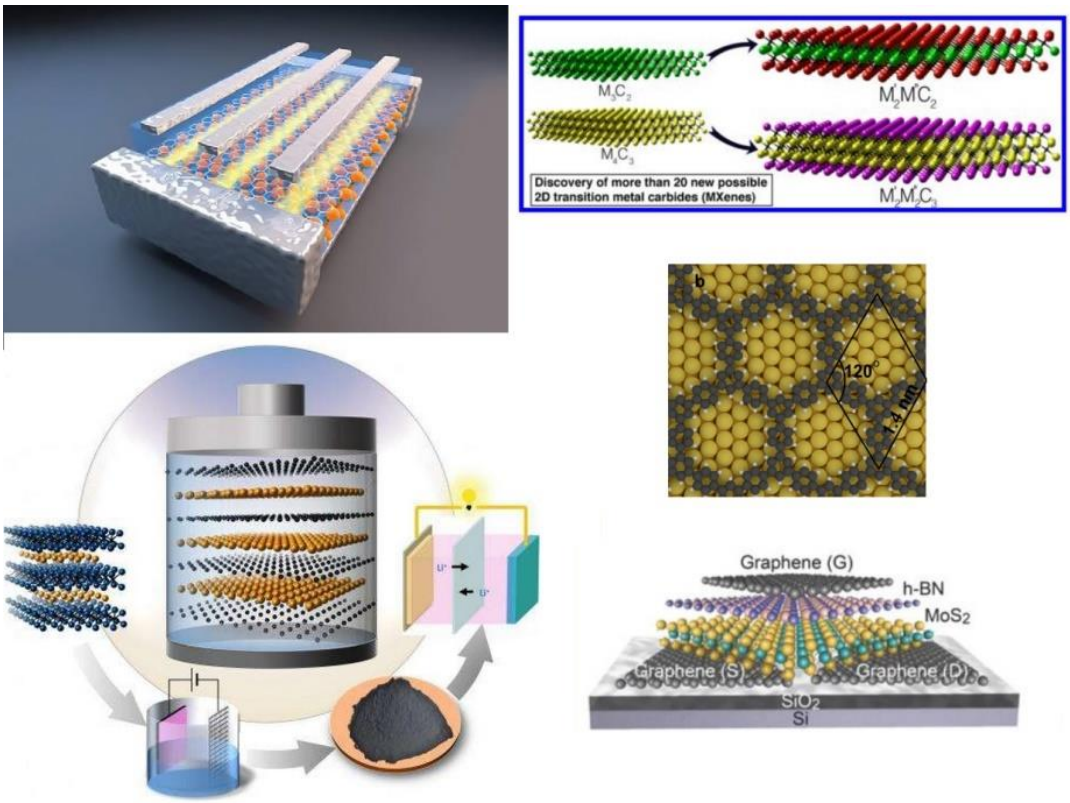

Figure 1.2: Numerous families of 2D materials and applications researched after graphene (Adopted from [8][9][10][11]).

The field is very young by scientific standards yet one can claim it is the fastest growing experimental field in modern times based on facts such as the original paper published in 2004 being the most cited experimental paper of the twenty first century [12].

On a very interesting side note, it seems that in all revolutions of material structures, carbon was the element that started it. An ironic coincidence considering it is the central element of complex lifeforms on earth.

1.2 Graphene

Graphene was theoretically studied longer than it was experimentally proven to exist [13][14]. While synthesizing graphene might be as simple as using a pensile to write something on a piece of paper, reports on what resembles monolayers of graphitic materials date back to only 1961 [15][16]. The Transmission Electron Microscopy (TEM) community is familiar with such thin materials even though back then TEMs did not have the resolution to determine if they were indeed monolayers.

The first work published by Geim and Novoselov which conclusively demonstrated monolayer graphene was of very high quality graphene that was unambiguously a monolayer of carbon. The robust nature of the initial discovered material set the trend for future work which was clearly defined. Notable mention should be given to Philip Kim et al. for his high impact publication of the experimental observation of the quantum hall effect in graphene [17] and Walt de Heer et al. who also contributed greatly to the field [18].

Carbon has four electrons in its outmost valance band. The final sp_2 bond remains free and forms what are called the π bonds which provide graphene with its electron transport properties.

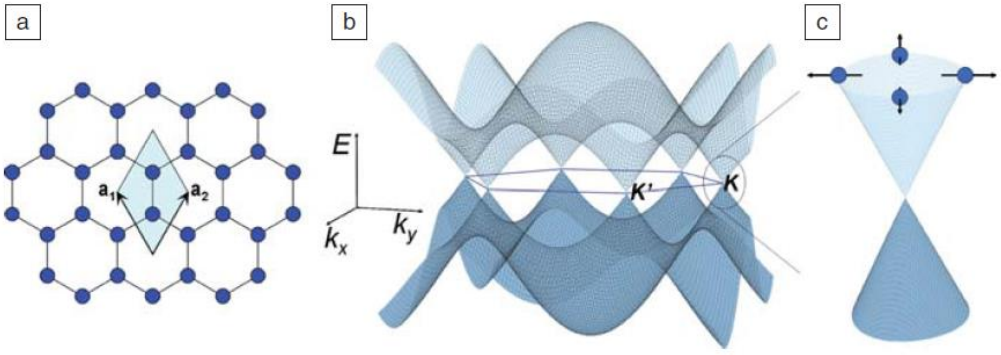

Figure 1.3: a: Graphene honeycomb lattice b: Band structure c: Energy band linear dispersion relation (Adopted from [35])

Electrons moving in such bands behave like zero effective mass Dirac fermions due to the linear band energy dispersion as illustrated in figure 1.3. Ballistic transport has been reported [19][20] and when suspended as in figure 1.4, electrons can travel in graphene with mobilities exceeding 10^6 $cm^2/V.s$ [21].

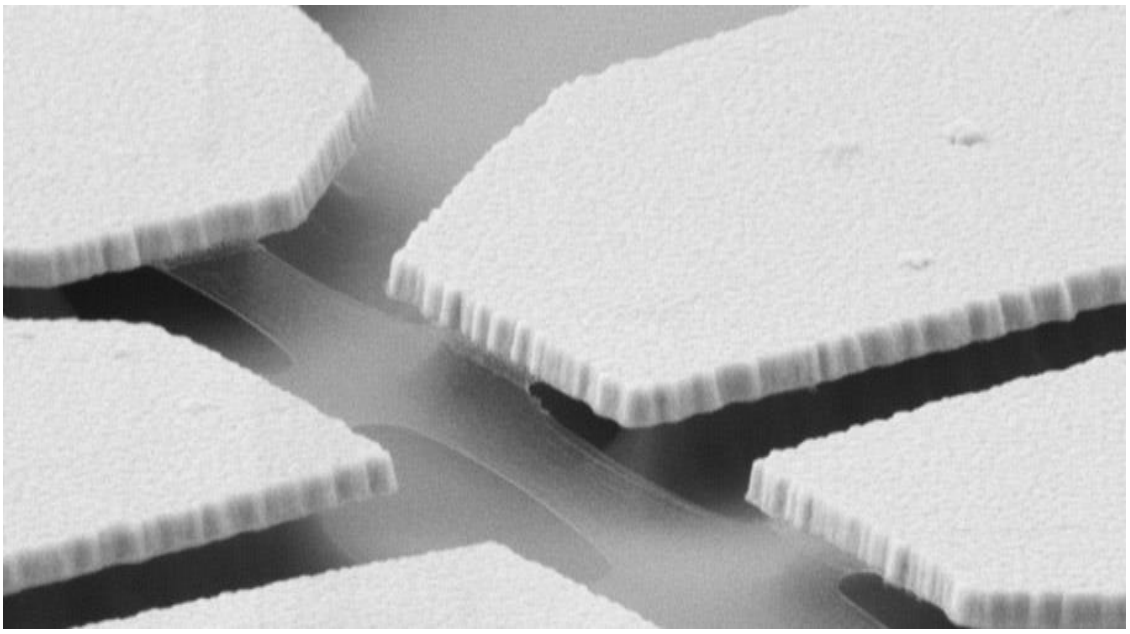

Figure 1.4: Suspended graphene (Adapted from [22])

The honeycomb structure also provides it with exceptional strength being 100 times stronger than steel. Absorption, for a materials comprised of a single monolayer, is high at around 2.3% value [23] and opens up the opportunity, being a semi-metal material that passes a lot of light through, to be a potential replacement to technologically important materials such as Indium Tin Oxide (ITO).

Although graphene is the oldest material in the 2D material family, it is still among the most technologically relevant. For example, its high conductivity for a monolayer, coupled with its semi-transparent, properties make it an excellent candidate for electrode applications in solar cells [24][25]. Certainly, it is among the most exciting

with recent reports showing experimental observation of superconductivity [26] and even laser propulsion levitating graphene [27].

1.3 Bilayer Graphene

For this dissertation, bilayer graphene plays a central role and exclusive detail will be presented in this section. While monolayer graphene garners more attention among 2D materials publication wise, bilayer graphene is a topic of intense research efforts as well. How the two layers of graphene come together is a very rich field of science yielding a lot of publications [28][29][30][31][32][33][34]. The details and forms of combining two layers of graphene are beyond the scope of this dissertation save for the simplest which will be detailed here and known as AB stacking.

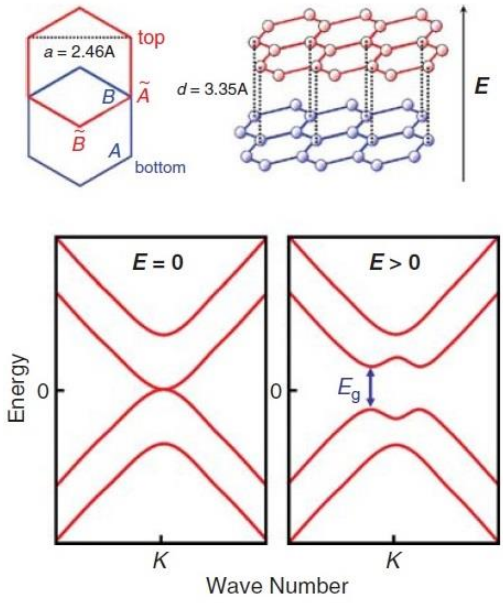

Figure 1.5: AB stacked bilayer graphene with bandgap opening at around 0.25 eV due to vertical field (Adopted from [35])

AB stacked bilayer graphene is of technological interest due to the ability to open a finite bandgap when applying a vertical field as illustrated in figure 1.5. This would possibly enable the manufacturing of electronics with gate controllable bandgaps. The maximum bandgap is 0.25 eV [36]. Fuhrer and Drew et al. reported the application of AB stacked bilayers in high performance bolometers illustrated in figure 1.6 [37][38]. However, their work was done using exfoliated graphene. This synthesis method yields high quality graphene but is limited in its application to large area synthesis which will be detailed in section 1.5.

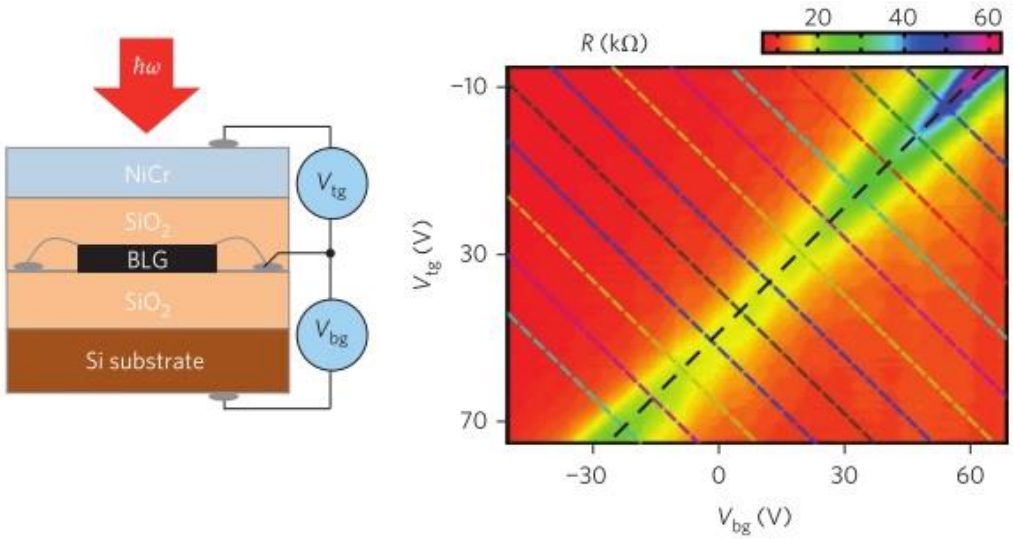

Figure 1.6: Bilayer graphene bolometer illustration with a plot of resistivity varying with controlled gate voltages indicating the opening of a bandgap (Adopted from [37])

What cannot be emphasized enough here is the crucial role the AB stacking plays if any of these properties are to be realized. Non-AB stacked bilayer graphene or indeed even non-uniformly AB stacked graphene simply either does not exhibit any of these proprieties or the performance can be detrimental in application.

1.4 2D hexagonal Boron Nitride and other Materials

Hexagonal boron nitride (h-BN) was the second 2D material to gain interest after graphene, led by the pioneering work of the Columbia University groups [39].

h-BN has the same hexagonal structure of graphene with a lattice constant of 2.52 *Å* making it a very close match. Furthermore, unlike graphene, it is an insulator. It has phonons very high in energy and a surface that is atomically smooth (figure 1.7). These properties are contributing factors to the enhanced mobility of graphene when h-BN is used as a substrate. Furthermore it has been reported that h-BN is a self-cleaning surface when coupled with graphene which eliminates much of the contaminants that work to degrade graphene mobilities[40]. All these properties make it the substrate of choice for graphene.

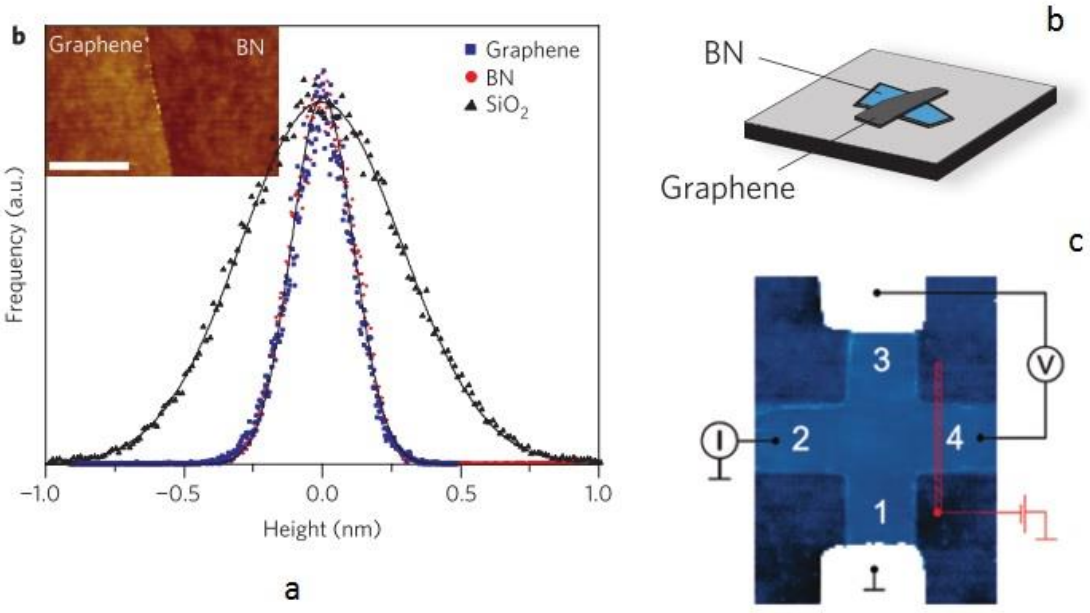

Figure 1.7: a. h-BN smooth surface roughness b. Graphene on h-BN substrate illustration c. h-BN graphene encapsulation devices record highest mobilities in literature (Adopted from [39][41])

Other complete families of two dimensional materials have gained attention as well. Mentions should be given to silicone [42][43][44][45], the two dimensional form of silicon, and black phosphorous, a 2D material similar to graphene but has the added property of a controllable bandgap [46][47][48]. Both materials are unstable though. Molybdenum Disulphide (MoS_2) with a whole host of metal dichalcogenides gained a lot of attention, being 2D semiconductors, but mobilities and other electronic properties fall short of the Graphene/h-BN combination [49].

1.5 Current Graphene Synthesis Methods

1.5.1 *Exfoliation*

The initial experiments led by the Manchester University research groups and others raised a lot of excitement. The scotch tape method pioneered by the Manchester group yielded very high quality graphene usually in the few micron size. While it is arguably the reason behind the whole graphene phenomenal rise because of the acceptability of this method, this is not the whole story. Even with contrast enhancing substrates such as using silicon dioxide on a silicon substrate (SiO_2/Si) [50] monolayers are very difficult to find and often in the few tens of microns size. Research in itself was challenging let alone the thought of scaling up to industry production levels which so far did not happen using the scotch tape method. Clearly alternative synthesis forms are needed.

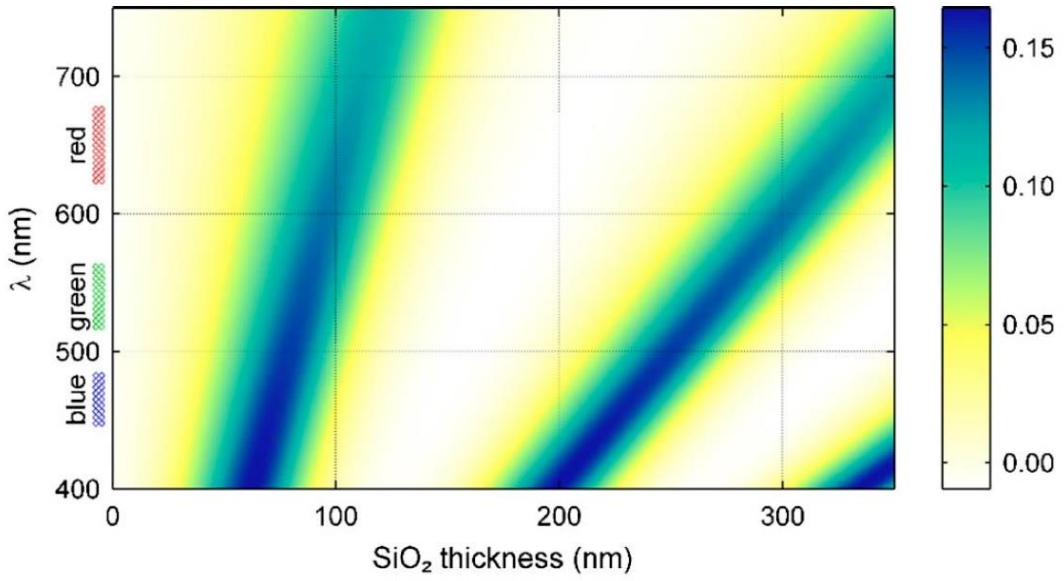

Figure 1.8: Graphene contrast as a function of wavelength and SiO_2 thickness. Optimization of thickness improves graphene visibility (Adopted from [50]).

Graphene, being the wonder material that it is, has no shortage of alternative synthesis methods. Indeed one fails to find another material out there that had such amusing scientific papers published on its synthesis. Detonation growth and animal feces for starting material are on that list [51][52]. In this section, the more prevalent methods will be presented.

1.5.2 Chemical Vapor Deposition

As of the time of this dissertation, the leading method of graphene synthesis is Chemical Vapor Deposition (CVD) on catalytic substrates such as copper. This synthesis method started back with the leading work of [53][54][55]. The reason why it gained popularity is the relative low cost and simple requirements needed to setup a typical CVD chamber. Growth temperatures are typically in the 1000 ^oC range. The synthesized graphene area is mostly limited by the size of the starting catalytic substrate. Indeed even at the early stages, groups were reporting role to role production of very large area graphene [56]. Currently, most commercial providers of

graphene rely on the CVD method. However CVD graphene has its shortcomings. It is generally hard to control the growth to achieve monolayer uniformly throughout the substrate. This problem has been minimized currently, but it was a challenging problem in the earlier days of CVD graphene. The other major problem with CVD graphene is that the way it grows is by nucleation on the catalyzing grains of the substrate. These grains have random orientation. This random orientation of the starting nucleation ends up creating grain boundaries once the graphene grains in turn coalesce as shown in figure 1.9. Cornell and Columbia University groups led by Prof. Muller reported extensively on this issue [57].

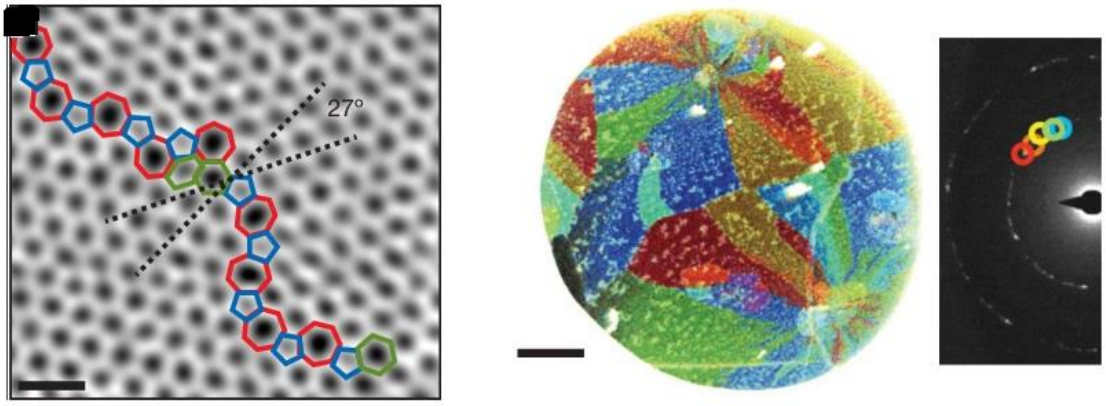

Figure 1.9: Grain boundaries of CVD graphene revealed by TEM methods (Adopted from [57])

While the effect of these grain boundaries is highly debated in the field, the consensus is that graphene, with fewer of them, is better quality graphene [58][59]. Research work has gone into improving the grain size of CVD graphene [59] and the results are sufficiently impressive to challenge exfoliated graphene which sets the benchmark in quality. Groups have reported centimeter grain size [60] even though their method requires over 10 hours of growth time which is prohibitively expensive to scale up. CVD graphene also typically requires transfer off the metal catalytic substrate it is

grown on and this procedure, which will be touched upon in section 3.1, will almost always introduce a host of imperfections ranging from physical damage to the graphene, to charged and uncharged contaminants [61][62][63][64]. Another limitation of CVD graphene is the stacking order of bilayers. Obtaining AB stacked bilayer graphene is challenging with the CVD method. With the grains being randomly oriented in a monolayer, it is expected that the stacking order of bilayers is random. Added to this, the CVD method is inherently challenging to control the uniformity of layer numbers. The first layer of graphene covers the catalytic nucleation sites and any subsequent growth tends to be less controllable due to this.

1.5.3 SiC Epitaxial Graphene

Epitaxial Graphene (EG) growth by high temperature annealing of Silicon Carbide (SiC) is the second oldest method of graphene synthesis [18].

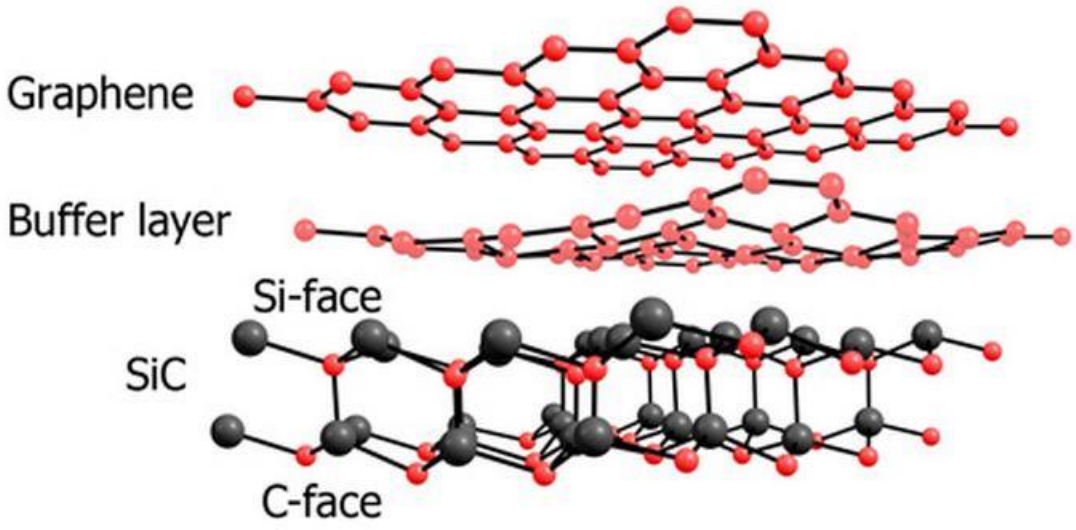

Figure 1.10: SiC EG illustration (Adopted from [65])

The details of SiC EG growth will be presented in section 2.2. SiC EG grows in a carpet like form [66] with seemingly no grain boundaries. This growth is dictated by the crystal lattice of the SiC substrate. Furthermore, any subsequent layer growth is still dictated by the SiC crystal lattice. This has a profound effect on layer orientation being predominantly AB stacked as will be presented later on. The growth temperature is high at around 1600 ^{o}C.

One more method of synthesis that shows a lot of initial promise is the epitaxial growth of graphene on a germanium substrate [67][68][69]. This method has high technological relevance since germanium is a CMOS compatible substrate that is touted to play a major role in future electronics. The graphene grown by this method is epitaxial, so it shows less of the randomness found in conventional metal CVD methods. This method of synthesis though is at a very early stage with little research done compared to CVD and SiC EG as of the time of this dissertation.

1.6 Motivation for Pursuing Transferred Epitaxial Graphene

There are three main motivations behind pursuing Transferred SiC Epitaxial Graphene (TEG). The first is that the SiC substrate tends to cause mobility limiting anomalies that will be detailed in section 2.5. Second is the possible use of more favored substrates such as h-BN. And the third motivation is the possible reuse of the SiC substrate.

In this dissertation the procedure for monolayer and bilayer EG growth will be detailed in chapter two. Chapter three will cover the literature on what has been done in this field and then present the transfer method we developed using gold adhesion layers and how, for the first time, we successfully transferred high quality monolayers

and bilayers. Chapter four will present structural characterization of the transferred graphene in which we show detailed Raman studies that were made possible by transferring graphene to a Si_2O/Si substrate, and Transmission Electron Microscopy (TEM) studies that show the conclusive structure of the transferred graphene and that were never done before nor have been possible if not for the successful transfer. We thoroughly conclude that the structural studies show AB stacked bilayer graphene. In Chapter five, we present the fabrication of characterization devices that enabled us to measure electronic properties of the transferred graphene and further study the AB stacked bilayers. We show large gains in mobility for transferred monolayers due to negating the substrate effects after transfer and we show how the bilayers have significantly different electronic properties. In the end of chapter five, a study of annealing and moisture absorption of the bilayers is presented. Chapter six will present work done in improving h-BN CVD growth by electropolishing the substrate. We also present the successful transfer of CVD graphene on CVD h-BN and electrical characterization in comparison to different substrates. The dissertation is concluded with a prospective and future outlook for TEG.

CHAPTER 2

GROWTH AND CHARACHTERIZATION OF EPITAXIAL GRAPHENE

In this chapter, the process of growing monolayer and bilayer EG using cold wall furnace growth is presented. An intercalation procedure was developed for formation of bilayers from monolayers.

2.1 Cold Wall High Temperature Growth Furnace

SiC is a wide bandgap semiconductor with strong covalent bonding energy in the range of $\sim 5\ eV$. This necessitates very high temperature furnace growth in the range of 1600 ^{o}C in order to break such bonds and sublimate silicon and allow remaining carbon atoms to stitch together forming graphene. Regular quarts tubes cannot withstand temperatures higher than about 1200 ^{o}C. This necessitates cold wall furnaces. Our setup shown in figure 2.1 is a stainless steel cold wall chamber with water running through piping of the stainless steel walls as coolant allowing the furnace to go up to 1750 ^{o}C without melting the steel enclosure. There are two, upper and lower, heating elements which are made of tungsten. Samples are loaded into the chamber using a regular graphite holder.

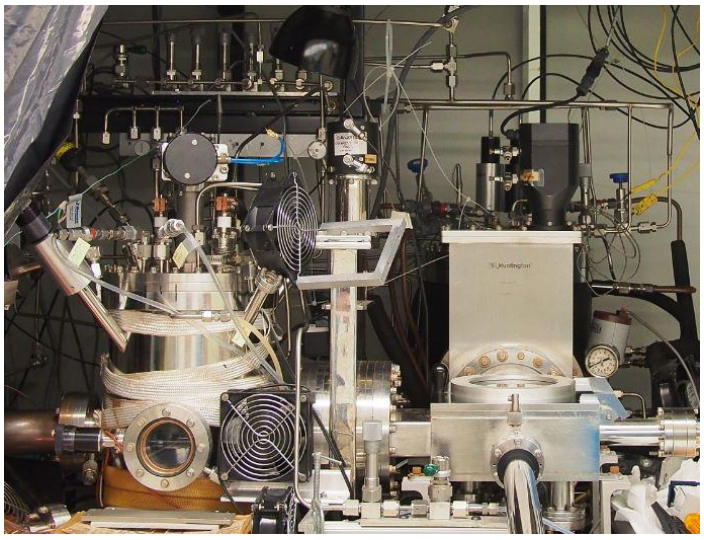

Figure 2.1: Purpose built SiC epitaxial graphene chamber utilizing water cooled cold wall steel reaching temperatures as high as 1750 ^{o}C.

Growth temperature is monitored using both a pyrometer and a thermocouple. The pyrometer reading is the main source of temperature measurements conducted during growth. Careful calibration is necessary for the pyrometer gauge as its readout values vary with the index of refraction of the material being measured. The usual procedure is to calibrate its temperature readout before sample growth.

Due to water vapor and other contaminants sticking to the wall of the stainless steel chamber, it is necessary to keep it under ultra-high vacuum all the time. Water vapor is especially crucial to get rid of as the water molecules break up at high temperature and both hydrogen and oxygen can cause rough surface morphology of the EG growth. Ultra-high vacuum is achieved using a turbo pump as well as regularly baking out the chamber to very high temperatures to release any water molecules stuck to the walls of the chamber. Our chamber was setup with an automatic gas flow pressure controller as well as being able to allow the flow of ultra-high purity argon for necessary growth procedures.

2.2 Silicon Carbide Epitaxial Graphene

SiC comes in many crystalline polytypes. The most technologically relevant to this dissertation is 6H and 4H. The former is the one used here. Due to the nature of SiC crystal structure, the two faces of the wafer are not interchangeable. The upper face, normally referred to as **(0001)** in Miller indices, is called the silicon face (Si-face) and the lower face **$(000\bar{1})$** is called the carbon face (C-face).

The study of **$(000\bar{1})$** EG was not pursued in this dissertation. Growth on the **$(000\bar{1})$** face tends to be very rapid with little to no control over the number of layers, orientation, or even morphology. Growth nucleation seems sporadic with little control. The graphene grown on the **$(000\bar{1})$** side is akin to multilayer graphene [70][71]. Growth on the **(0001)** face is well studied in the field of graphene, dating back to the original work of Berger and de Heer et al. [18]. It is interesting to note that the de Heer paper was published in very close time proximity to the original work of Geim and Novoselov.

When temperature rises to 1600 ^{o}C in SiC, the silicon atoms sublimate off the substrate leaving the carbon atoms behind to stitch together and form graphene. The early work of Berger and de Heer et al. [18] was done by annealing **(0001)** SiC at high vacuum pressures. This method is known to yield rough surface morphology. The nucleation is non-uniform as well. Earlier studies were conducted using this method since it is almost as early as the Geim paper. A lot of literature reported monolayer graphene when their characterization leaves a lot speculation.

EG synthesis quality improved considerably when Johansson et al. and Seyller et al. independently reported atmospheric growth using argon ambient [72][73]. This worked to suppress the rapid sublimation of silicon atoms and the slow release

allowed the remaining carbon atoms more time to stitch together and this had a profound effect on the morphology of the EG.

A little more detail is necessary on the growth to better facilitate the understanding of core problems facing EG. The first to consider is the surface morphology of SiC before growth. SiC wafers are grown to crystalline form much akin to the silicon industry's methods. This necessitates growing ingots that need to be cut into wafers. The angles, at which these ingots are cut, play a major role in growth. This angle creates what is known as steps on the surface of the SiC. The step sizes are critically dependent on the cutting angle of the wafer. The size of these steps in turn plays a major role in the quality of the graphene grown. Zakharov et al. verified experimentally how graphene growth changed with wafer miscut angle [74].

When the temperature is first raised in SiC, the steps come together forming larger terraces in what is called "step bunching" as illustrated in figure 2.2. These terraces can be up to 10 *microns* in width and hundreds of microns in length. The edges of the terraces are usually referred to as "step edges" and are usually in the 10 *nm* height range. These step edges are of inferior crystal quality. They are full of defects [75] and play a very crucial part in growth as will be detailed next.

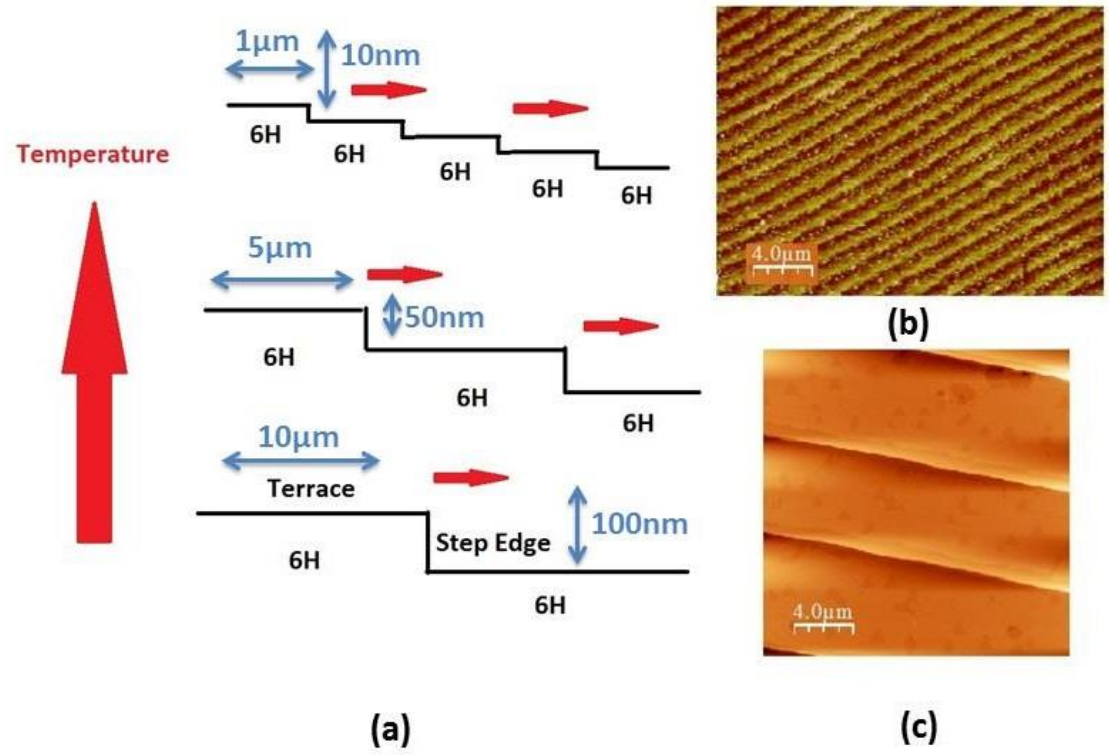

Figure 2.2: a. Illustration of step bunching in SiC as temperature is raised. b. AFM of SiC steps before bunching c. AFM of SiC graphene after step bunching.

When the temperature is further raised, the silicon atoms first start leaving the SiC surface through the step edges. The growth of graphene on step edges is considerably more energetically favorable over the terraces to the point that a number of layers are formed on the step edges first [75]. This can be up to 4 layers and some report even more [75][76][77]. Eventually, when the temperature is raised further, the graphene growth migrates to the terraces through either side of the initial step edge growth [75]. At some point, all the films coalesce as illustrated in figure 2.3 and numerous sources have shown this growth as being continues carpet like growth [66].

It is important to note at this point that the multilayer growth of the step edges is still present under this "carpet graphene". Indeed further bilayer growth and so on continues through these extra layers.

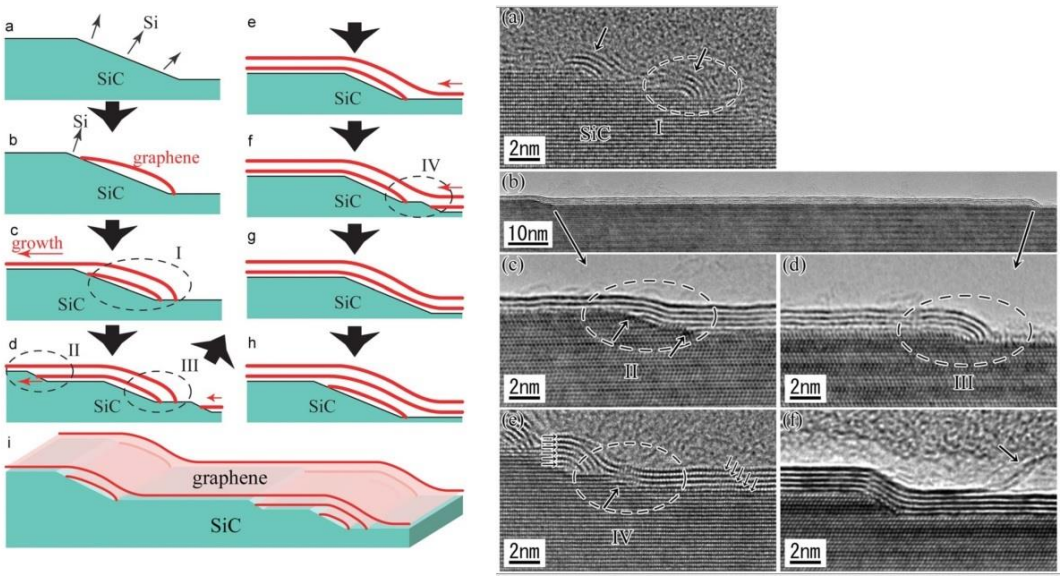

Figure 2.3: Illustrations and TEM images of SiC EG formation showing the role of step edges in initial growth (Adopted from [77]).

2.3 Monolayer Growth Procedure

The initial critical step in TEG is the accurate control of the number of layers as well as the quality of grown material. The samples used in this growth were of 1200 X 1200 *micron* size. Towards achieving high quality monolayer growth throughout the area of the samples, extensive research work was done in optimizing our system. We developed a growth heat cycle that relied on accurate time steps and the flow of argon to control the sublimation rate of silicon.

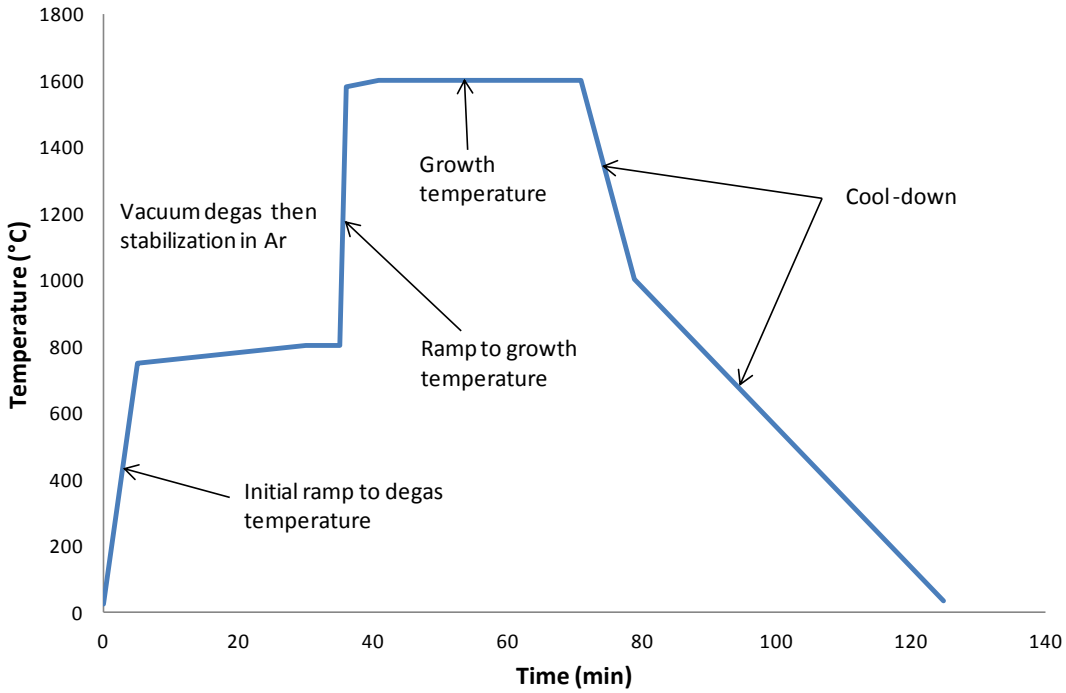

Figure 2.4: Heating cycle for monolayer EG growth.

In our analysis, we have found the following procedure to yield the most repeatable good results. For our growth procedure we clean the SiC using regular solvent cleaning and load it into the chamber and leave it overnight in ultrahigh vacuum at around 3 X 10^{-8} *Torr* to outgas any contaminants on the surface. Following the heat cycle illustrated in figure 2.4, the temperature is then raised to 800 ^{o}C for one hour as a

further outgassing cleaning step. 2000 SCCM of argon flow is kept steady for 5 minutes at 750 Torr to stabilize the system. The temperature is then rapidly raised to 1600 ^{o}C for graphene growth and kept for 15 minutes. After that, the temperature is gradually lowered down to 900 ^{o}C and then power is shut off the filaments to allow for room temperature cool down. The sample is left in the chamber for one hour to cool down before it is taken out.

We specifically chose to use 1600 ^{o}C for a 15 minute growth after studying various growth temperatures and time intervals and observing the number of layers yielded as shown in figure 2.5. We have experimentally verified that the increase of temperature or time would result in more layer growth. For optimizing growth, it is preferred to keep the growth time as short as possible while increasing the temperature and at the same time, use a reasonable growth time length that would allow accurate control of monolayer growth. The reason why rapid growth is preferred is that it limits the number of layers grown on step edges and yields more uniform growth.

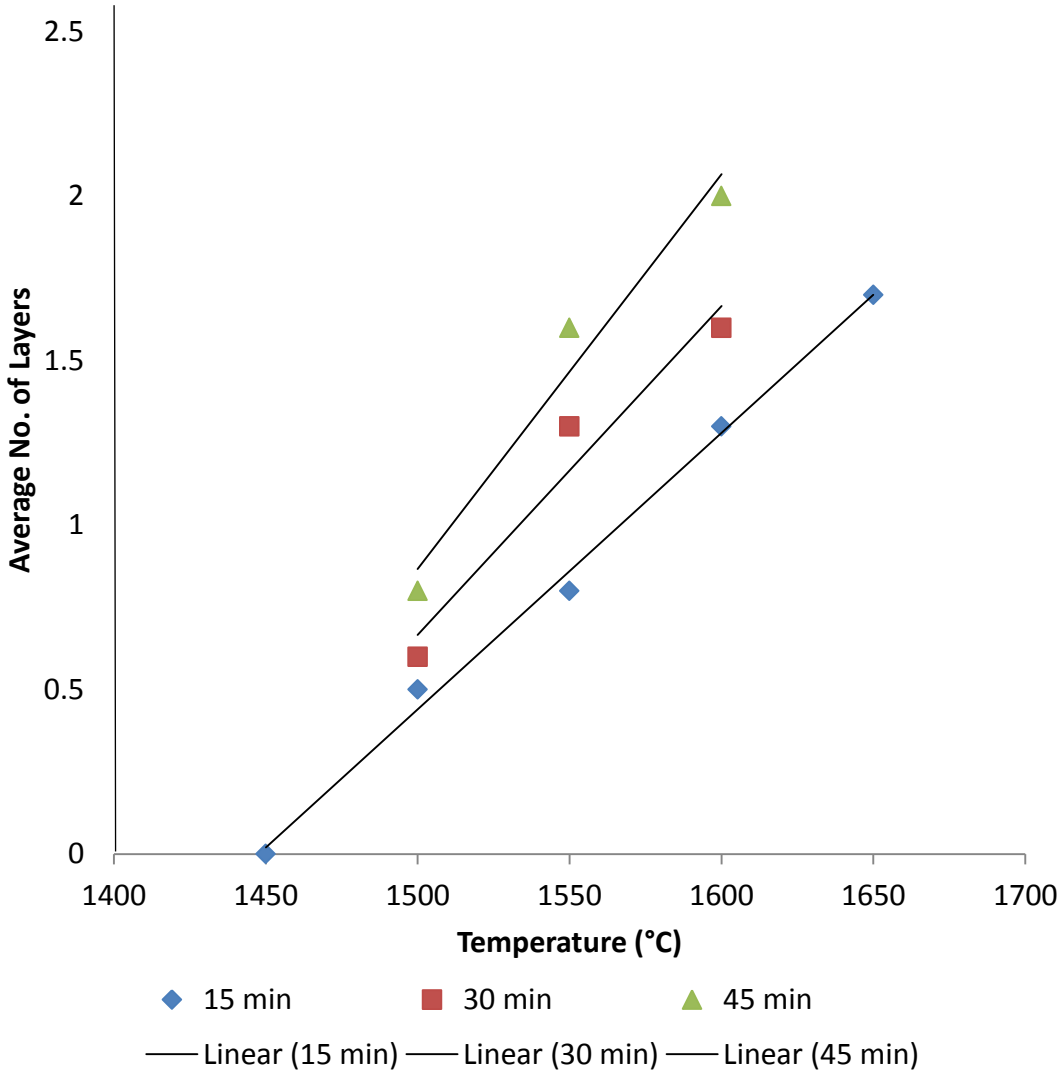

Figure 2.5: Plots of the number of graphene layers grown as a function of temperature for 15 min, 30 min and 45 min growth times.

The number of layers was further confirmed using X-ray Photo-electron Spectroscopy (XPS). Using XPS, it is possible to distinguish the carbon peaks indicating the number of layers. XPS is a surface analysis tool that only goes about 10 *nm* into the material. It can simultaneously measure the binding energy and the number of electrons emitted from the material due to X-ray bombardment. Because both the buffer layer and the EG layer are composed of carbon, and because they have different binding energies that XPS can measure, it is possible to distinguish the buffer layer from EG. For instance, at 1450 ^{o}C, XPS in figure 2.6 would indicate that only the components of a buffer layer and bulk SiC exist, and that no EG was grown. The overlaid spectra shows how XPS can measure the progressive rise in intensity of the EG C 1s signal (peaking towards about 284.8 *eV*) and progressive attenuation of the intensity of the SiC C 1s signal (at about 283.7 *eV*) with increase in temperature. This indicates more EG layers being grown with higher temperature.

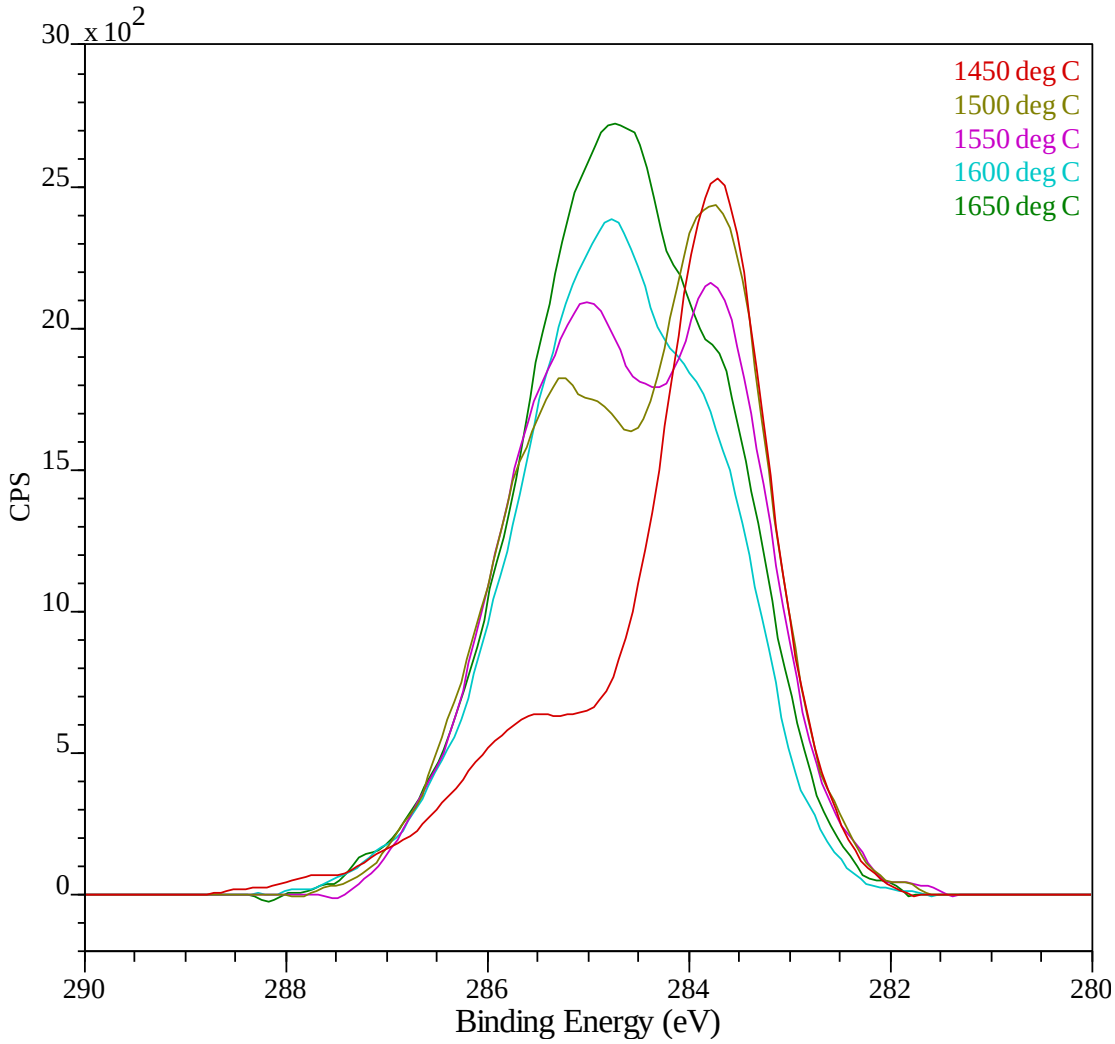

Figure 2.6: Overlay of XPS high-resolution C 1s spectra for 15 min growths at 1450, 1500, 1550, 1600 and 1650 °C.

We have found that generally 1600 ^{o}C was the optimal growth temperature and we worked towards optimizing growth time that would yield tight control of monolayer growth as shown in figure 2.7.

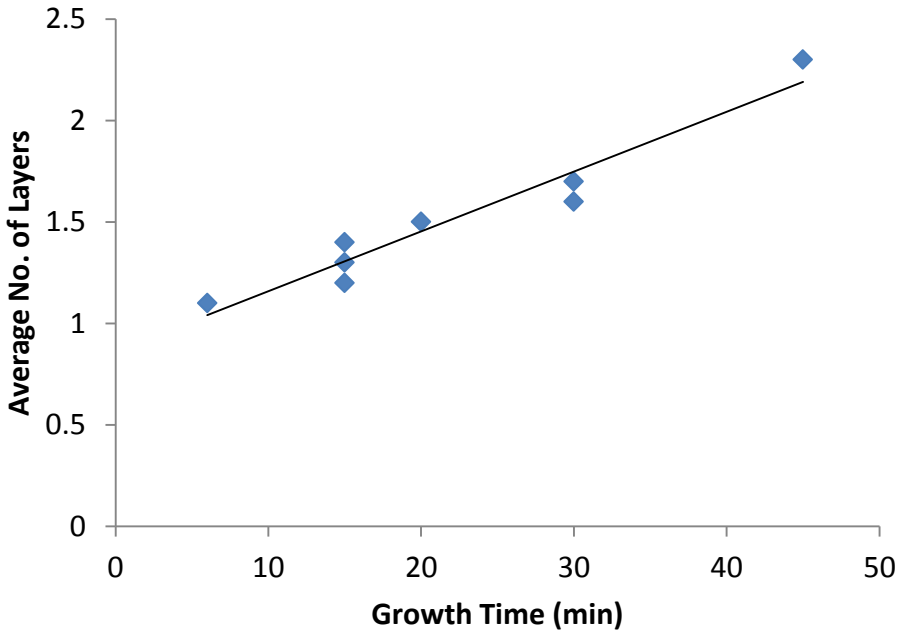

Figure 2.7: Plot of the average number of graphene layers grown as a function of growth time for 1600 °C growth.

Finally, some samples were processed for hall mobility measurements. Again, the trend we observed is that growth at 1600 ^{o}C for 15 minutes gave us the highest mobility values with the lowest carrier concentration as shown in figure 2.8.

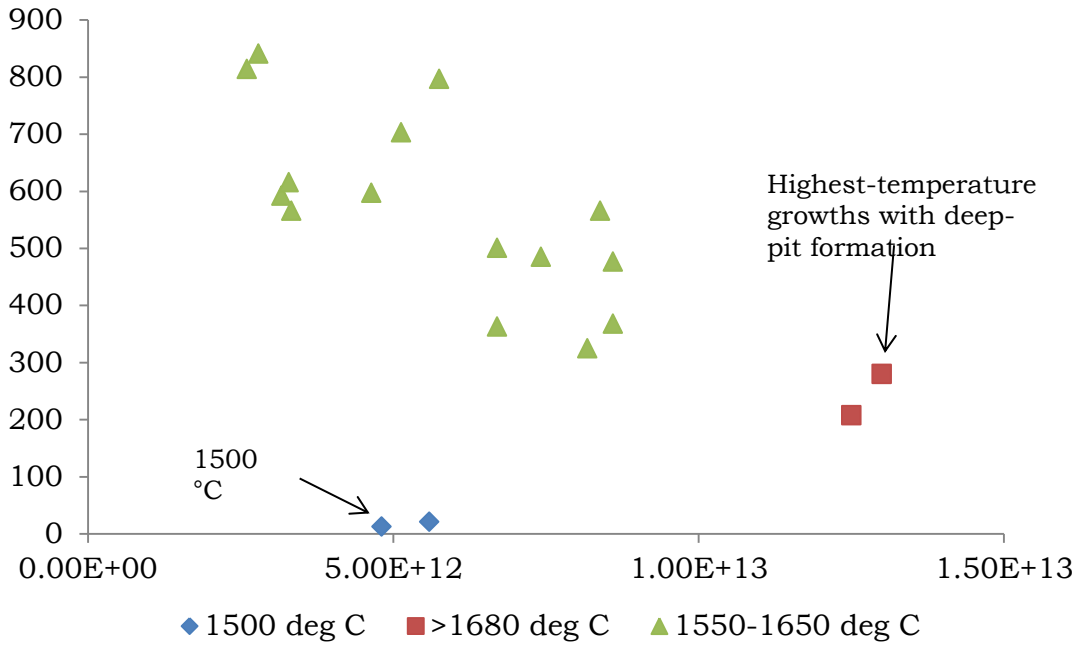

Figure 2.8: Hall measurements of carrier mobility versus carrier density where growth temperature of 1600 ^{o}C shows optimal performance.

It is worth mentioning that, in general EG growth, it is favorable to condition the surface by hydrogen etching to remove polishing imperfections and further increase the size and quality of the terraces [73]. We unfortunately did not have such facilities to conduct this pre-growth treatment and chose to optimize growth without using it.

To recap on the growth steps of EG, as the temperature is raised up to 1450 ^{o}C, silicon atoms start sublimating from the step edges forming the first layers of graphene. As temperature is raised to 1600 ^{o}C graphene starts migrating from the step edges onto the terraces where it stitches together to form a carpet like growth. The sample is then cooled down and is ready for further characterization and processing.

2.4 Pre-Transfer Raman and Atomic Force Microscopy Characterization

Prior to transferring EG, the quality of the grown layers has to be assessed per each sample grown. Also, the characterization methods used have to be non-destructive to allow further processing steps. Raman and Atomic Force Microscopy (AFM) were used to achieve this.

Raman has proven itself to be the leading quick and easy method of characterizing graphene [78]. This holds true for SiC EG as well. It is a versatile tool for graphene characterization with publications detailing information about the graphene layers that can be inferred from the Raman signal.

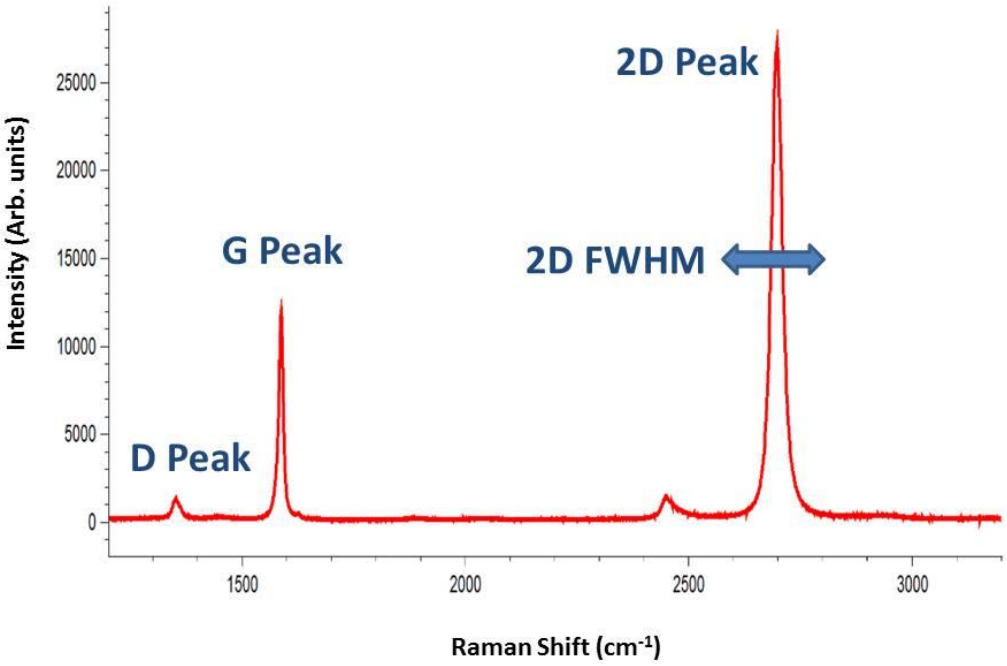

Figure 2.9: Typical Raman signal from graphene with labeling on the main characterization peaks.

Referring to figure 2.9, in graphene Raman characterization, there are three main peaks used: 2D, G, and D. These peaks are located at 2700 cm^{-1}, 1580 cm^{-1}, and 1350 cm^{-1} respectively. The leading Raman signal observables in graphene are as follows: First the 2D peak position, shape, and the full width at half maximum (FWHM). A Good quality monolayer will have a Lorentzian sharp peak at around 2700 cm^{-1} with a FWHM 30 cm^{-1} or less [79]. A shift in peak position is usually an indication of stress. A non-Lorentzian shape tells you there is something wrong, such as the band structure of graphene or contamination. And a FWHM that is thicker either indicates that the graphene is not strictly monolayer (or indeed not a monolayer at all) or that the graphene quality is poor. The second leading observable is the 2D/G ratio. For a good quality monolayer this should be over 2. Third is the D/G ratio. This ratio is the best indicator of the quality of graphene [80][81]. The lower it is, the better the quality of the graphene. One other indicator worthy of mention, but is generally considered extreme, is the G peak showing shoulders. This is an extreme case and is usually either caused by a lot of contamination residue or very high strain values [82][83].

Usually, graphene is characterized by the sharpness of the 2D peak, the sharpness of the G peak, the 2D/G ratio, and the G/D ratio. Unfortunately, EG is not as easy to characterize using Raman. The first issue is that the signal from EG on SiC is weaker than in more favorable substrates such as thickness optimized SiO_2/Si. Second, the substrate gives off a signal right where the D and G peaks are expected to be. We usually subtract the background substrate in Raman post processing as shown in figure 2.10. Yet still, it is not as clear as the case of a SiO_2/Si substrate and leaves a lot for speculation. The FWHM of the 2D peak is usually a good indicator of the number of payers but this is not an accurate method when applied to EG when it is on SiC. It is however possible to conclude graphene growth and even approximate the number of layers.

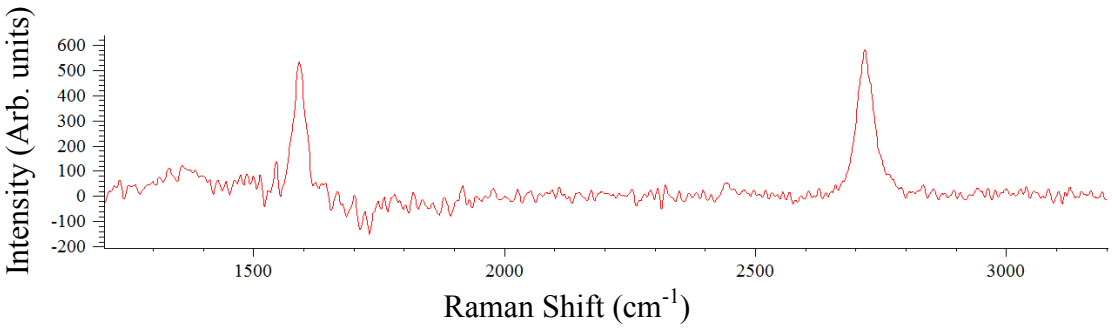

Figure 2.10: Typical Raman of EG before transfer. The background SiC signal was subtracted.

The second most important characterization method is AFM. Using a very sharp tip on a cantilever that deflects a measurable laser beam, AFM is able to probe the surface of a material down to a single atom. AFM can show clear surface morphology of the SiC indicating how successful the growth was. It is in many ways, a better characterization method than Raman. The phase image of the tapping mode AFM can distinguish monolayers from bilayer. AFM phase image records the delay of the cantilever oscillation and is sensitive to the adhesion of the material among other things. Due to monolayer and bilayer graphene having different adhesion properties, AFM phase image can distinguish between them. Using AFM, it was possible to study the structure of the micro-terraces before they are step bunched at high temperature.

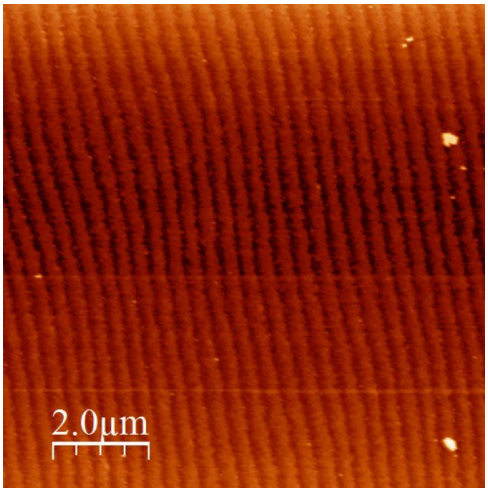

Figure 2.11: AFM image of SiC surface steps before growth and step bunching.

Once the SiC is raised to high temperatures and the steps bunch together along with the formation of graphene, it is possible to use AFM to distinguish monolayer from bilayer growth where the phase image shows bilayers as being darker in color as shown in figure 2.12. It is also possible to distinguish monolayers from bilayers using amplitude where the bilayers are a few nanometers recessed bellow the monolayers.

The surface morphology of the SiC generally varies across the wafer and, in accordance; the uniformity of monolayer growth varies. The proceeding transfer work depended on the starting material and it is possible to optimize it as we have done.

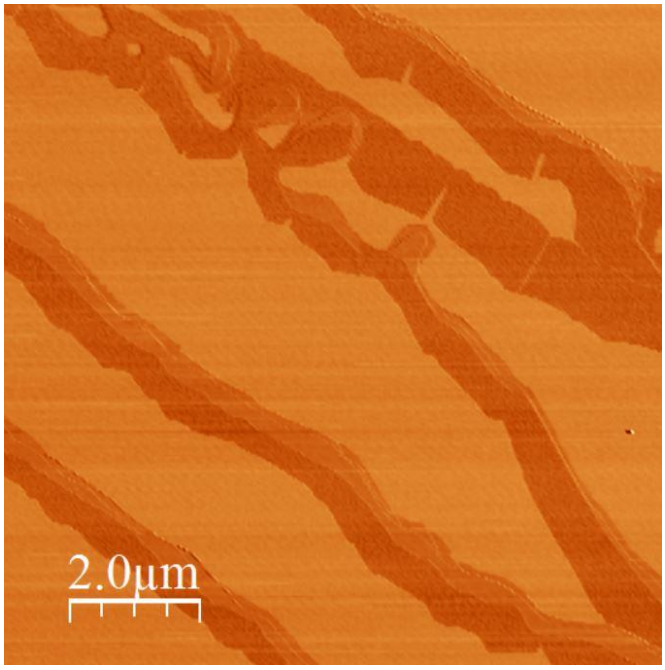

Figure 2.12: AFM phase image showing non-ideal growth where lighter portions are monolayer EG, and darker portions are bilayer EG.

To summarize this section, Raman is first used to indicate the successful growth of EG by the formation of a 2D peak. Subsequently AFM is used to confirm the quality of the monolayer growth by observing the phase image indicating the uniformity. Both these characterization steps are non-destructive and have no subsequent effect on the quality of the TEG.

2.5 Intercalation and Bilayer Graphene Synthesis

As illustrated in the previous section, it is possible to accurately grow monolayer EG by careful control of growth temperature and time. Clearly, it would also be possible to optimize the growth for uniform bilayers. However, we chose to pursue an alternative method of bilayer synthesis which we have found to yield more controllable results. This method relied on releasing what is called the "buffer layer" by high temperature hydrogen intercalation.

When EG is formed by sublimating the silicon atoms at high temperature, the silicon atoms also leave the first underlying SiC layer as well. However, this underlying layer, which is commonly referred to as the buffer layer, is strongly attached to the SiC substrate. Studies have shown that this layer is a carbon rich reconstruction of the SiC surface and is electrically inert [84]. What is critical about this buffer layer is that it is partially, but strongly, covalently bonded to the substrate. And the EG layer is weakly covalently bonded to this buffer layer. The EG 2D Raman peak is shifted, indicating the film is stressed [85].

In the process of intercalation, hydrogen atoms at high temperature are used to passivate the covalent bonds between the buffer layer and the SiC substrate. This allows the buffer layer to be released as illustrated in figure 2.13. Our studies indicated that this buffer layer is effectively just another layer of graphene after being released. Numerous groups have found the same result [86][87][88][89].

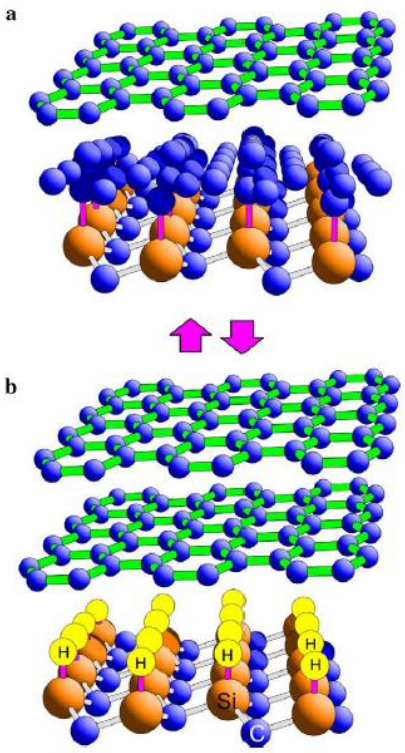

Figure 2.13:Intercalation releasing the buffer layer forming bilayers (Adopted from [89])

There are other forms of intercalation using different gas species [90][91][92] that will not be touched upon in this dissertation.

For our process specifically, we grow monolayers of graphene using the optimized growth method explained in the previous section, and then we intercalate only when we want to release the buffer layer in order to create bilayers. This is done by flowing hydrogen at a temperature of 1050 ^{o}C in a separate multi-purpose cold wall CVD furnace. We found this method to be the most reliable and accurate method of obtaining high quality bilayers.

CHAPTER 3

EPITAXIAL GRAPHENE TRANSFER

In this chapter, an overview of transfer methods for graphene is presented and more detail is given for the specific case of EG transfer and what is reported in literature. The various transfer methods that we have attempted will be detailed before moving on to the successful method of using gold as an adhesion layer. The transfer of Monolayer Transferred Epitaxial Graphene (MTEG) and Bilayer Transferred Epitaxial Graphene (BTEG) will be presented in the results of this section. This is among the first successful transfer of high quality atmospheric growth EG reported in literature. The chapter will explain challenges faced for transferring EG and will also conclude with a section on a study of adhesion energies that can be inferred from our experiments which sometimes agreed and others contradicted adhesion energies reported in literature.

3.1 Overview of Transfer Methods for 2D Materials

Transfer methods, being a pivotal part in the success story of 2D materials, understandably had a lot of deep and technical research devoted towards them. Indeed it is very easy to argue that the unprecedented rapid research development of graphene in its very early stages, is due to the success of the scotch tape transfer method pioneered by Geim and Novoselov [6]. Such inexpensive and technically straightforward transfer method allowed researchers all over the globe to rapidly access this field of research. Eleven years onward and the scotch tape method is still relevant and popular in use. In initial investigations we often isolated monolayer exfoliated graphene in the tens of micron size as shown in figure 3.1 but it was

challenging to obtain such sizes.

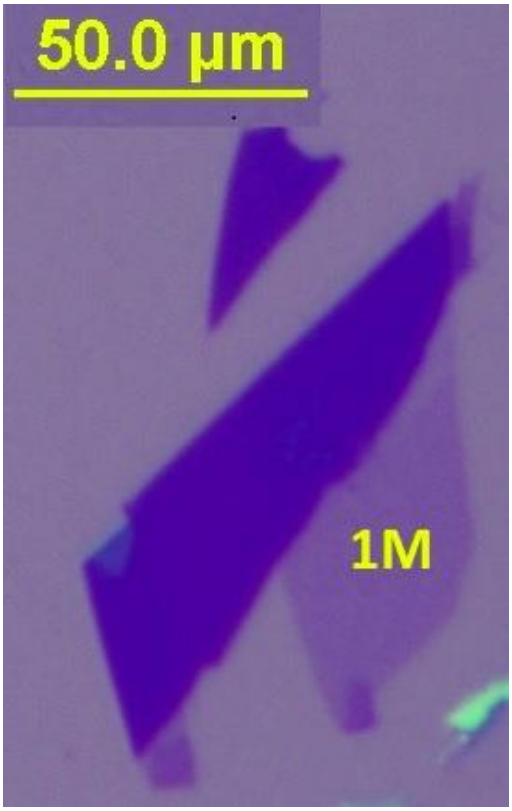

Figure 3.1: Exfoliated monolayer graphene we isolate.

Another very popular method of transfer is using Poly(methyl methacrylate) (PMMA) as a supporting substrate while etching off the original substrate. This method was made popular because it is among the best ways of transferring CVD graphene grown on copper where the copper is dissolved in etchants. Other transfer methods worthy of mention is, Polydimethylsiloxane (PDMS) stamps [93], the use of release material that is claimed to leave very clean surfaces [62], and more sophisticated layered transfers [94][95][96]. All continue to push the boundaries of clean, and damage free transfers. Unfortunately none of these transfer methods are applicable to SiC EG. The partial covalent bonding of this type of graphene to the SiC substrate as previously explained in section 2.5 makes it adhere more strongly and therefore, trying to transfer it off

directly using scotch tape or other prevalent methods will either damage it severely or will fail altogether to cleave it off the substrate. Methods utilizing the etching of substrate to release graphene are a challenge in the case of SiC. SiC is a very difficult material to etch. Groups have successfully etched SiC using photoelectrochemical methods [97] but to the knowledge of the author, none have succeeded in demonstrating monolayers conclusively.

3.2 Literature on Epitaxial Graphene Transfer

The very first exfoliated graphene isolated by Geim and Novoselov, were of very high quality. As a matter of fact, they are still the standard of high quality graphene today by which all other synthesis methods are measured against. This makes the transfer literature of that form of graphene synthesis clear and straightforward. Unfortunately, this is not the case with SiC EG transfer. The quality of the graphene that is epitaxial grown varies a lot in literature, and the transfer method and success vary accordingly. The most striking variation one must carefully observe is the morphology of the starting EG. As discussed in the previous chapter, it was not until the work of [72][73] in growing at atmospheric argon, did the quality of EG become uniform all throughout the wafer. Yet groups have published on the transfer of EG before then.

The method of choice for transferring EG is to use a metal as an adhesion layer to EG before mechanically exfoliating it off the SiC substrate. The preceding carbon nanotube community was using metals (often gold) to transfer nanotubes [98][99] as illustrated in figure 3.2 so this is a continuation of previous methods.

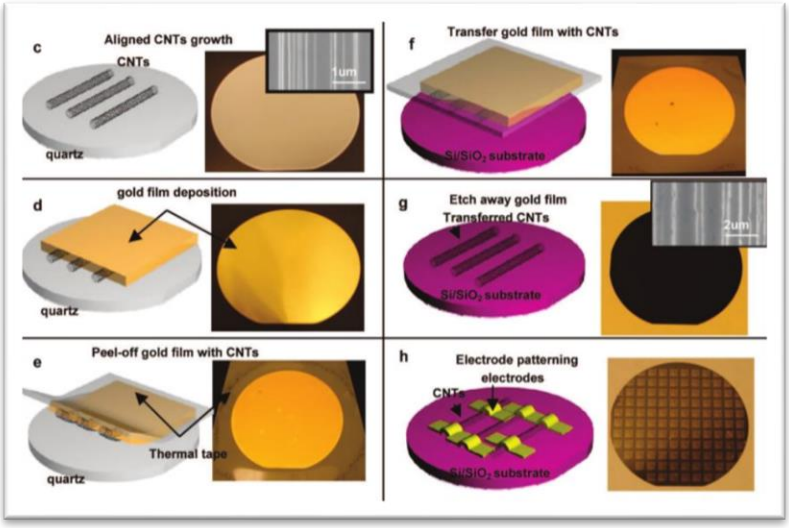

Figure 3.2: Early carbon nanotube research relying on gold adhesion layers for transfer and alignment (Adopted from [98])

Earlier reports on transferred EG [100][101][102][103] were done using high vacuum annealed samples. EG formed by high vacuum annealing is known to be flaky with non-uniform growth throughout the sample. This makes the actual transfer easier because you are transferring parts, rather than all, of the graphene layer and the number of graphene layers is not tightly controlled. So, transferring such graphene is somewhat akin to transferring graphene off graphite. Graphene adhesion energy tends to be weaker when the surface morphology, or number of layers is non-uniform [104]. Also, the final transferred graphene tends to be of inferior quality. This is reflected in low mobilities often reported as well as the Raman peaks which show low 2D/G ratios and wide 2D peaks. These are all indications of lower quality graphene as will be details in the next two chapters.

3.3 Attempts in Transferring High Quality Epitaxial Graphene

The first method attempted in transferring EG was the simple PMMA spin and then the peel off of PMMA using sharp tweezers as illustrated in figure 3.3. This method was unsuccessful.

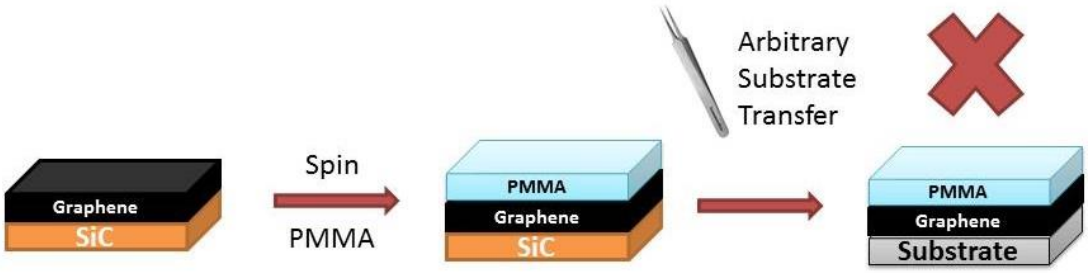

Figure 3.3: Schematic of PMMA transfer method that ultimately proved unsuccessful in transferring EG.

Due to the partial covalent bonding between EG and the SiC substrate, the PMMA adhesion energy was not enough to transfer SiC EG. We also attempted to use sophisticated PMMA transfer aiding methods such as the bubbling technique that was developed with our collaborators and detailed in [105] but success was very limited. EG bonding to substrate was clearly strong.

Our first successful attempt in transferring SiC EG relied on using gold as an adhesion layer to the graphene and then spinning PMMA on top of the gold to mechanically transfer the Au/Graphene layer using a sharp tweezer as illustrated in figure 3.4.

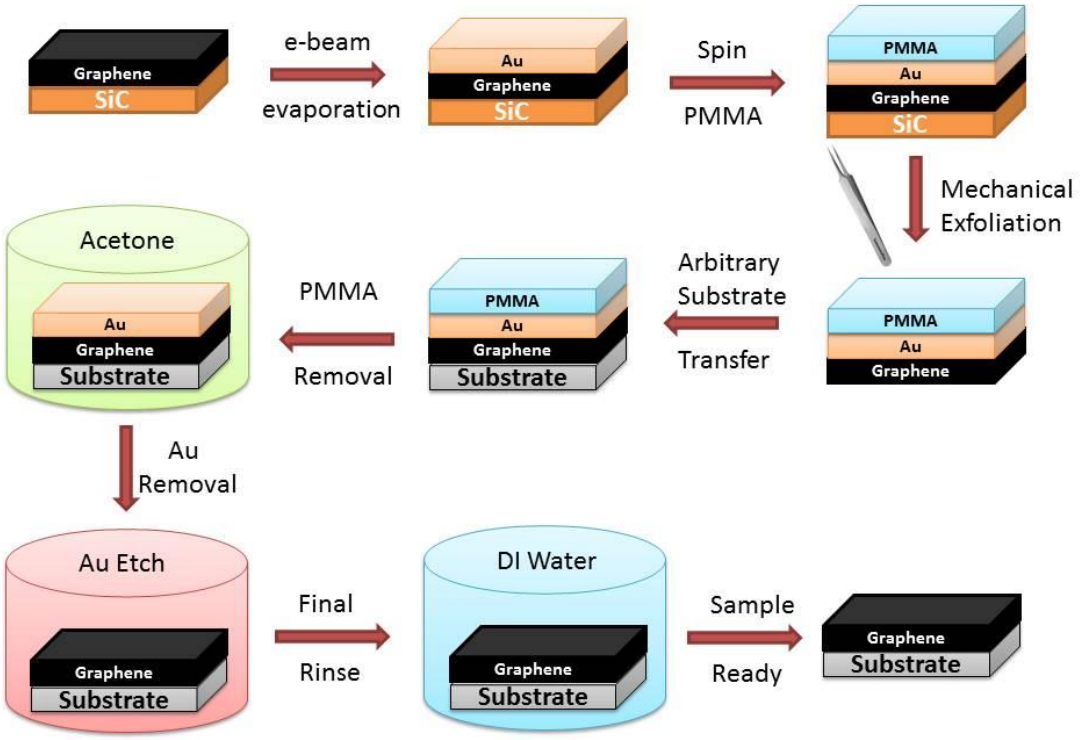

Figure 3.4: Illustration of the Au/PMMA transfer method.

Both our group [105] and [106] independently reported the successful transfer of monolayer EG off high quality SiC sublimation back around the end of 2013. Our work did crucially show suspended monolayer EG prepared for TEM studies and we were the first to show this.

The Au/PMMA method was initially a successful method for transferring EG but this method was marred with difficulties. For one, we had to peel off the Au/PMMA using a sharp tweezer and we could never get large areas using this method. And even after successful transfer of the often small areas, no larger than a few hundred microns, we lost even more of it in dissolving the PMMA in acetone and subsequent gold etch. Furthermore, Raman analysis often showed shoulders on the G peak which were not investigated further as to what was causing them since this method was dropped in

favor of the Au/PVA method illustrated in the next section. Device fabrication was challenging as well because the films were often very small allowing for a limited number of devices to be fabricated. They were also often discontinues and making a working device with multiple connections proved challenging.

3.5 The Au/PVA Transfer Method

Throughout this investigation it was found that depositing gold as an adhesion layer to EG and then using Poly(vinyl alcohol) (PVA) tape for mechanical exfoliation, yielded the most success. The illustration of this method is shown in figure 3.5.

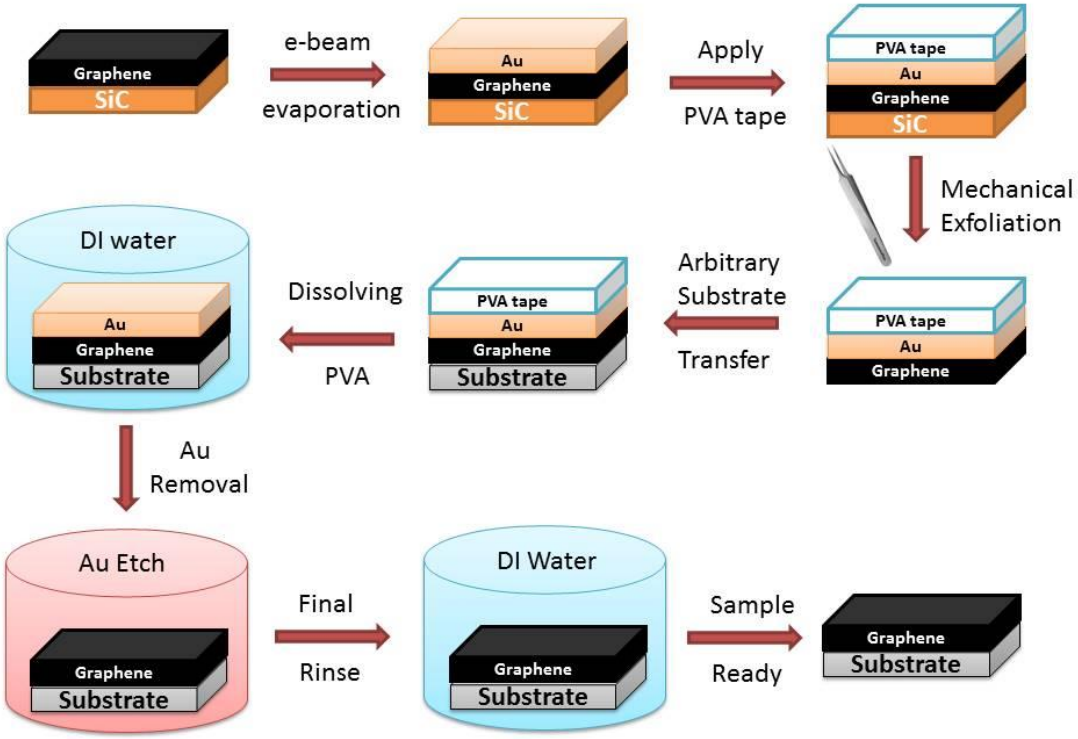

Figure 3.5: Illustration of the Au/PVA transfer method.

For one thing, as will be shown in the next section, the Raman showed very clean and ideal peaks for the transferred graphene. Microscope inspection showed little residue

if proper cleaning procedure is followed. Furthermore, the strongest advantage to using this method is that it allowed the complete transfer of all graphene regardless of substrate size. In our investigation, it was typical to transfer 6000 X 6000 *micron* films as shown in figure 3.6. And there was no limitation to transferring 12000 X 12000 *micron* films or lager if we intended to. The microscope images, such as figure 3.7 would often show hundreds of microns of continues monolayer films.

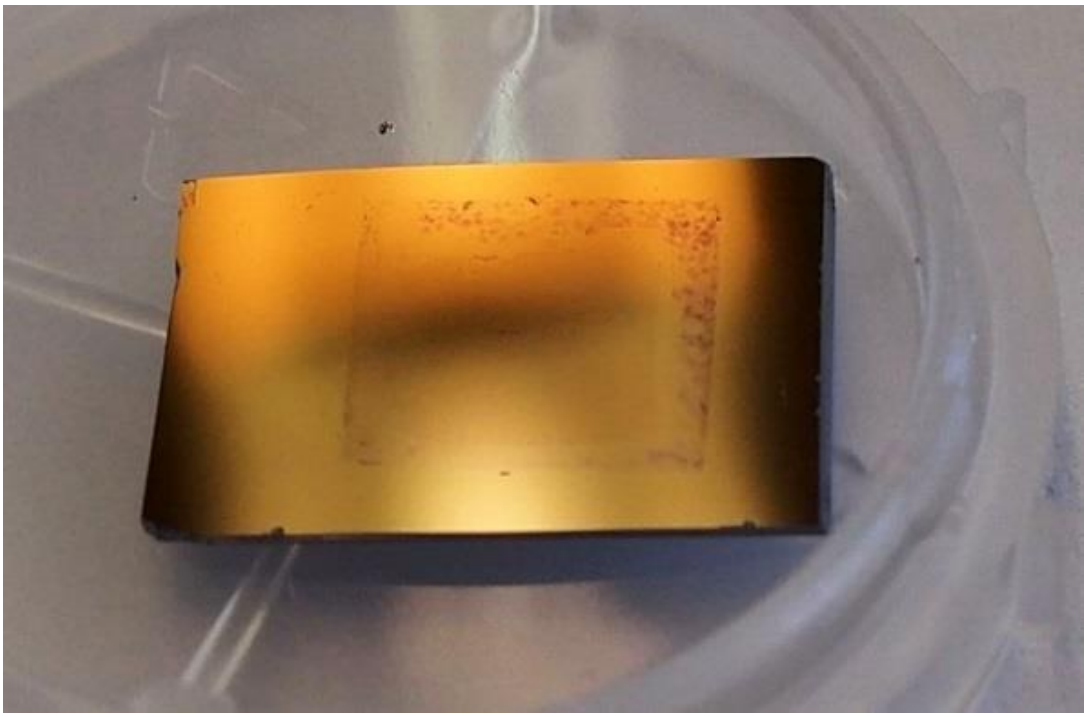

Figure 3.6: 6 X 6 mm MTEG on SiO_2/Si substrate.

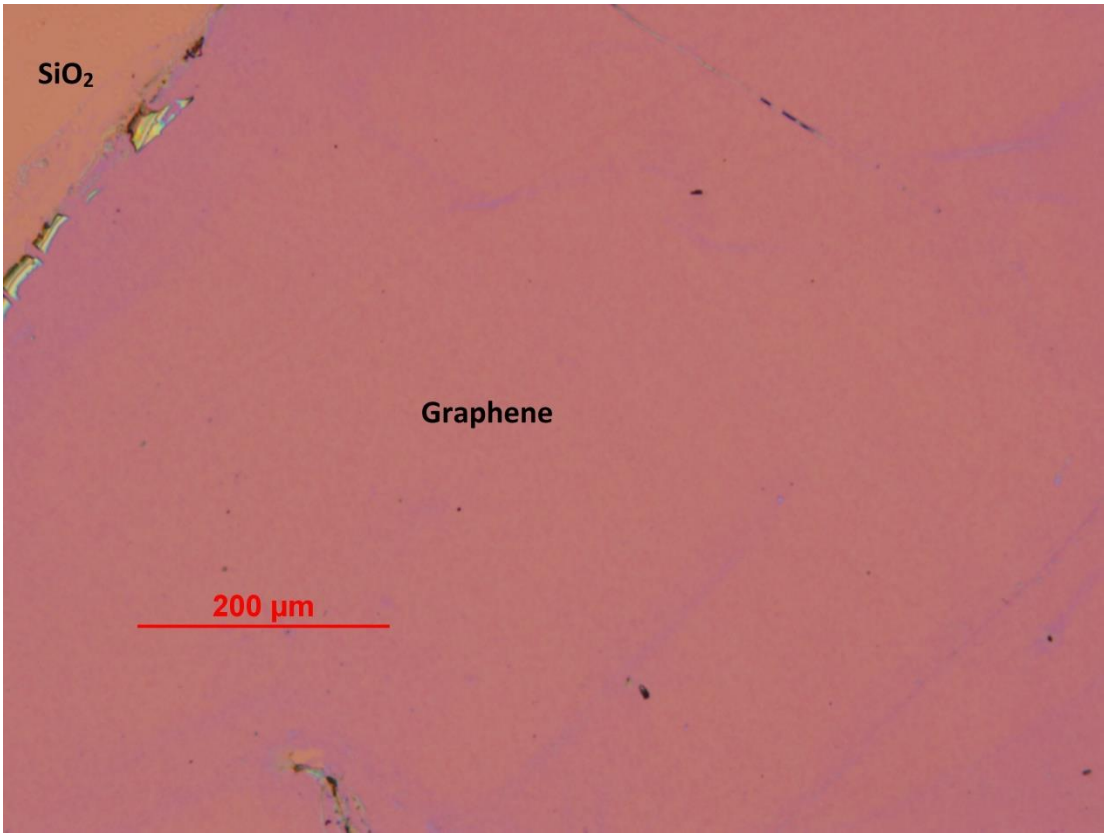

Figure 3.7: Microscope image of MTEG showing large areas in the hundreds of microns range.

There were, and indeed still are, challenges to this method. For one, earlier on, PVA residue was significant. This was solved by prolonged DI water rinsing. Another problem faced during this research which was very surprising, is that usually placing the PVA tape in DI water for the dissolving step, went on smoothly with no trouble. But when we switched to using wafers from a different supplier, the films suddenly started to completely delaminate during the PVA dissolving step. Numerous experiments went into trying to fix this problem and it somehow seems that the adhesion varies from one substrate to anther significantly as shown in figure 3.8. It varies in a way that is difficult to predict.

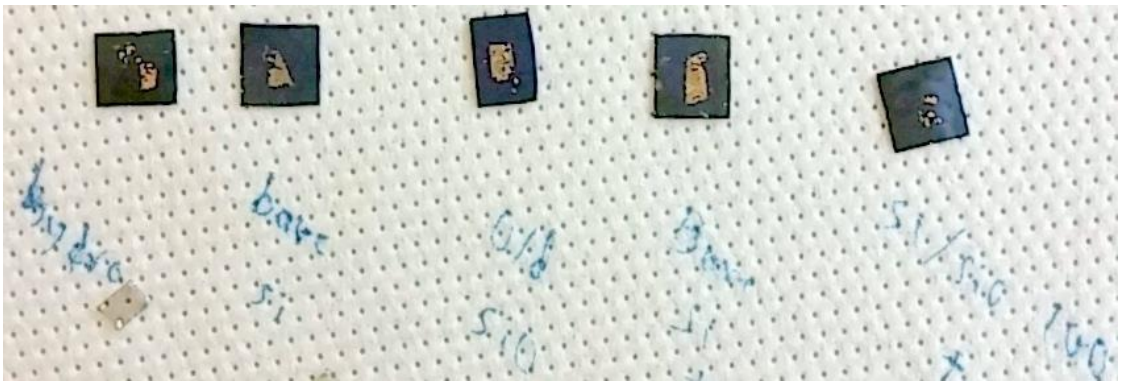

Figure 3.8: Image depicting the adhesion problem faced in transferring the PVA/Au/Graphene stack to various substrates. In the image, it is shown how the transferred stack is lost during dissolving PVA in DI water. This varies by substrate. This problem was resolved later on using a modification to the transfer procedure.

Eventually this problem was solved by using a slightly wet cotton swab to wet the PVA tape, and then very slowly peel off the PVA tape as opposed to leaving the PVA in DI water allowing the chance for it to delaminate. It was still challenging to succeed even using this method. But after using this method, it was possible to transfer to any substrate type and hence no further investigation was carried out as to why there was such a large disparity in the adhesion of the transferred stack based on substrate.

The final challenge, which has still not been overcome, is the fact that the films can break up during the transfer probably due to the mechanical nature of it. Figure 3.9 shows how bad the films can crack.

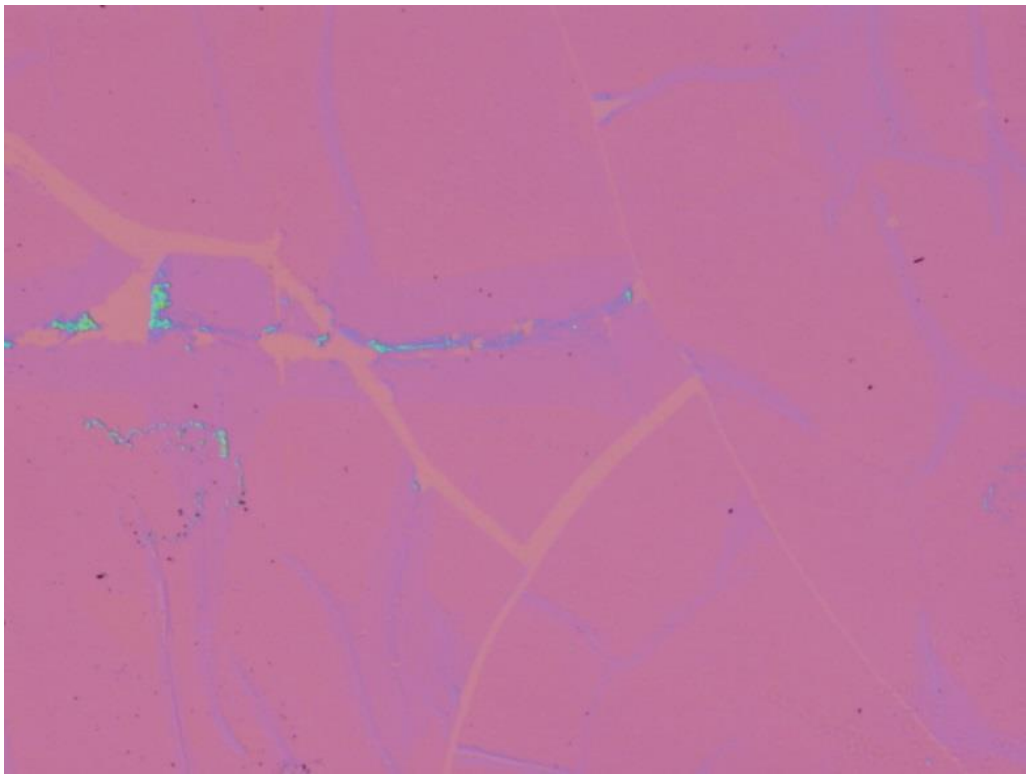

Figure 3.9: Microscope image of MTEG showing the cracked film problem.

Parallel investigations were carried out in the hope that using PDMS stamps would solve this problem. However the repeatability of PDMS stamp method was limited and due to the difficulty and cost of obtaining EG samples, this method was not investigated further. A final note about the cracks in films is that it is not clear if the cracks are due to the transfer method or due to the growth conditions not being optimized, or indeed even a combination of both. Certainly there are evidence, that both contribute to this problem.

To summarize the detailed step by step Au/PVA transfer method, we first evaporate a 100 *nm* gold film using an e-beam evaporator. We then use PVA tape along with tweezers to mechanically exfoliate and place the stack on any substrate of choice. A damped cotton swab is used to slowly wet the PVA tape while mechanically peeling it

off slowly. The sample is left in running DI water for about 10 minutes to clean the PVA residue. Potassium Iodide and Iodine Complex, which is a standard chemical, is used to etch the gold adhesion layer. The sample is left in the gold etchant for at least 20 minutes. The gold etch does not leave any residue, nor does it attack the graphene. Samples were left for hours sometimes with no graphene damage or characteristic difference. The sample is taken out and rinsed with DI water for about 10 minutes to get rid of any contaminating residues. The sample is then ready for characterization or further processing for device fabrication.

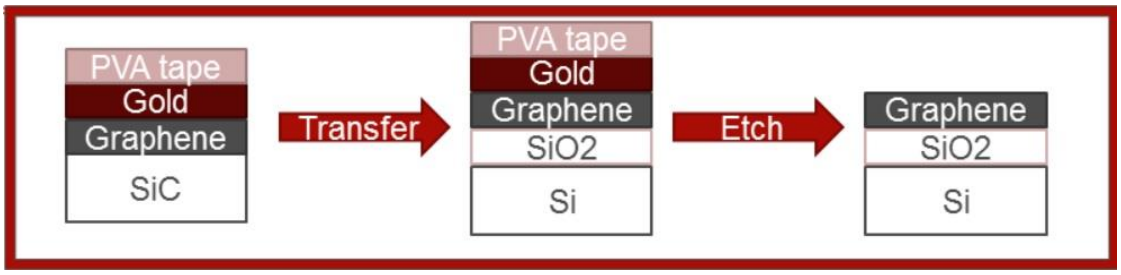

Figure 3.10: Schematic overview of PVA/Au transfer method.

3.6 Adhesion Energy

The extensive work done on testing the transfer of EG gained us significant insight on the adhesion energies of various materials we tested. During the course of this investigation we tried PMMA, as well as a host of metals that included Cr, Al, Pd, Au, and Ni. We eventually did settle on using Au as the adhesion layer because all other materials tested either, did not adhere strongly to EG, and hence fail to transfer it, or further processing caused significant or complete loss of the graphene film. Further detail per each specific adhesion layer is given in table 3.1. This section will summarize our findings on using these materials and what we can infer from comparing against adhesion energy values obtained from literature.

Neil et al. [107] reported that the adhesion energy of EG to the SiC substrate is $3.0 \pm^{1.6}_{1.0}$ J/m^2. Assuming PMMA has a similar adhesion energy to PDMS which is measured for few layer graphene to be 0.176 J/m^2 [108], this would explain why PMMA, will not transfer EG off SiC. We have confirmed the failure of PMMA to transfer EG experimentally. This result is true even when elaborate methods such as the bubbling technique [105] was used.

The repeated and reliable success of transferring monolayer EG off SiC using gold as the adhesion layer raises very interesting points about the adhesion energy of Graphene/Au. To the knowledge of the author, the only paper that talks about the adhesion energy of graphene to gold is the simulation work done by Hamada et al. [109]. In that paper, Graphene/Au adhesion is calculated to be around 0.7 J/m^2. This is the paper that was sighted for the work of Kim et al. when they chose nickel over gold as the adhesion layer [106]. But Judging by the fact that we had nearly 100% success transferring monolayers using a gold adhesion layer multiple times and that the monolayers were continues over hundreds of microns, it would seem the 0.7 J/m^2 theorized by [109] is greatly underestimating the Graphene/Au adhesion energy which

at least should be more than the Graphene/SiC adhesion energy of 3.0 $\pm^{1.6}_{1.0}$ J/m^2. We have further successfully used a gold adhesion layer to transfer CVD graphene off copper and did so repeatedly with complete film coverage and 100% yield. Graphene/Cu adhesion is measured to be 0.7 J/m^2 [110]. This is further evidence that Graphene/Au adhesion is higher than the 0.7 J/m^2 value calculated in [109].

The successful transfer of bilayer graphene synthesized by hydrogen intercalation gives very good insight as well. Graphene/Graphene adhesion energy is low at 0.3 J/m^2 [111]. Since for transfer, the bilayers must remain intact, it is safe to assume that after intercalation, the adhesion energy of graphene to the SiC substrate must be less than the 0.3 J/m^2 value between the two graphene layers.

Adhesion energies were reported for Graphene/Cu 12.75 J/m^2 Graphene/Nickle 72.7 J/m^2 in [112]. However these values are very high and do not seem to hold true experimentally in our work.

In all the above statements and conclusions we assume no surface roughness effects on adhesion energy [104]. This is a valid assumption, knowing that the step edges in SiC are about 10 *nm* high and the gold deposition on top of graphene is done using e-beam evaporation which is a very uniform film deposition.

TABLE 3.1 Adhesion Energy and Experimental Notes

	Adhesion Energy J/m^2	Reference	Experimental Notes
Graphene/Graphene	**0.3**	[111]	Intercalated bilayers did not separate during transfer indicating EG layers show similar adhesion pattern to exfoliated graphene layers.
Graphene/SiC	**$3.0 \pm^{1.6}_{1.0}$**	[107]	Non-metal based adhesion layers tested were too weak to transfer EG confirming strong adhesion energy of EG to SiC.
Graphene/SiC Intercalated	**<0.3**	**--**	Intercalated bilayer transfer did not separate the layers indicating the adhesion energy to SiC after intercalation must be lower than 0.3 J/m^2 which is the adhesion energy of two graphene layers.
Graphene/PDMS (close to PMMA)	**0.176**	[113]	Failed to transfer EG. Adhesion energy too low.
Graphene/Copper	**0.7**	[110]	Au was experimentally used as an adhesion layer to transfer graphene off Cu substrate indicating that graphene adheres to Au stronger than Cu.
Graphene/Gold (likely incorrect)	**0.7**	[109]	Au used as an adhesion layer successfully and repeatedly transferred EG off SiC substrate indicating the adhesion energy is at least higher than 3 J/m^2 contrary to current literature.
Graphene/Ni	**3.5**	[114]	Ni films often caused high stress that would crack the films and fail to transfer. Optimizing Ni thickness was not pursued since Au was successful. Also, transferred films that did not crack would delaminate in the Ni wet etch step and sample would be lost.
Graphene/Al	**$< 3.0 \pm^{1.6}_{1.0}$**	**--**	Failed to transfer EG, indicating that the adhesion energy of Al must be less than 3 J/m^2.
Graphene/Pd	**--**	**--**	Pd was difficult to clean off in etching step

CHAPTER 4

TRANSFERRED EPITAXIAL GRAPHENE STRUCTURAL CHARACTERIZATION

In this chapter, detailed structural analysis is presented on TEG using optical microscopy, Raman, and TEM. Miscopy shows the difference in contrast between monolayers and bilayers, while Raman shows all the characteristic peaks that are sharply defining monolayers and bilayers as well as the uniformity of the films. TEM show a direct image of monolayers and bilayers along with other more sophisticated characterizations that will be detailed.

The structural characterization confirms the transfer of high quality MTEG and evidence of AB stacked BTEG.

4.1 Optical Characterization

Optical characterization was made possible by transferring EG. Although a monolayer of graphene only absorbs about 2.3% of light, it is still visible under a microscope if a proper substrate is used to enhance its contrast. This is certainly another one of the crucial reasons why the original Geim and Novoselov research work was successful in identifying a monolayer of graphene. This was even formally investigated in a paper titled "Making Graphene Visible" [115], where it is shown that if graphene is placed on a SiO_2/Si substrate with a thickness of either 90 *nm* or 285 *nm*, peak contrast is achieved through interference effects with the substrate. However, in the case of SiC, it is a transparent substrate so graphene on top of it is not visible at all because there is

no interference effect enhancing its contrast. Due to this reason, an optical microscope is of limited use in the case of EG on SiC. An illustration of this effect is shown in figure 4.1. This is a simplified illustration as the actual effect is more complex.

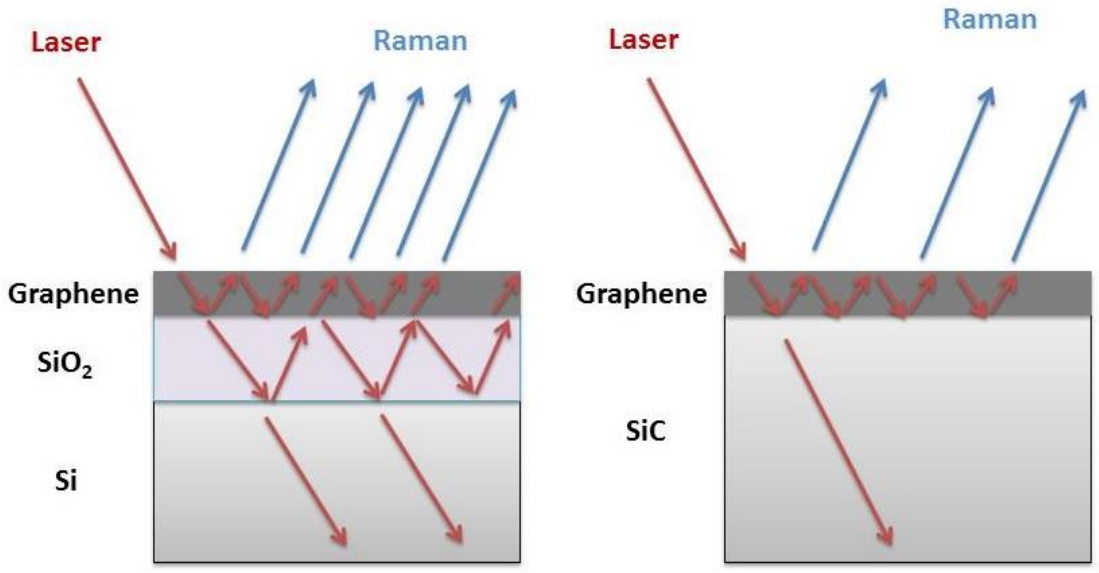

Figure 4.1: Illustration of the interference effect of thickness optimized SiO_2 substrates as opposed to SiC substrate

The first sign of successful EG transfer that we observed is the very clear visibility of a monolayer and a bilayer once transferred off SiC and on to a SiO_2/Si substrate with optimized SiO_2 thickness. As a matter of fact, the visibility and contrast were so great; you can even distinguish monolayers from bilayers by naked eye let alone visibly see the graphene on the substrate. Figure 4.2 shows a monolayer on the top substrate and a bilayer on the bottom substrate. The contrast is not true to real life due to limitation of the photo-image taken. In real life, the contrast is strongly visible.

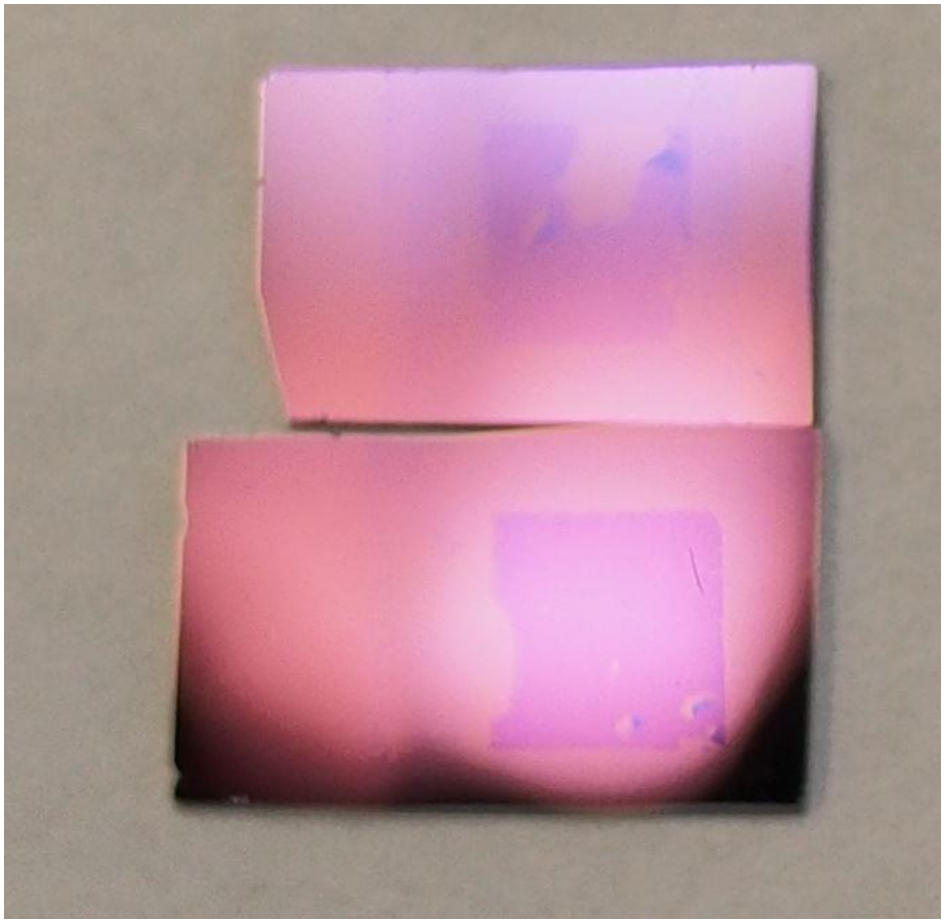

Figure 4.2: 6 X 6 mm MTEG (top) visible contrast distinguishable from BTEG (bottom) by naked eye.

Being able to see the monolayers and bilayers helped significantly in the fabrication steps as well. As mentioned in the previous sections, cracks in the graphene film due to either transfer or misgrowth can be crucial in fabricating successful devices and being able to visibly see your marked graphene greatly enhanced the chances of successful device fabrication.

4.2 Raman Characterization

Raman was the next characterization technique to have greatly benefited from transferring EG. For one thing, the substrate Raman background no longer overlaps with the crucial signifying peaks of graphene, allowing a better study of the D and G peaks where they are very clear and no background subtraction is necessary which often obscured results. The other very significant contribution of transferring EG, is that the Raman benefits from the interference effect much the same way as in the case of microscopy. The Raman signal counts are greatly enhanced when the EG is transferred onto a SiO_2/Si substrate with optimized SiO_2 thickness as can clearly be seen in figure 4.5. This leads to significantly enhanced peaks that allowed for careful 2D/G peak ratio, and FWHM measurements. And this intern was a crucial step in conclusively identifying monolayers from bilayers which is otherwise an approximate procedure using Raman alone and without transfer.

For MTEG Raman (figure 4.5) we found the 2D peak to be positioned around 2700 cm^{-1}. This would indicate a release of strain as the original 2D peak, when the graphene is on SiC, is either blue shifted or red shifted which varied by location on the SiC substrate. Also, the position of the 2D peak is consistent in being at 2700 cm^{-1}. This positional consistency is not the case before transfer as we observed and others reported [85]. The FWHM was at about 30 cm^{-1}, the D peak was a sharp Lorentzian and the 2D/G peak was consistently over 2, the G/D peak was often over 20. All indications of not only conclusive monolayers, but comparatively high quality TEG so far as Raman characterization is able to indicate.

Bilayer graphene is more technical in Raman characterization. For exfoliated AB stacked bilayer graphene, the 2D peak exhibit very rich characteristics. As a matter of fact the 2D peak is the most important peak in graphene characterization in general as it clearly evolves with the number of layers [78]. Our concern is with bilayers though

and for bilayers the 2D peak is actually composed of the summation of four separate Lorentzian peaks. Earlier in this research, the 2D Raman peak of exfoliated graphene bilayers were fitted to the summation of four Gaussian peaks using MATLAB to verify the distinctive 2D peak of exfoliated bilayer graphene as shown in figure 4.3. Gaussians were used as an approximation to make the analysis easier.

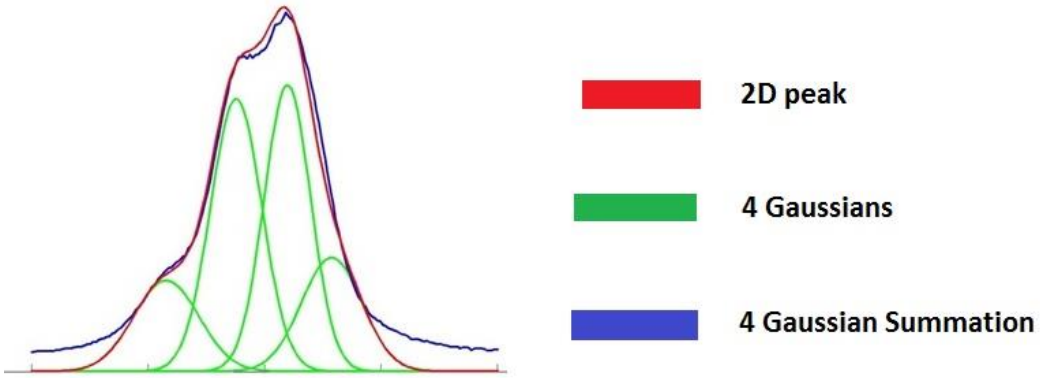

Figure 4.3: 2D peak of exfoliated bilayer graphene verified by fitting the summation of four Gaussians uisng MATLAB.

Ferrari et al. in his original work on Raman characterization of graphene [79], presents the best explanation of this characteristic 2D peak. He attributes it to the selectivity of photon emission based on the band structure of graphene. And this selectivity will give four possibilities and hence the four peaks as shown in figure 4.4.

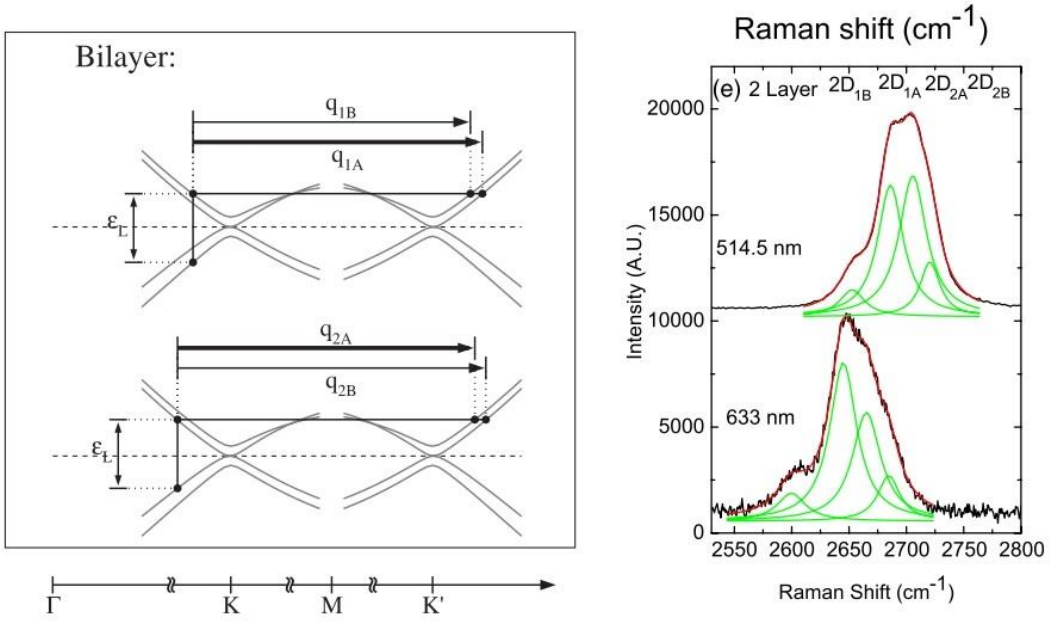

Figure 4.4: Original Ferrari et al. work explaining bilayer 2D peak using energy band transitions (Adopted from [79])

In the case of the Raman of the BTEG (figure 4.5), the 2D/G ratio is usually in the 0.85 range, and the 2D peak FWHM is around 60 cm^{-1}. These values are in agreement with literature so far as bilayer graphene goes. The major anomaly is the 2D peak not exhibiting the characteristic four peak components of exfoliated AB stacked bilayer graphene. This anomaly is also found in CVD bilayer graphene that is said to be AB stacked [116]. It would seem that only exfoliated graphene shows the ideal 2D peak. We still do believe the bilayers are AB stacked in our case as further evidence of this will be presented in the TEM section. We believe the 2D peak not exhibiting the expected characteristics is due to it being very sensitive towards imperfections in the band structure of bilayer graphene. Dislocations are known to cause very wide k value energy bands and they might play a role large enough to obscure the 2D peak's dependence on band structure.

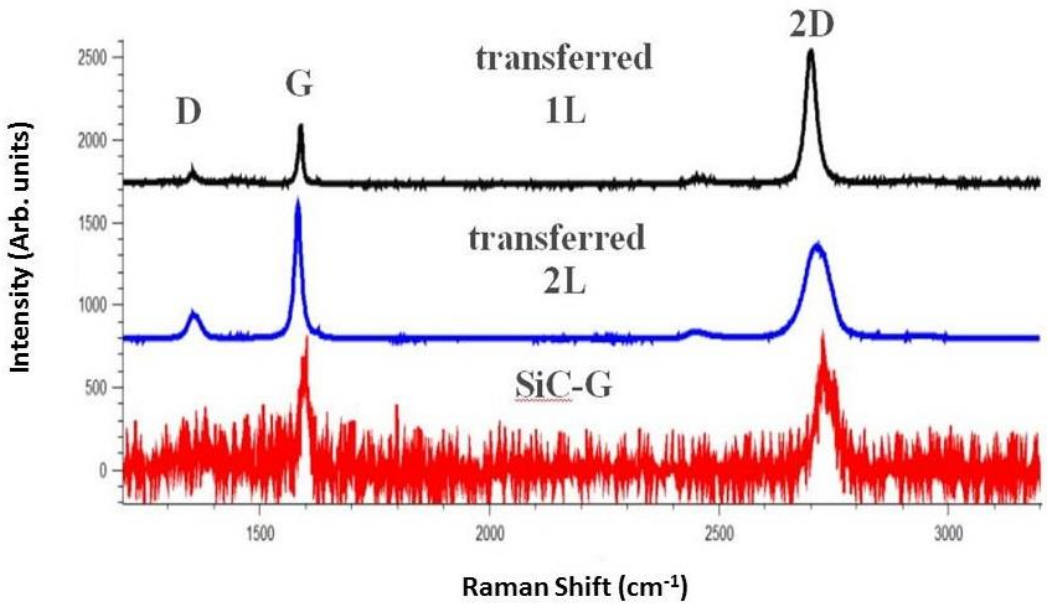

Figure 4.5: Raman of EG on SiC before transfer (Red), Raman of MTEG (black), and Raman of BTEG (blue)

On the topic of bilayer graphene, it was possible to sometimes observe bilayers formed by having MTEG that tear apart during transfer and fold back. These are clearly visible under a microscope. They provided a clear reference to rotated TEG bilayers. The Raman characteristics of these folded bilayers are surprisingly similar to monolayers and very different from AB stacked bilayer graphene as shown in figure 4.6.

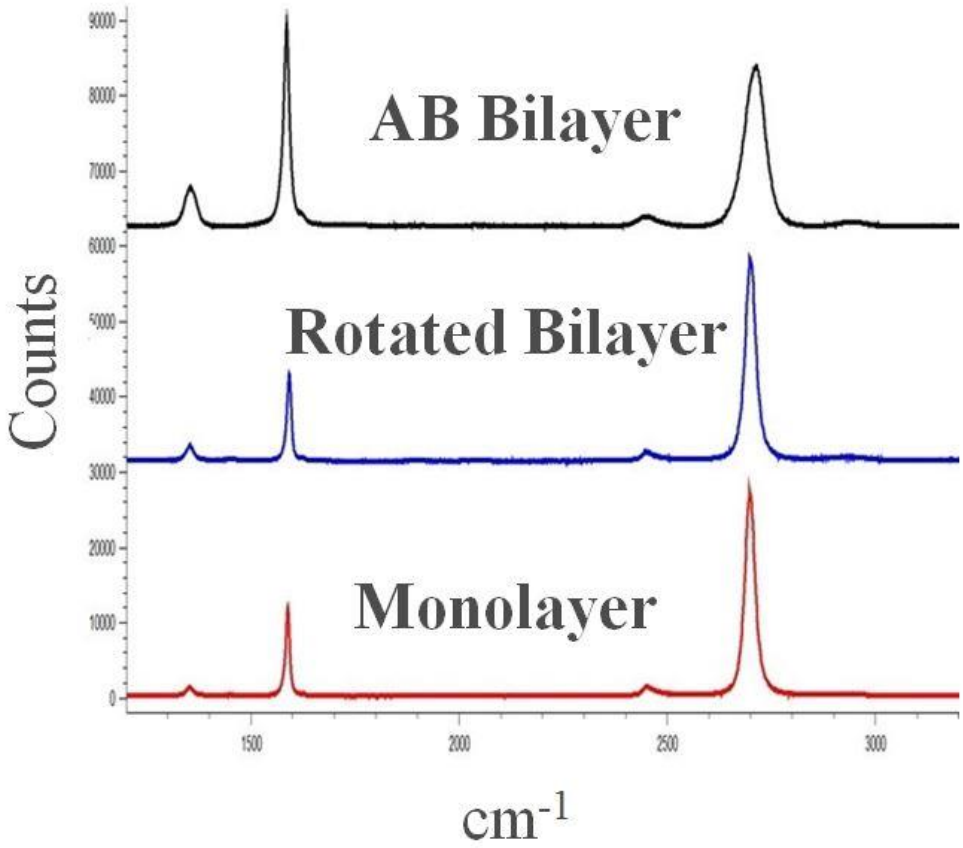

Figure 4.6: Raman of TEG: AB stacked bilayer (black), random oriented bilayer (blue), and monolayer (red)

This seems counter intuitive, but other research groups have shown the same result [117][118]. The 2D peak actually evolves as the two layers are rotated as shown in [118]. This was further indication that the BTEG we obtain by growth and intercalation rather than folded MTEG, are at the very least of very little rotation no greater than 3^{o} if any rotation at all. Else the Raman 2D peak would have resembled rotated bilayers.

To emphasize the uniformity of the AB stacking of BTEG, a two dimensional Raman map was done on an arbitrary area of 150 X 150 *microns*. The Raman laser would raster across the area in steps of 3 microns and record the Raman spectrum per each spot. The 2D peaks are the same all throughout, indicating no rotation. The 2D peak

intensity of the raster is overlaid on top of the BTEG area shown in figure 40.

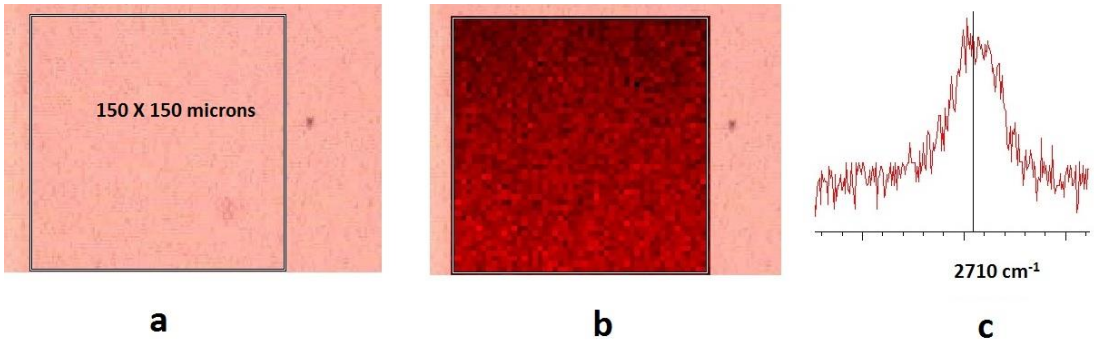

Figure 4.7: Two dimensional Raman mapping of BTEG over 150 X 150 *micron* area indicating AB stacking uniformity. a. 150 X 150 micron square area BTEG. b. Raman 2D peak intensity overlay. c. Typical 2D Raman peak.

This section is concluded by mentioning that CVD graphene was also used as a reference point for MTEG. The CVD graphene was transferred using the same exact method as MTEG. The Raman characteristics which are shown in figure 4.8 are of 2D peaks located at 2700 cm^{-1} with a 2D/G ratio of 2.8, a FWHM of 33.5 cm^{-1} and a G/D peak around 20, all indicating very close values to MTEG. We did not attempt to transfer CVD bilayers as they are more difficult to obtain and stacking order would be an issue.

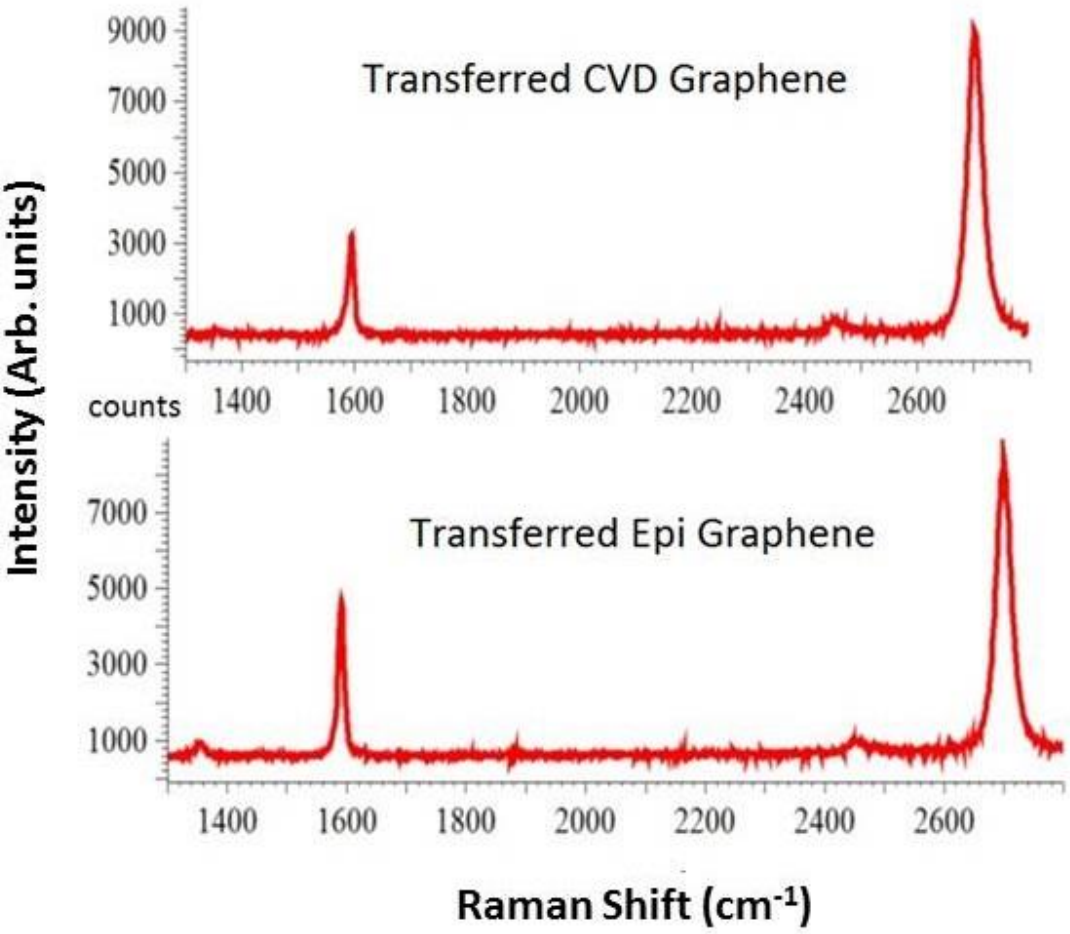

Figure 4.8: Raman of transferred monolayer CVD graphene (top), and MTEG (bottom)

TABLE 4.1 Raman Characteristics of Graphene Layers.

Raman Table	2D/G	FWHM (cm^{-1})	G/D (Approximate)
MTEG	**2.1**	**29.5**	**20**
AB stacked BTEG	**0.85**	**62**	**5**
Rotated BTEG	**2.3**	**31**	**5**
Monolayer CVD graphene	**2.8**	**33**	**20**

4.3 Transmission Electron Microscopy Characterization

Graphene being a monolayer of carbon atoms arranged hexagonally with only 2.46 Å apart puts specific constraints in it being a 2D material. The conclusive observation of a 2D material should be done in a suspended form in order to not have the underlying 3D substrate appear. Transmission Electron Microscopy (TEM) is the tool of choice for this task since it is possible to create magnified images of suspended 2D materials on holy grids showing what is close to individual atoms.

We have collaborated with the Rümmeli group to conduct extensive TEM studies of TEG. During this collaboration we would transfer the EG monolayers and bilayers onto an arbitrary substrate and ship the samples to our collaborators in Germany and then our collaborators in turn would carry out another transfer procedure to take the graphene films off this arbitrary substrate and onto the TEM holy grid. The details of

this procedure were published in [105]. The EG layers survived two mechanical transfers before going into the TEM, a testament to how robust EG can be.

During this collaboration we have successfully obtained TEM images of both suspended monolayer and bilayer graphene. The MTEG show the clear honeycomb structure expected of graphene and the BTEG showed a visible contrast indicating more than one layer as can clearly be seen in figures 4.9 and 4.10. These images were very consistent throughout the different spots taken on the suspended films, further bolstering the claim of very uniform monolayer and bilayer growth respectively.

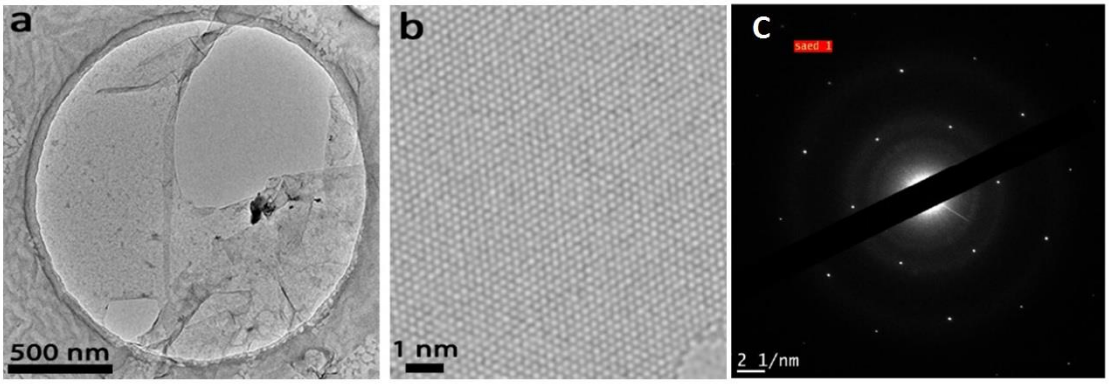

Figure 4.9: a. Holy grid image of suspended MTEG b. TEM image of the honeycomb structure of MTEG c. SAED diffraction pattern of MTEG.

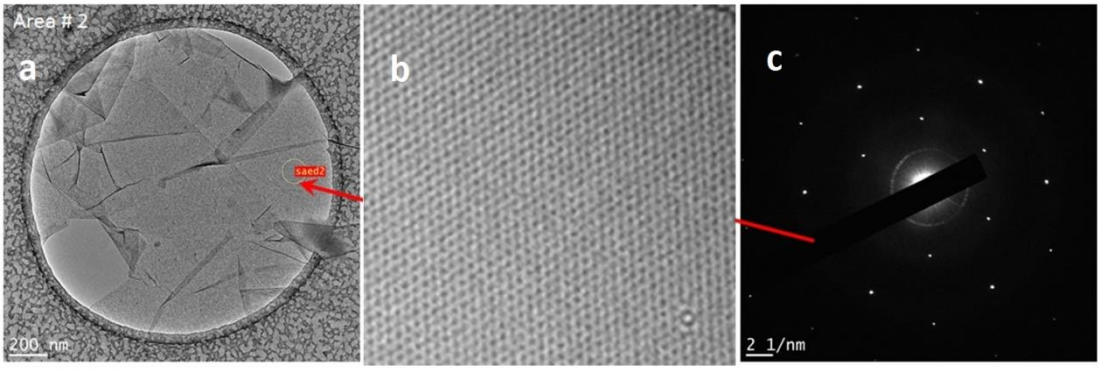

Figure 4.10: a. Holy grid image of suspended BTEG b. TEM image of the honeycomb structure of BTEG c. SAED diffraction pattern of BTEG.

Furthermore, we obtained Scanning Area Electron Diffraction (SAED) images. The MTEG SAED showed only one set of diffraction pattern as expected for monolayer graphene. The BTEG more crucially, also showed only one set of diffraction pattern as shown in figure 4.10 in expected accordance to AB stacking. Also, the intensity plot taken from the SAED image of the BTEG in figure 4.11 showed the very distinctive and unmistakable pattern of AB stacked bilayer graphene reported in literature [119]. This is a very clear and conclusive indication of tight AB stacking for if the bilayers were rotated slightly, there would be two sets of diffraction patterns and also the intensity plots would not show the distinctive pattern of AB stacking.

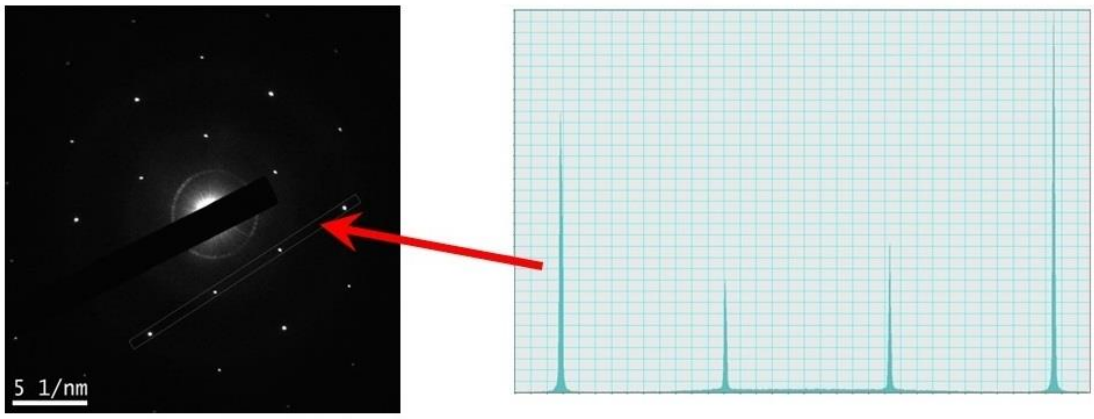

Figure 4.11: Intensity plot obtained from BTEG SAED.

The BTEG is truly an interesting material. When transferred off SiC and onto the TEM holy grid, it would look like aligned bilayers with none of the moiré effect that is usually exhibited in rotated bilayers. Furthermore, it was possible to etch off parts of the first graphene layer using the electron beam of the TEM and reveal the underlying layer. This is shown in figure 4.12. Both graphene layers seemed aligned and further supporting the evidence of AB stacking.

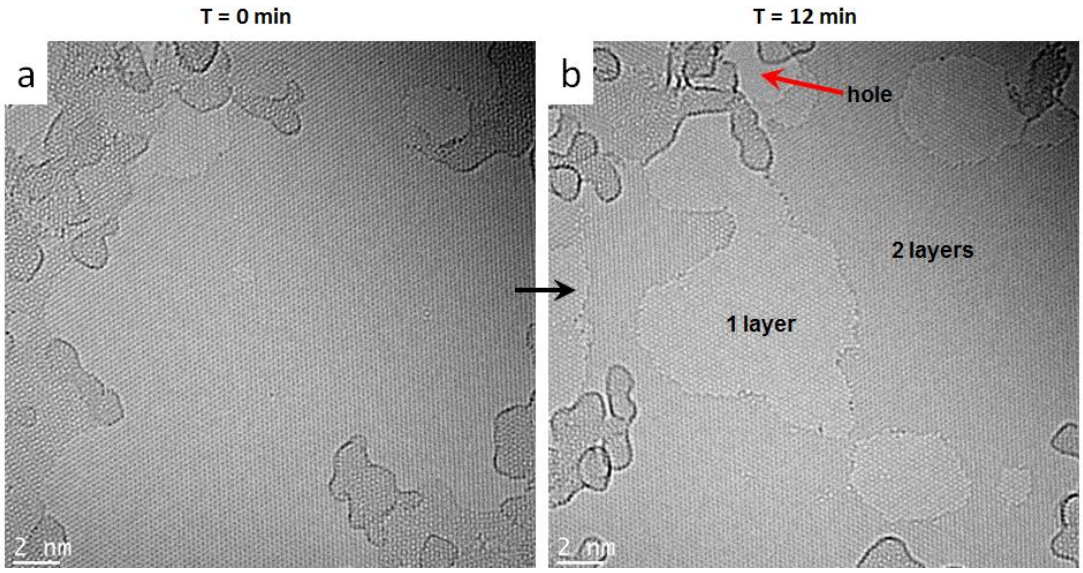

Figure 4.12: a. Initial BTEG. b. Parts of first layer etched off by TEM electron beam 12 minute exposure.

This section is concluded on mentioning the occasional observed rotated BTEG under the TEM. Rotated bilayers have been both theorized and observed to show a moiré effect by multiple sources [120][121][122][123]. This moiré pattern is illustrated in figure 4.13. In the case of using a TEM, folded MTEG that form rotated BTEG were just as observable as they were in microscopy and Raman characterization. These rotated BTEG are formed by MTEG layers that tear and fold back and are not to be confused with the AB stacked BTEG that are formed by intercalation before transfer and that are the main subject of this dissertation.

These rotated BTEG however, allowed us to observe TEM images of the aesthetically beautiful moiré effect of folded graphene using SiC EG as shown in figure 4.1.4. To the knowledge of the author, this has never been demonstrated before in literature using the SiC epitaxial form of graphene.

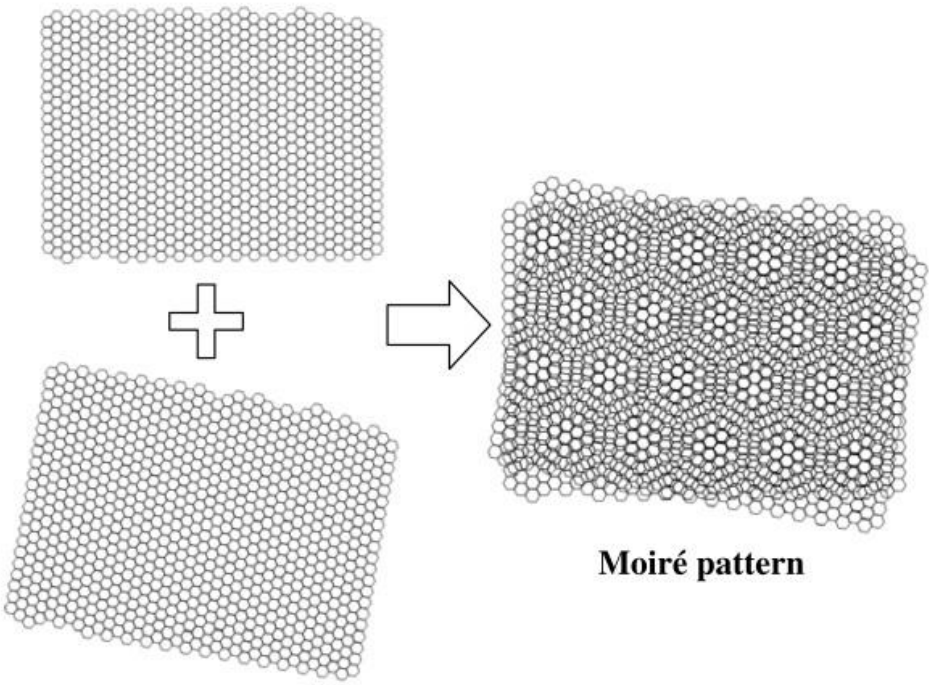

Figure 4.13: Visualization of the moiré pattern arising from combining two graphene monolayers at a 10^{o} angle (Adopted from [120])

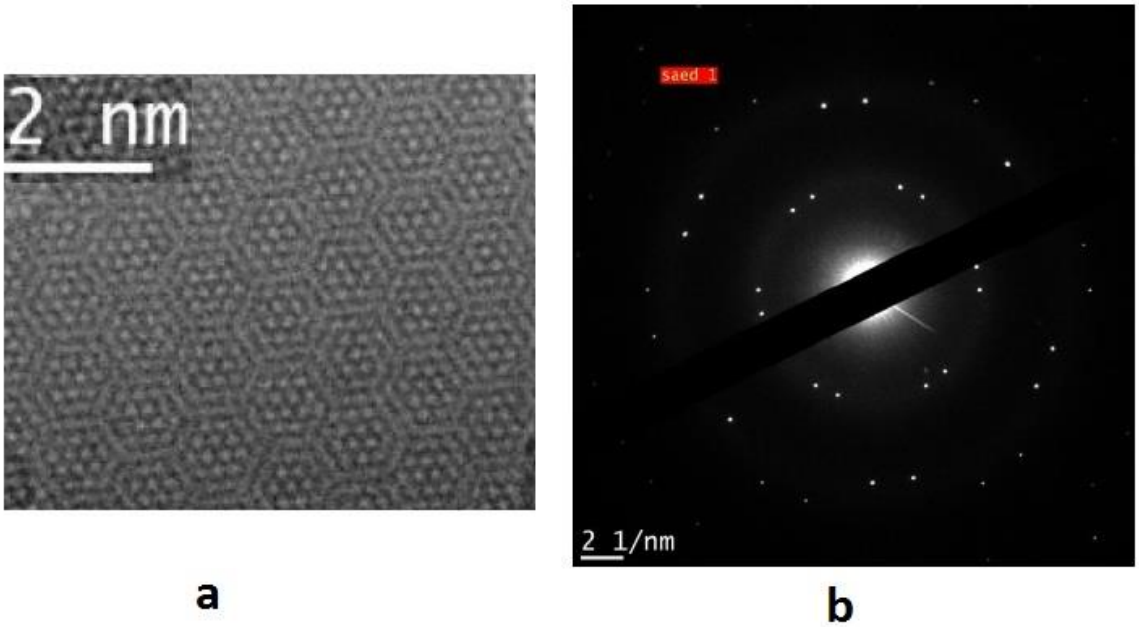

Figure 4.14: TEM image of rotated BTEG from folded MTEG where the moiré pattern is clearly visible. b. SAED diffraction pattern showing two rotated sets.

CHAPTER 5

TRANSFERRED EPITAXIAL GRAPHENE ELECTRICAL CHARACTERIZATION

In this chapter, electrical characterization methods are carried out on TEG using mainly Transmission Line Measurement (TLM) structures and Field Effect Transistor (FET) structures. All measurements were conducted at room temperature. We measure the contact resistance for MTEG and BTEG using common contact resistance methods, which is a first and was never reported elsewhere. The TLM measurements allowed us to gain insight on the difference of mean free path between MTEG and BTEG.

The fabricated FETs are used to show monolayer mobility gains higher than two times once transferred off the SiC substrate as well as significantly lower carrier concentrations. Only one other research group reports such results. Mobilities of BTEG are measured as well which is not reported anywhere else in literature as of the time of this dissertation and is an important contribution considering the potential of this method for large area AB stacked bilayer synthesis. Other details on the electrical properties of TEG will be given such as carrier independent mobility and universal mobility calculations. An annealing section for the MTEG and BTEG FET structures will report unique characteristics that distinguish MTEG from BTEG as well as the unique BTEG moisture absorption properties. Finally, the chapter will conclude with some explanation on carrier mobility limiting factors related specifically to EG.

5.1 Fabrication

For the electrical characterization of TEG, we relied mainly on fabricating FETs. Other devices fabricated were TLMs for measuring contact resistance, and Van der Paws as well as Hall bars for Hall measurements. Unfortunately, it has proven too much of a challenge to get any Hall measurements out of TEG. The low yield as well as what seems to be micro-cracks along with the challenging wiring of Hall measurements prevented any successful measurements. So we relied mainly on the FET structures for electrical characterization.

SiO_2/Si, with optimized SiO_2 thickness, was the preferred choice of substrate. It allowed for backgating the devices. It also made TEG visible for ease of fabrication. We were ultimately vying for using h-BN as a substrate but unfortunately the research did not progress fast enough to reach that stage. Usually the SiO_2 was either 285 *nm* or 100 *nm* thick. 90 *nm* oxide would have been optimal but was not used during this investigation due to availability. The thinner 100 *nm* oxide thickness was preferable over thicker 285 *nm* oxide because it allowed reaching the Dirac point at lower voltages as a consequence of the equation:

$$\mathrm{n} = \frac{\varepsilon_0 \varepsilon_r \mathrm{V_G}}{\mathrm{te}} \qquad (5.1)$$

Where n is the carrier concentration, ε_0 is the dielectric constant of free space, ε_r is the relative dialectic constant, V_G is the gate voltage, t is the gate thickness, and e is the electron charge.

Fabrication steps followed traditional lithography procedures. Sheiply SPR-220-3µm photoresist was mostly used. Although the thickness of the photoresist did not allow for optimally sharp features, it did help in etching and contact deposition steps as it allowed for longer etch times and allowed contact lift off without LOR respectively. In

a regular process, photoresist is used as a cover material to etch TEG into device mesas using oxygen plasma Reactive Ion Etch (RIE). A 10 second etch time is usually sufficient to etch TEG. Another layer of photoresist is then exposed and used as a masking layer for metal contact lift off. The metal contact layers are deposited using electron beam evaporation. More details on metal contacts are given in the next section. The sample is left in acetone overnight for the lift off process and the devices are cleaned afterwards with Isopropanol (IPO) and prepared for electrical characterization. Final fabricated devices are shown in figure 5.1. Throughout the extensive work done in fabricating devices out of TEG, it was found that it is best to make processing compromises in order to minimize the processing steps and simplify the process as much as possible. This produced better yield which was more crucial in the case of TEG.

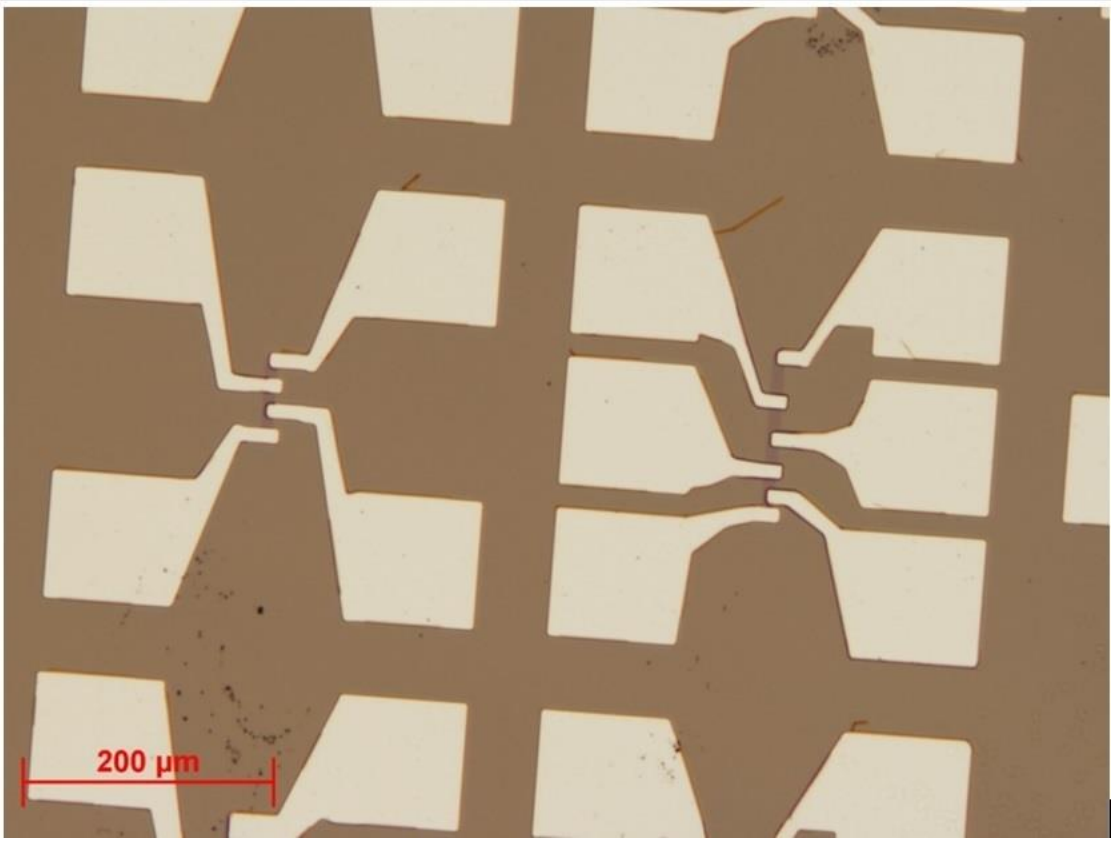

Figure 5.1: Typical fabricated TEG FETs and TLMs.

5.2 Contact Resistance

Contact resistance is among the main focus issues in the graphene community when looked upon from a device prospective. Earlier on in graphene research, contact resistance values were very high. Research has progressed significantly since then. There are sophisticated contact methods such as the one presented by the Columbia University groups where they contact graphene from the side in what they call a one dimensional contact [124]. This was too technical for us to pursue. Another method of getting good contact resistance is to slightly damage the graphene through ion bombardment [125][126]. This method allows for improved contact through the sides of the patches created. However this method has to be optimized and considering the difficultly we faced in getting TEG devices to work; it was not a viable option.

We opted to use conventional contact methods of electron beam evaporation of metals onto graphene mesas, which is the widely used method in the 2D materials research community. Initially, we used 10 *nm* of titanium as an adhesion layer to graphene and about 150 *nm* of gold as the contact metal. This yielded very high contact resistance values that dominated the electric characteristics of the initial devices. It was necessary to use four point probing in such a case to measure the intrinsic properties of the TEG without the contacts dominating its properties. Adopting alternative recipes [127][128] we later switched to using 0.5 *nm* of titanium as an adhesion layer and palladium as the main contact metal with a thickness in the range of 150 *nm*. The 0.5 *nm* titanium was thought to be a patchy deposition that allowed palladium to be the real contact metal, with titanium mainly just acting as a supporting adhesive. The contacts were afterwards, excellent to the point that the field effect mobility values measured using two point contact where hardly any different from four point contact measurements. And the Dirac point shift was negligibly small.

5.2.1 2p-4p Method

Contact resistance measurements were conducted using two different methods. The first method, which will be referred to as "2p-4p", was to measure the two point probe resistance of the FET structure, and then to measure the four point probe resistance of the same FET structure as illustrated in figure 5.2.

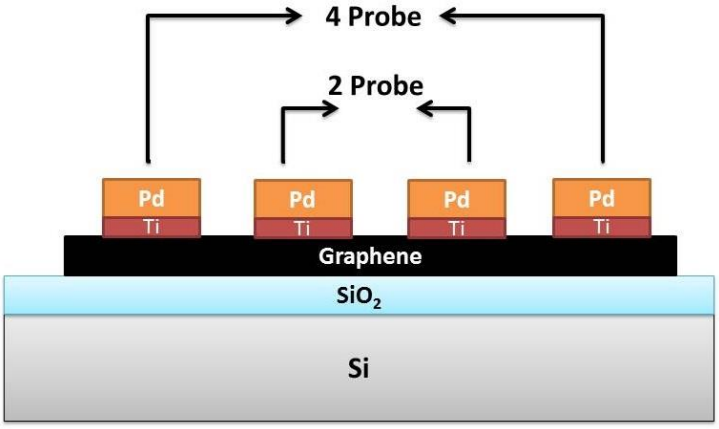

Figure 5.2: Schematic of contact resistance measurement.

We then have two sets of resistance values. Using the following equation:

$$R_c = W\left(\frac{R_2 - R_4}{2}\right) \qquad (5.2)$$

Where R_C is specific contact resistance (Ω.µm), W is contact width, R_2 is the two point probe resistance, and R_4 is the four point probe resistance. This equation states that you can get the contact resistance by canceling out the graphene resistance from the total resistance (which is $R_4 - R_2$ in this case) and then you are left with the contact resistances on both sides. You divide that value by two to get contact resistance per each side and then multiply the value by contact width to get the final specific contact resistance.

For 2p-4p FET, measurements, we obtained an average specific contact resistance value of 1021 Ω.µm for MTEG and 2630 Ω.µm for BTEG. The value obtained for the BTEG is in close proximity the specific contact resistance value measured using the TLM method shown next. The MTEG value however is significantly higher than the TLM value. We attribute this discrepancy to the quality of the specific MTEG used for this measurement being slightly lower than the one used in the TLM set and therefor adversely affecting the contact resistance value.

5.2.2 TLM Method

The second method, commonly referred to as the TLM method, relies on varying the length of the conducting material between the contacts while keeping the width of the conducting material constant as illustrated in figure 5.3.

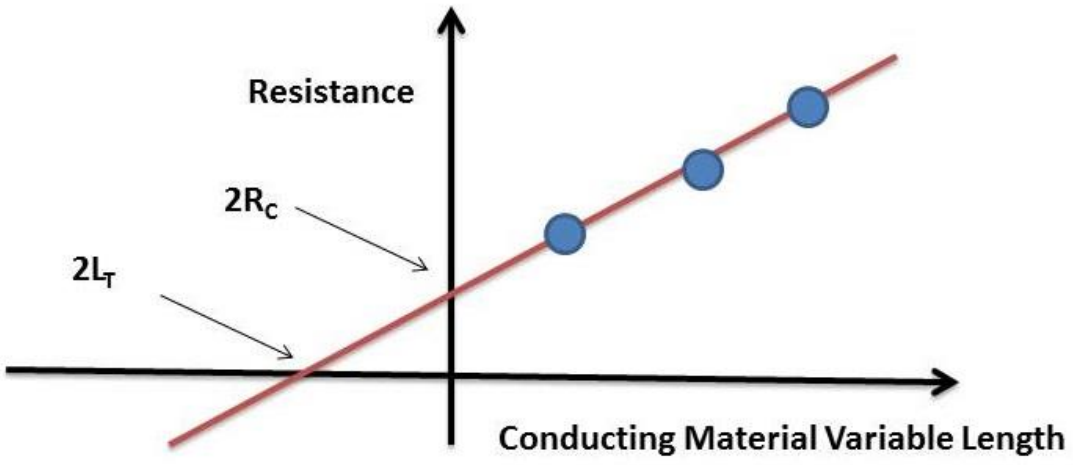

Figure 5.3: Illustration of TLM theory.

Plotting the resistance values verses the conducting material length; we get a y-axis intercept that gives $2R_C$ which is the contact resistance. The x-axis intercept would normally give us $2L_T$, the transfer length. However, as detailed in [128][129] this x-axis value of L_T is usually a poor fit in the case of graphene. This is due to: (1) transport in graphene under the metal contact is partially ballistic, and not completely diffusive, (2) the metal contact dopes graphene and therefor the sheet resistance of graphene under the metal contact is dissimilar to graphene in the channel.

Xia et al. [128] showed that the transfer length in metal-graphene contacts can be expressed using the following set of equations:

$$\lambda = \frac{\pi V_F \tau}{2} \quad (5.3)$$

$$\lambda_m = \frac{\hbar V_F}{\pi \eta} \quad (5.4)$$

$$L_T = \sqrt{\lambda \lambda_m} \quad (5.5)$$

Where λ is the carrier mean free path, V_F is the Fermi velocity, τ is the scattering time, η is the metal-graphene coupling strength, L_T is the transfer length, and λ_m is the metal-graphene coupling length. In the devices fabricated, we were successfully able to obtain a set of TLM measurements for MTEG and three sets of measurements for BTEG. The values obtained are plotted in figure 5.4 with error bars for the three sets of BTEG measurements.

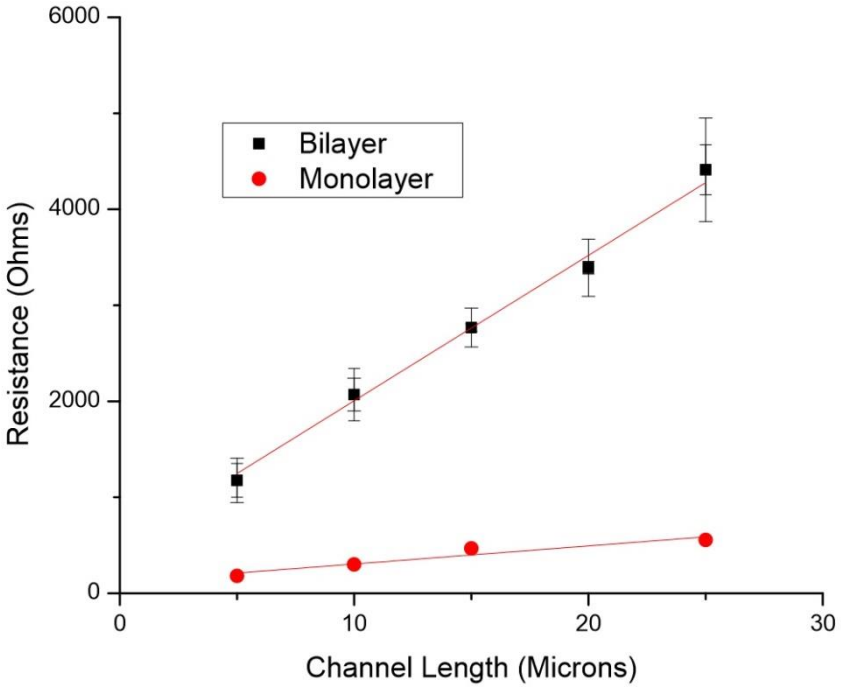

Figure 5.4: TLM measurements for MTEG and BTEG.

TLM measurements gave specific contact resistance values of 585 Ω.µm for MTEG and 2310 Ω.µm for BTEG. The specific contact resistance value of MTEG is respectable and comparable to leading values in literature using the same contact schemes which range around 200 Ω.µm [128]. The reason why it is higher in the case of MTEG is that generally, contact resistance is dependent on the quality of the graphene being contacted. While TEG is competitive with other large area graphene synthesis methods in terms of quality, it falls short in comparison to exfoliated graphene specifically which is the benchmark for graphene quality and is also the benchmark used in setting the good contact resistance values reported in literature. Specific contact resistance values for bilayer graphene are not as widely studied as in the case of monolayers. However, it is generally expected that R_C for the bilayers

should be higher than the monolayers since carrier mobilities in bilayers are known to be significantly lower than in monolayers while carrier concentration is not significantly higher as to offset the carrier mobility advantage of monolayers. Therefore the values obtained for BTEG are very reasonable and within expectation.

The x-axis intercept also gains a lot of insightfulness to the properties of MTEG compared to BTEG. While the x-axis intercept does not give an accurate value of the transfer length L_T, it should be safe to assume that the ratio of the transfer length from the x-axis intercepts to the monolayers and bilayers should be a usable property. From our data, the ratio of the MTEG transfer length (L_{T1M}) to the BTEG transfer length (L_{T2M}) is calculated to be $L_{T1M} / L_{T2M} = 2.5$.

It should be safe to assume that the metal-graphene coupling length (λ_m) is approximately the same for MTEG and BTEG since the same metal contact and metal deposition process are used. It should also be safe to make the approximation of Fermi velocities for MTEG and BTEG are equal. The Fermi velocity of monolayer graphene on SiO_2 is generally approximated to be ~ 6×10^6 *m/s* and bilayer graphene on SiO_2 was measured by other groups to have a Fermi velocity of 6.01×10^6 *m/s* [130]. So, it should be a valid approximation since in our case, both MTEG and BTEG are on the same nominal SiO_2 substrate.

Using these approximations and looking at the transfer length set of equations (5.3-5.5), one can infer by knowing the L_{T1M} / L_{T2M} ratio, that the carrier mean free path (λ) of MTEG is 6.25 times that of BTEG. In turn, the scattering time (τ) of MTEG is 6.25 times that of BTEG.

5.3 MTEG FET Characterizations

FETs were used for measuring the field effect mobility of TEG. In the simplest setup, two point probing was used where two points contacting the graphene would act as the source and drain of the FET structure. The gate voltage is modulated from the substrate beneath the graphene which is commonly referred to as backgating. Through sweeping the backgate voltage (V_{GS}) while running a low voltage between the source and drain (V_{DS}), the carrier concentration of graphene is modulated and the drain current (I_D) responds to V_{GS}. For all the FET measurements V_{SD} is set at 0.1 V. The field effect mobility can then be approximated from the linear part of the response curve using the following simplified FET equation:

$$\mu = \frac{L}{W}\frac{1}{V_{DS}}\frac{1}{C_{ox}}\left(\frac{I_D}{V_G}\right)_{linear} \quad (5.6)$$

Where μ is the field effect mobility, L is the device active area length, W is the device active area width, V_{DS} is the voltage between the source and drain, ε_0 is the dielectric constant of free space, ε_r is the relative dialectic constant, t is the gate thickness, I_D is the drain current, and V_{GS} is the gate voltage.

Earlier on in this research, four point probing (figure 5.5) was used for measuring the field effect mobility as it has the benefit of canceling contact resistance effects and therefore giving the true intrinsic value of mobilities as well as removing any ambiguities invasive contacts could cause in shifting the Dirac point [131]. Approximating the field effect mobility follows the same method as two point probing with replacing the appropriate variables. Equation 5.6 is used for this. What changes here is that the sweeping variables are V_{DS} and V_{GS}, rather than V_{DS} and I_D in the case of two point probing.

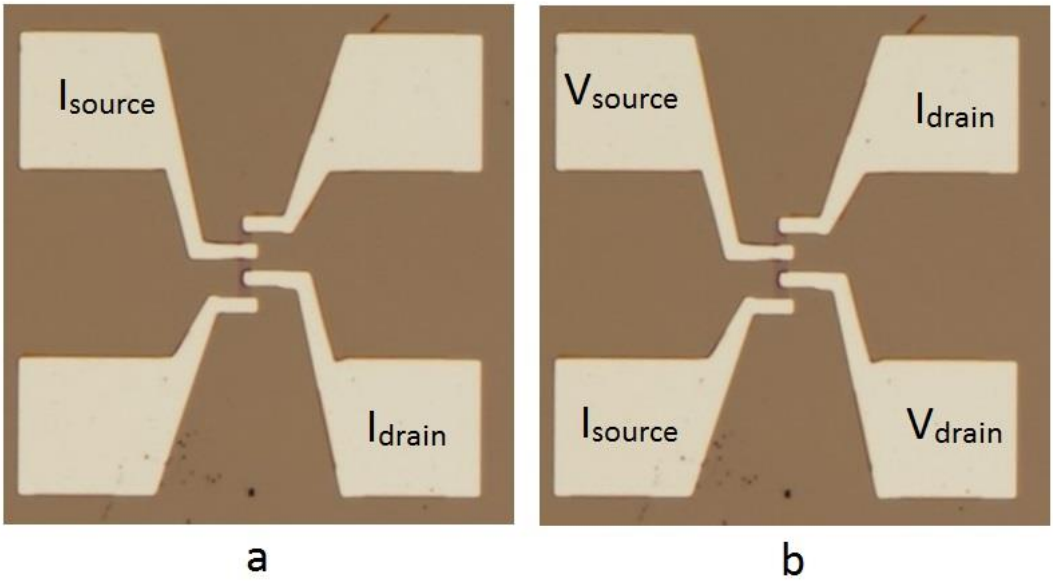

Figure 5.5: a. Probing setup for two point probe b. For four point probe.

Micro-cracks (figure 5.6) are a limiting problem in TEG. Device yield was very low, often no higher than 5%, and the surviving devices would, intern either not backgate at all, or would give low field effect mobility values. Through optimizing the transfer process and minimizing device fabrication steps as well as careful study of these micro-cracks, we were able to obtain very promising field effect mobility measurements for TEG.

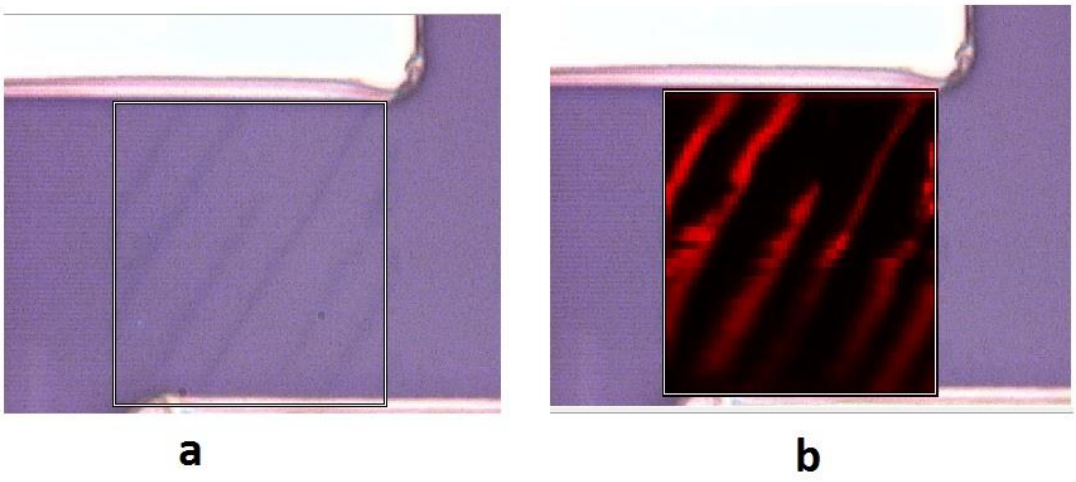

Figure 5.6: Micro-crack issue with TEG. a. Microscope image of a 10 X 10 μm square with MTEG active device having a lot of tear. b. Raman mapping of the same MTEG active device showing which areas have graphene left.

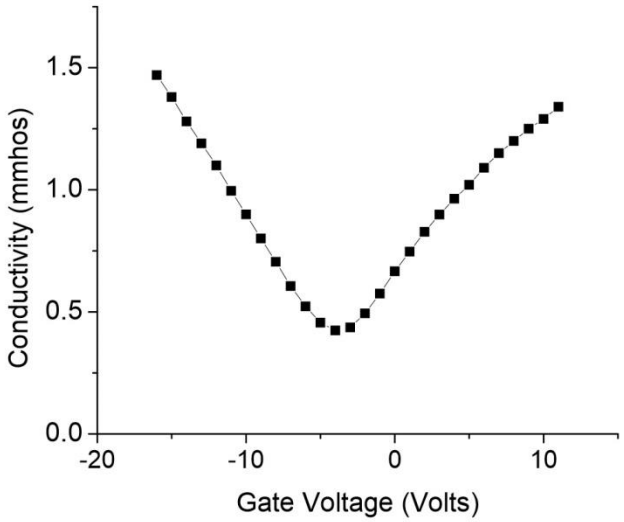

Figure 5.7: Conductivity curve for MTEG.

Figure 5.7 shows a typical conductivity curve we obtain from MTEG. It shows the typical bipolar Dirac behavior of a monolayer of graphene. Graphene on SiC tends to be n-doped. When it is transferred off the substrate, it is expected to be slightly p-doped as other forms of graphene synthesis. Our devices did show p-doping but occasionally they showed n-doping as well (figure 62 is a case in hand). This cannot be attributed to the palladium contacts as palladium causes p-doping [132]. Also, this cannot be attributed to defects in the TEG, as defect studies also show p-doping [133]. The very thin titanium (0.5 *nm*) used as the adhesion layer for the palladium contacts might be a source as titanium dopes graphene negatively [132]. However, even when four point probing is used, which eliminates contact effects, we did occasionally see n-doping. We attribute this n-doping to the gold etchant step in our processing. Oznuluer et al. grew graphene on a gold substrate [134] and they etched off the gold using the same etchant we used. They show very heavy n-doping for their devices. So evidently, this gold etch step is the source of this contamination. This is not a limiting factor in the gold transfer of TEG as this problem is easily solved by proper cleaning of gold etchant. Which is why, we only occasionally run into these n-doped devices.

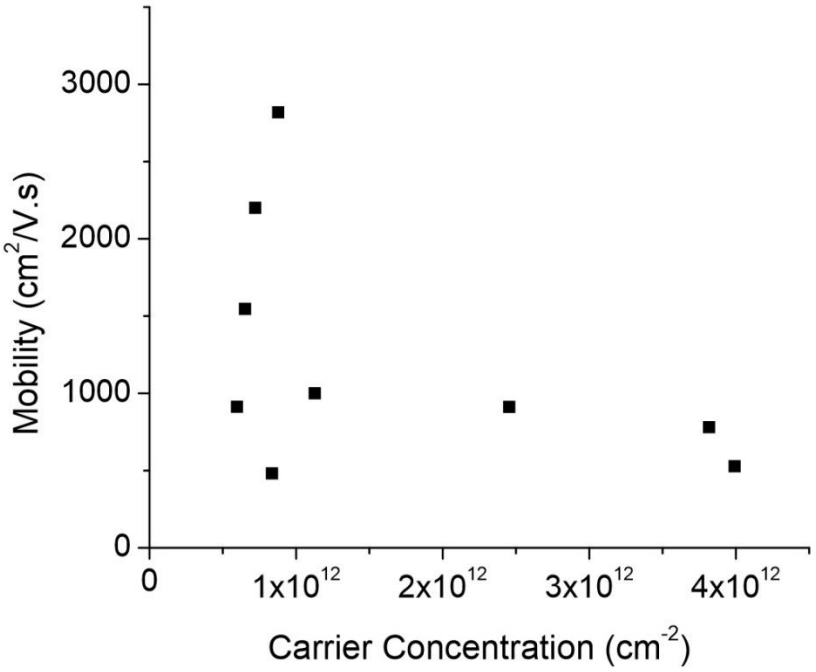

Figure 5.8: MTEG field effect mobility Vs. carrier concentration.

Figure 5.8 shows the field effect mobilities of MTEG FETs plotted against carrier concentration. As it shows in that figure and is typical for only a monolayer of graphene, mobility is higher at lower carrier concentration which is not the case for bilayers [135]. Electrical characterization shows the unique characteristics of monolayer graphene.

The mobilities were promising with a high value reaching 2800 $cm^2/V.s$. The average MTEG was at around 1700 $cm^2/V.s$ with an average carrier concentration of approximately 1.5 X 10^{12} cm^{-2}. These are exemplary results considering the fact that the starting EG on SiC would normally get an average hall mobility of around 700 $cm^2/V.s$ and an average carrier concertation of around 7 X 10^{12} cm^{-2}. This represents a mobility gain of more than a factor of two. It shows that a lot of the negative effects of the SiC substrate have been mitigated.

Further studying the transport characteristics of MTEG, we calculated universal mobility curves for some of the devices fabricated using the method of [136]. Figure 5.9 shows the hole universal mobility curves for these devices.

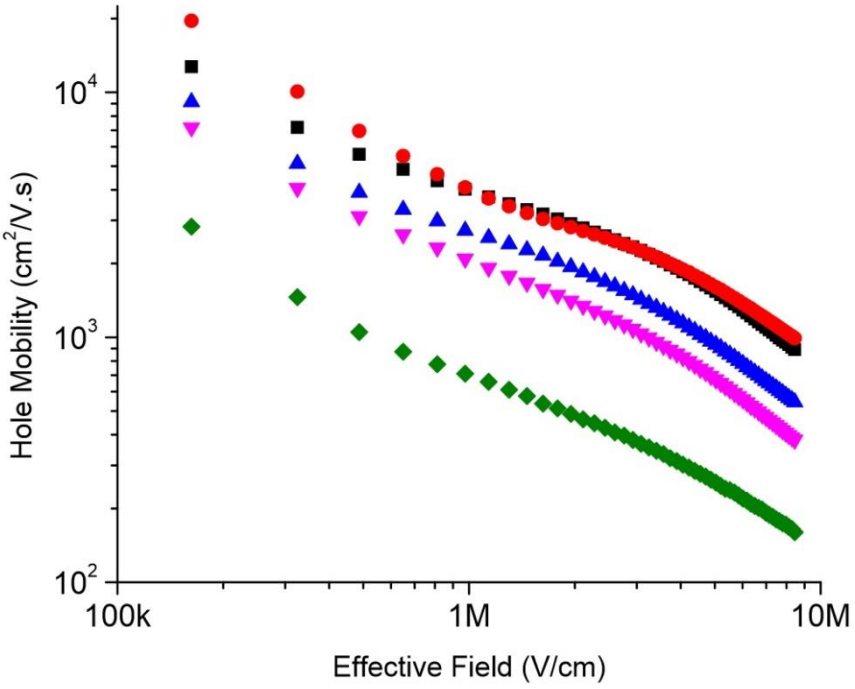

Figure 5.9: MTEG hole universal mobility curves.

While a SiO_2/Si substrate is not the ideal substrate for studying the transport properties of graphene, it does give a good reference point to compare transport results with literature. For our MTEG devices specifically, in referring to figure 5.9, we see high mobility values at low transverse electric fields. This shows that charged impurity scattering is not a major issue in MTEG. This is to be expected as our transfer method is a dry transfer and no charged particles should be trapped between the transferred graphene and the substrate. At around 0.5 *MV/cm* in figure 5.9 phonon scatting starts to dominate. This is expected for a SiO_2/Si substrate as reported by Chen et al. on the

extrinsic performance limits of graphene on a SiO_2/Si substrate [137]. Tirado et al. [136] showed the universal mobility curves of exfoliated graphene on a SiO_2/Si substrate. The same scattering patters for exfoliated graphene in that study are observed in our MTEG. At higher fields in figure 5.9 beyond about 2 *MV/cm* mobility further drops in what seems to be the same effect experienced in silicon MOSFETs, which is namely surface roughness scattering [138].

These results for MTEG are good and competitive with CVD graphene, the current leading large area graphene synthesis method. However, CVD graphene has been reported to give mobilities as high as 11,000 $cm^2/V.s$ on SiO_2/Si substrates [139]. Commercially available CVD graphene on SiO_2/Si substrate is quoted at field effect mobilities of 2000 $cm^2/V.s$ [140] which is much lower and is a conservative value closer to real performances of CVD graphene. The high values reported in literature on CVD graphene are optimized devices. But even taking this into account, SiC mobilities still seem lower than what they should be. So the general question is, why does EG after transfer, fall short of expectations?

This seemingly upper limit to the mobility of EG shows elsewhere in literature. Early studies of EG predicted an intrinsic limit of EG mobility [141] at around 5800 $cm^2/V.s$. Intercalation studies of EG on SiC to mitigate the substrate effects without transfer, yield mobility values no better than 3100 $cm^2/V.s$ [142][143]. Even suspending graphene, which is known to yield mobilities in the range of 1×10^6 $cm^2/V.s$ [21] for exfoliated graphene, could only give an estimated mobility of 5000 $cm^2/V.s$ in the case of suspended EG [144]. Multilayer growth on the step edges might be a source for mobility degradation with sources reporting as high as 10 fold mobility degradation [145][146]. But in our investigation we made sure that the devices measured were indeed only monolayer and furthermore, the mobility increasing with decreasing carrier concentration shown in figure 54 is a unique propriety of monolayer

graphene, so this cannot be the reason. Grain boundaries might be the reason for this underperformance [58] but multiple sources have shown EG to be a carpet like material.

We speculate that the reason behind this less than optimal EG mobility is that the graphene that grows on step edges is full of structural defects as comprehensively studied in [75]. Furthermore due to SiC wafer miscut [147] making these defects in step edges appear as correlated line defects [148], they work as a true limiting factor in the mobility of EG. And although transferring EG off the SiC substrate does mitigate substrate effects such as film stress, and substrate doping of graphene, the mobility is still ultimately limited by these defects.

To further expand on this point we used the self-consistent transport model of [149] which fits conductivity to a density-independent mobility attributed to the long range charged impurity coulomb scattering:

$$\sigma^{-1} = (ne\mu_c + \sigma_0)^{-1} + p_s \quad (5.7)$$

Where σ is the conductivity, n is the carrier concentration, e is the electron charge, μ_c is the carrier independent mobility, and σ_o is the residual conductivity at the Dirac point, and p_s is the contribution to resistivity from short range scattering.

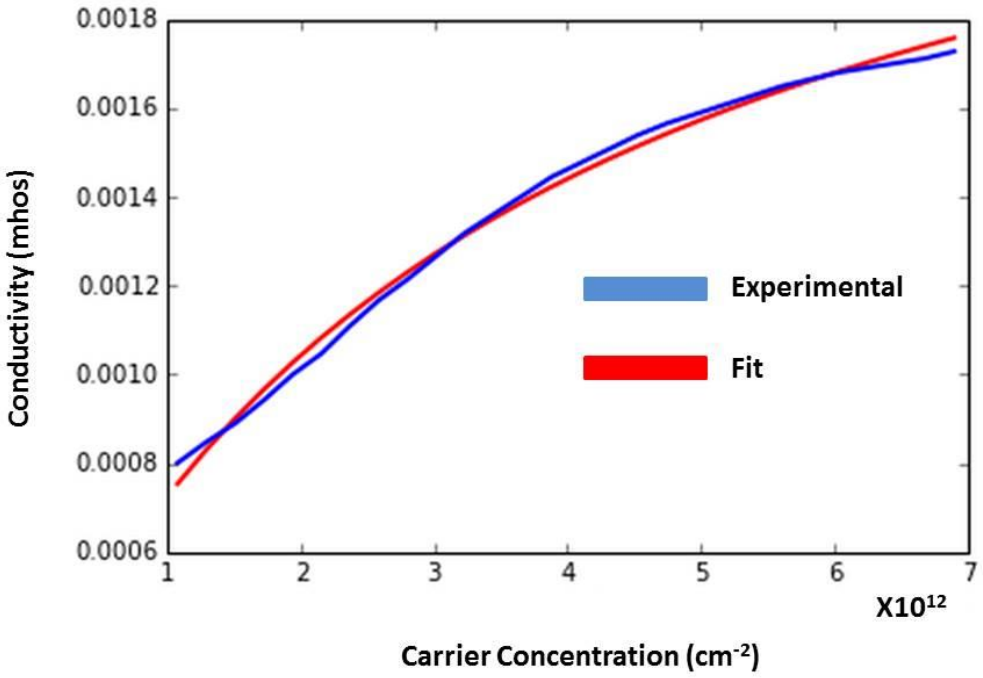

Figure 5.10: Density independent mobility fitted to experimental curve of MTEG.

When fitting the slope of our data to the carrier independent mobility equation in figure 5.10 we got a mobility of nearly 4000 $cm^2/V.s$ for a device that shows a field effect mobility of 2000 $cm^2/V.s$ when the normal FET equation is used. What this in effect is saying, is that the mobility limited by long range scattering is higher. Meaning it is the short range (defects) scattering that is limiting the mobility. While this is not conclusive evidence that indeed the structurally defective EG growing in the step edges, is the main cause of mobility limitations, it does add supporting evidence.

It should be possible to experimentally show substantial evidence to this line defect speculation. If the mobility of MTEG is measured against the direction of transport on the TEG and the plot of this directional mobility showed variation with only one direction yielding high mobility, then this would be strong supporting evidence that

the line defects from step edge growth is the major mobility limiting factor. Furthermore, if it were possible to fabricate devices from the TEG coming from the terraces where the EG quality is believed to be higher, than this would show the real limit of TEG transport properties. Unfortunately, the low yield we experienced during this investigation did not allow us to pursue these specific experiments and they will be the topic of future research.

To summarize this section, MTEG FET structures show mobilities in the range of 1700 $cm^2/V.s$ which is competitive with commercially available CVD graphene. While it does fall short of record setting mobilities by CVD graphene that can go up as high as 11,000 $cm^2/V.s$ even on SiO_2/Si substrates, these values come from optimization of the CVD graphene synthesis method over several years with various groups investigating CVD graphene. The mobilities reported from initial CVD graphene synthesis were much lower. TEG has very limited investigations in comparison. Without doubt, TEG would show more promising results if further research went into optimization of this synthesis method.

5.4 BTEG FET Characterization

For characterizing the FETs of BTEG it was necessary to anneal the FET structures in argon ambient at 300 ^oC for two hours. We observed that annealing BTEG improved mobility on average by about 25%.

The reason for this we believe is due to the synthesis method of the bilayers. Back in chapter 2, it was shown that the bilayer EG was obtained by hydrogen intercalation. This introduces a lot of hydrogen ions that are absorbed by the bilayers. Bilayer EG seems to have very good absorption properties as will be shown in the next section. These hydrogen ions remain trapped in the bilayers even after transfer and device fabrication and are only released after annealing. Since the intercalation step is done at

elevated temperatures and with high gas flow, the absorption of the hydrogen ions is a considerable dose of ionized impurities that cause coulomb scattering which degrade the mobility. This is evident by the Dirac point shift (figures 5.11 and 5.12) from over 50 volts before anneal to around 20 volts directly after anneal. This Dirac point shift, coupled with the fact that the mobility improves considerably after annealing and does not degrade subsequently after water vapor absorption with time, is what leads us to believe that hydrogen ions are trapped from the intercalation step of bilayer growth.

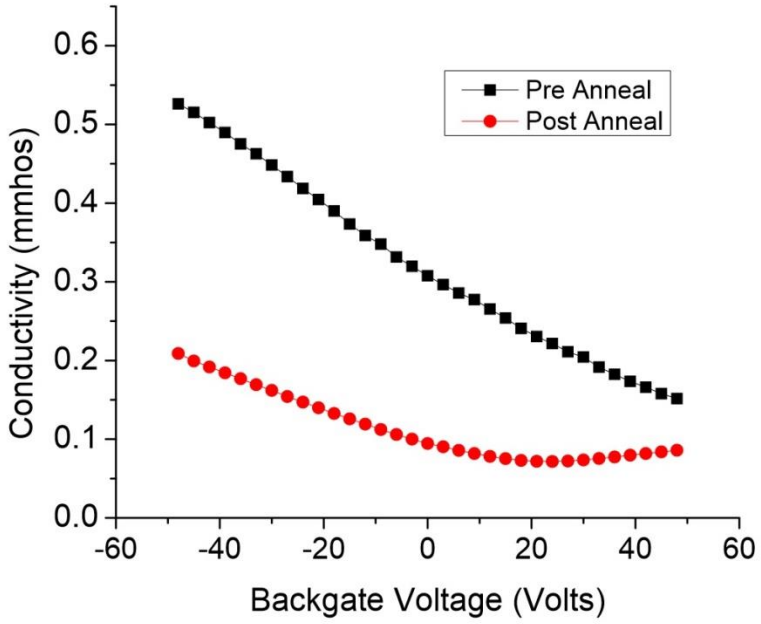

Figure 5.11: BTEG conductivity plot showing Dirac point shift with annealing.

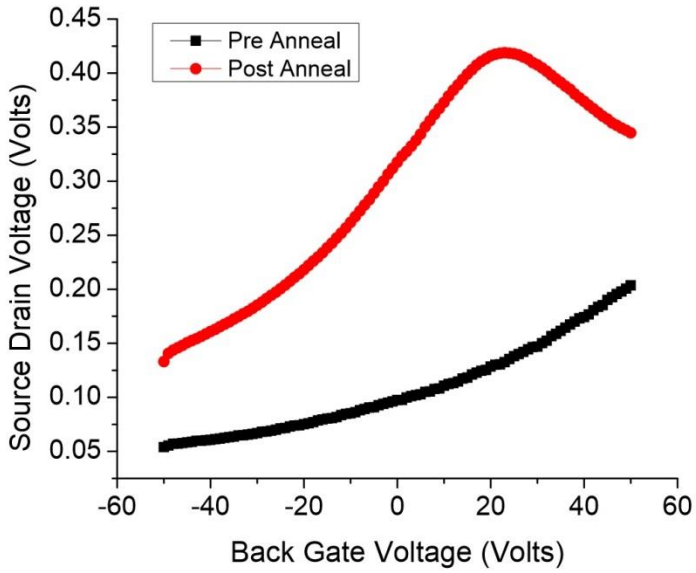

Figure 5.12: Voltage plots of BTEG Dirac point shift with annealing. The voltage plots emphasis the Dirac point shift more as opposed to the conductivity plots.

The conductivity plot of BTEG after annealing (figure 5.11) is representative of bilayer graphene. It shows lower conductivity values as is typical of bilayer graphene due to the lower mobilities. It also shows high intrinsic doping with the Dirac point typically at around 20V which is another common characteristic of bilayer graphene [135].

Figure 5.13 shows the field effect mobility of BTEG plotted against carrier concentration. The field effect mobility increases with increasing carrier concentration. This is the opposite of MTEG and is exactly the noticed behavior of exfoliated AB stacked bilayer graphene [135]. So this characteristic mobility increase with carrier concentration increase is supporting evidence of AB stacking for BTEG.

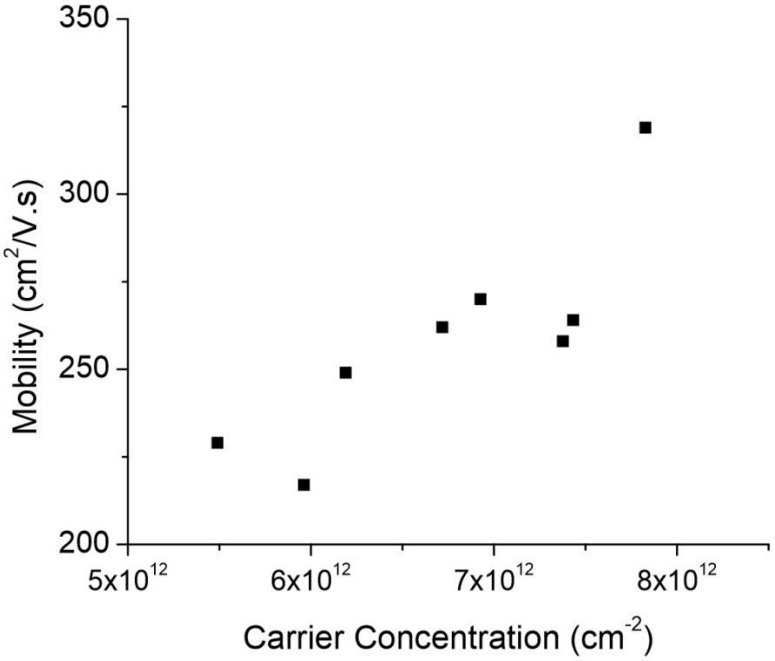

Figure 5.13: BTEG field effect mobility Vs. carrier concentration.

The field effect mobilities extracted from BTEG FETs were significantly lower than MTEG. The average field effect mobility was around 250 $cm^2/V.s$ and highest values only reached 330 $cm^2/V.s$. It is typical in exfoliated graphene that bilayer mobilities are 2 to 5 times lower than monolayer mobilities [150]. But in our case, this is almost 7 times lower. Granted that this lower mobility does further support the evidence of AB stacking as this shows that the two graphene layers are strongly coupled, it is still lower than expected.

We believe the reason for the lower than expected mobilities is the buffer layer that is released into a graphene layer during the bilayer growth. Other sources who use intercalation to release the buffer layer into a free standing monolayer do mention that this process yields less repeatable results than regular monolayer growth on SiC [144]. The buffer layer, while resembling a monolayer of graphene once released by

intercalation, still possess properties that are unique to it. Back in chapter 4 the D/G ratio was shown to be around 5. Pristine, exfoliated bilayer graphene does not show a D peak at all. This points towards BTEG having substantial defects. Since the D peak does not show so strongly in the case of MTEG, it appears that the released buffer layer indeed has more defects than a conventionally grown EG monolayer.

In conclusion to this section, we mention that the electrical characterization of BTEG do support the evidence of AB stacking. Despite our BTEG showing lower than expected mobilities, this does not necessarily limit its potential. Right now this is a viable method of obtaining large area AB stacked bilayer graphene. For the low mobilities, the growth and transfer procedure can be optimized as in the case of MTEG. Furthermore, alternatively, bilayers can be epitaxial grown without the intercalation step to release the buffer layer. This should eliminate the factor of the released buffer layer limiting the mobility.

TABLE 5.1 Transport Characteristics of Large Area Graphene Synthesis.

Transport Characteristics	Highest Mobility ($cm^2/V.s$)	Average Mobility ($cm^2/V.s$)	Average Carrier Concentration (cm^{-2})
MTEG on SiO_2	**2800**	**1700**	**$1.7X10^{12}$**
Monolayer EG on SiC	**900**	**650**	**$1X10^{13}$**
Best Results Monolayer CVD graphene on SiO_2	**11,000***		
Commercial Monolayer CVD graphene on Al_2O_3	**--**	**2000***	**--**
BTEG on SiO_2	**330**	**250**	**$6.7X10^{12}$**

* mobility values taken from [139][140] respectively.

5.5 BTEG Gas Absorption Properties

Annealing experiments were carried out on both MTEG and BTEG. The FETs we annealed in argon ambient at around atmospheric pressure at 300 ^oC for usually two hours.

After annealing, the samples are quickly taken out and electrically probed. For both MTEG and BTEG, the mobility did not change substantially over time after annealing. This is shown in figures 5.14 and 5.15 respectively.

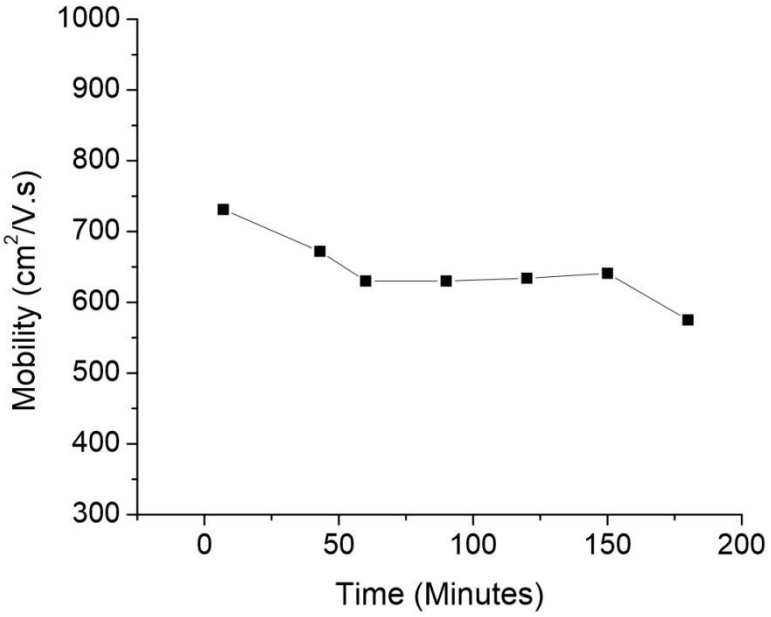

Figure 5.14: MTEG field effect mobility remaining constant over time after annealing.

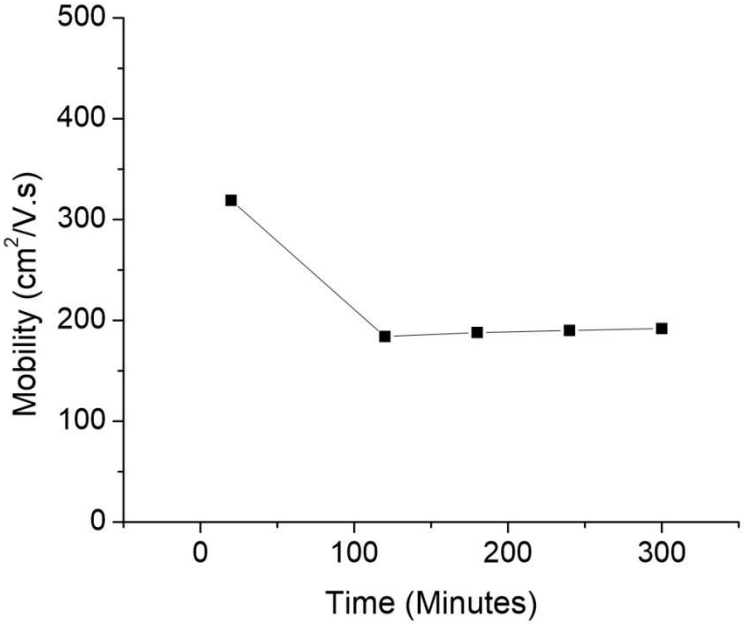

Figure 5.15: BTEG field effect mobility remaining constant over time after annealing.

However, the Dirac point did shift with time for both MTEG and BTEG. This is shown in figures 5.16 and 5.17 respectively.

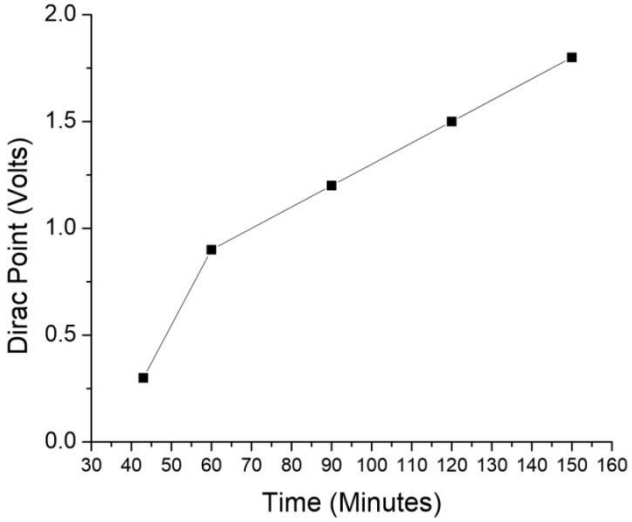

Figure 5.16: MTEG Dirac point shift with time directly after annealing.

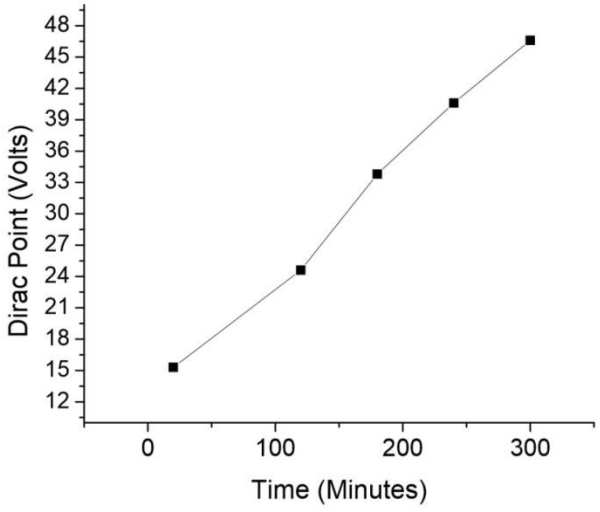

Figure 5.17: BTEG Dirac point shift with time directly after annealing.

This is a well-documented effect of graphene getting p-doped by ambient water vapor. Schedin et al. [151] shows this effect as well as also mentioning that the mobility does not degrade appreciably after absorption as it is in our case. This is an indication that the absorption is not substantial as in the case of bilayers being hydrogen intercalated. The more interesting observation here is that BTEG shows Dirac point shift with time that is 10 times faster than MTEG. From the conclusion of the previous section indicating that BTEG synthesized by releasing the buffer layer, has more defects than usual, this shows BTEG is a better gas absorber. This observation was also made by Hajati et al. [152] where they showed improved gas sensing properties of structurally defected bilayer graphene. This opens up a potential technological application for BTEG. Unfortunately, we were not able to further investigate this topic thoroughly but it is open for future research.

TABLE 5.2 List of Cornell Nano Fabrication Facility Tools used for Fabrication

Process Category	Tool Name	Description
PHOTOLITHOGRAPHY	ABM Contact Aligner	Flexible 200mm mask aligner with DUV light source
	GCA 5X Stepper	GCA 200 DSW i-line wafer stepper
	Heidelberg Mask Writer DWL2000	DWL2000 Laser Pattern Generator and Direct Writer
	GCA PG3600 Pattern Generator	Mask Pattern Generator
FURNACE PROCESSING	Wet/Dry Oxide – B2	MRL Industrial furnace for oxidation of silicon substrates
	Carbon Nanotube/Graphene Furnace	First Nano Carbon Nanotube and Graphene Furnace
COMPUTING	L-Edit CAD Software	L-Edit layout editor software by Tanner EDA
ELECTRICAL TESTING	IV Probe Station	IV measurement system with sense leads for four point probing
METROLOGY	FilMetrics Film Measurement Systems	F40/F50-EXR Optical measurement Systems for transparent thin film measurements
	P10 Profilometer	Equipment for measuring surface topology in the micron or finer scales
	Woollam Spectroscopic Ellipsometer	Variable angle Ellipsometer for full optical characterization of thin films
MICROSCOPES	AFM – Veeco Icon	Veeco atomic force microscopy for high resolution profilometry
	Nikon Eclipse L200N	High resolution microscope for device inspection
	Olympus Confocal Microscope	High resolution microscope for device inspection
	Zeiss Ultra SEM	Ultra-High resolution field emission SEM
ETCHING	Glen 1000 Resist Strip	Oxygen plasma resist tool. Used for forming Graphene
	Hamatech Hot Piranha	Automatic wafer processer for SC-1 & Piranha cleans
	Oxford 81 Etch	Oxford plasmaLab 80+ RIE System for fluorine based etching of oxide, nitride & silicon
	Oxford 100	Oxford PlasmaLab 100 RIE System for fluorine based ICP deep SiO2/glass etching. Used for etching SiC.
	PT720-740 Etcher	PlasmaTherm 720/740 Chlorine-based RIE system for Silicon & Aluminum Etching
	YES Asher	YES CV200RFS Oxygen Plasma Asher
THIN FILM DEPOSITION	Oxford ALD FlexAL	Atomic Layer Deposition of mainly Oxides
	SC4500 Evaporator	CVC SC4500 combination Thermal/e-gun evaporation system for depositing thin films of mostly metals
PACKAGING & MIS PROCESSING	Westbond 7400A Ultrasonic Wire Bonder	Gold wire bonder
	RTA – AG610	Rapid Thermal Anneal – AG Associates Model 610

CHAPTER 6

BORON NITRIDE RELATED WORK

6.1 Boron Nitride Chemical Vapor Deposition Growth

Much in the same line of graphene, boron nitride was early on realized as a technologically advantageous 2D material that needed to be scaled up because of the difficulties of working with small exfoliated flakes. As in the case of graphene, CVD is a leading synthesis method for h-BN. CVD growth of h-BN did not show the same level of success as graphene CVD because h-BN is more challenging to grow. Research groups were successful in obtaining 2 to 5 layer thickness of CVD h-BN [153] and later on, monolayer growth was demonstrated [154]. Large area, high quality multilayer CVD h-BN was only recently reported [155]. While, achieving large area single crystal domains in CVD h-BN is still an ongoing challenge with recent results [156] reporting 35 μm^2 domain sizes by electropolishing the substrate. The latest advancement [157] show single crystal domain with sides no larger than 100 μm. Obtaining high quality large domain h-BN is an ongoing topic and in our group, research was ongoing to improve h-BN CVD growth and implement it with graphene applications.

6.2 Copper Template Electropolishing

One of the main research efforts in CVD h-BN growth is to get high quality controlled large area single crystal monolayer growth. In our group it was observed and thought that the starting copper foils might play a major role in initial nucleation and subsequent growth. Figure 6.1 shows a sample monolayer CVD growth result

showing a lot of growth imperfections which were thought to be caused by the substrate. We wanted to investigate the effect of electropolishing the copper foils on the initial nucleation of CVD h-BN. Others have reported good results from electropolishing the starting substrate [156] but we wanted to make closer observations of the starting nucleation and subsequent progression to coalesced films.

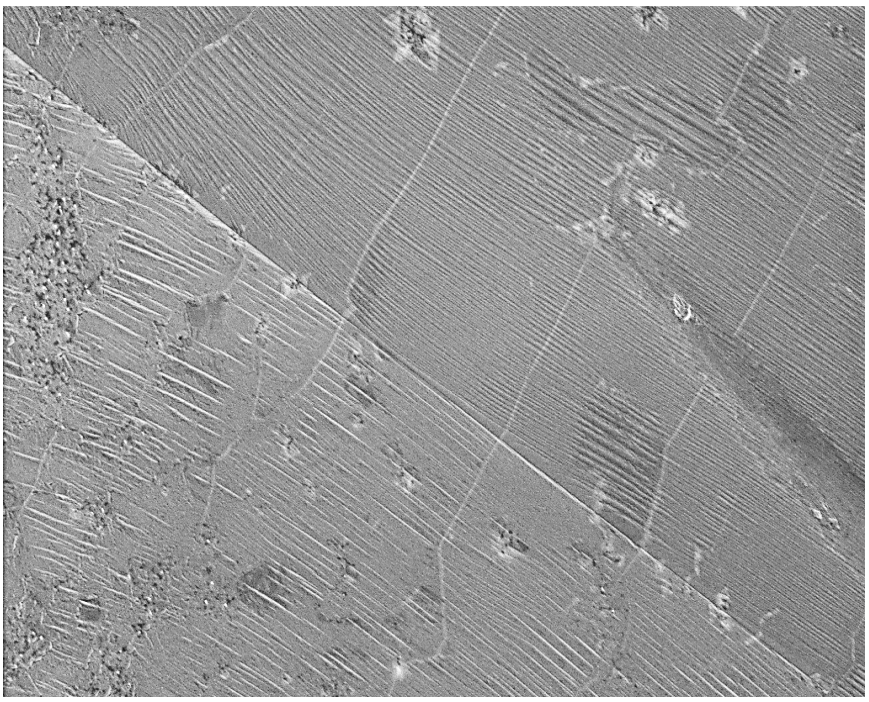

Figure 6.1: Coalesced h-BN films showing growth imperfections which are believed to be caused by the copper substrate before electropolishing.

The copper foils which are supplied from manufacturers and which we worked with often have a root mean square (RMS) roughness value of about 177 *nm* as we measured from AFM. This is due to rolling lines from the manufacturing process. These rolling lines can be as high as 800 *nm* as shown in figure 6.2.

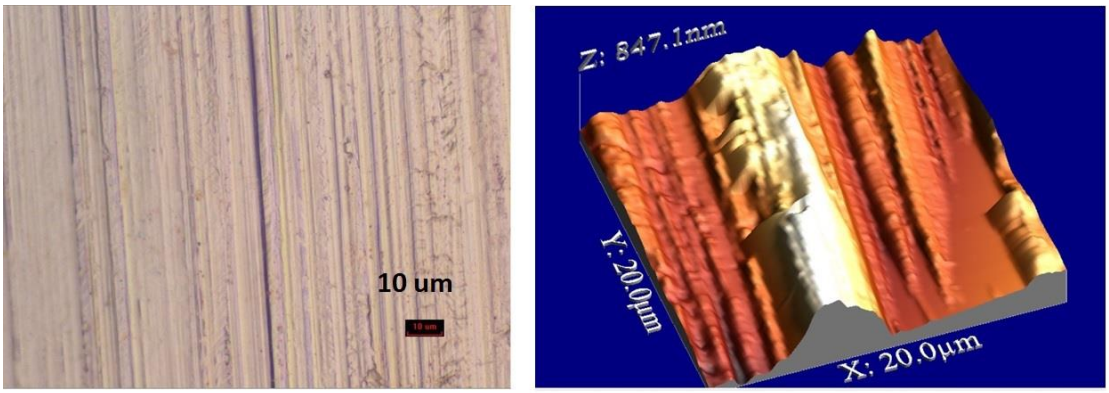

Figure 6.2: Rolling lines showing in unpolished copper foils a. dark field microscope image b. AFM image.

Kwon et al. reported that it was possible to reduce these copper rolling lines down to around 8 *nm* [158] using a simple yet optimized electropolishing procedure. We opted to reduce the surface roughness as much as possible on the copper foils using a simple electropolishing setup to see the effects on h-BN growth. The copper foils were first cleaned using heated TCE, Acetone, and IPO to get rid of all organic layers left from the manufacturer. The copper foils are then placed in an electropolishing solution composed of ethaline glycol, phosphoric acid, and DI water. The concentration of phosphoric acid was typically 2.17 molars. The setup is shown in figure 6.3. The solution is heated to 65 ^{o}C. A constant current power source was mainly used for the electropolishing but we also did utilize a constant voltage source for side experiments such as revealing the size of the copper grains after annealing. Throughout, the investigation we have found that electropolishing for about 10 minutes gave best results.

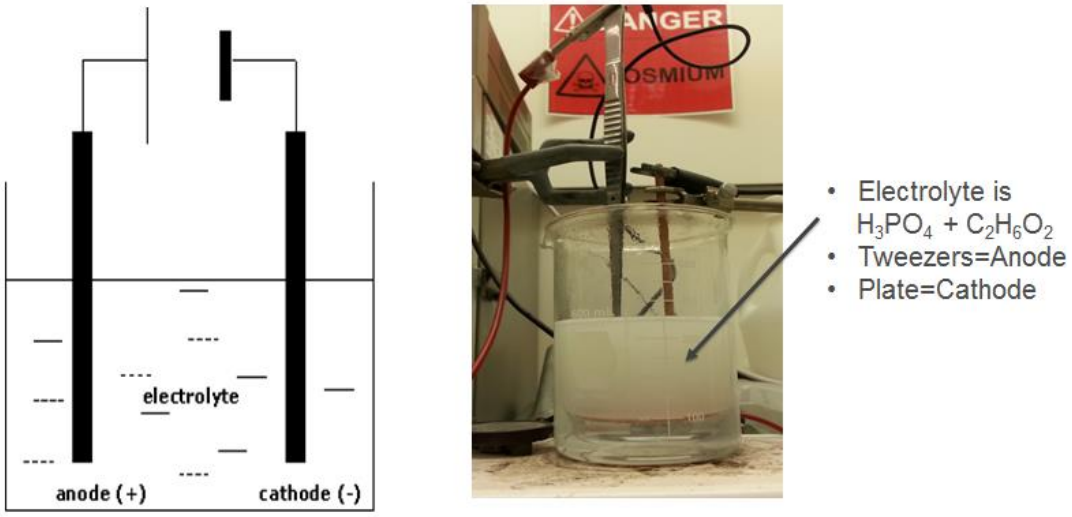

Figure 6.3: Electropolishing setup utilized for polishing copper foils.

Electropolishing has three main regions: (1) surface controlled kinetics etching, (2) mass transport controlled etching, and (3) gas formation etching. For the purpose of getting smooth surfaces, it is best to be in the second region where electropolishing is smooth and all grains of the material are polished equally resulting in a smooth surface throughout the material. However, we did Electropolish some samples in the first region. Because grains get etched at different rates in the first region, this enabled us to visibly observe how large the copper grains got after we annealed those particular copper foils. The grain sizes can be seen in figure 6.4. It was important to see the grains grow often to the size of a few millimeters square because having large grains is important for improving the quality of CVD films grown on it subsequently.

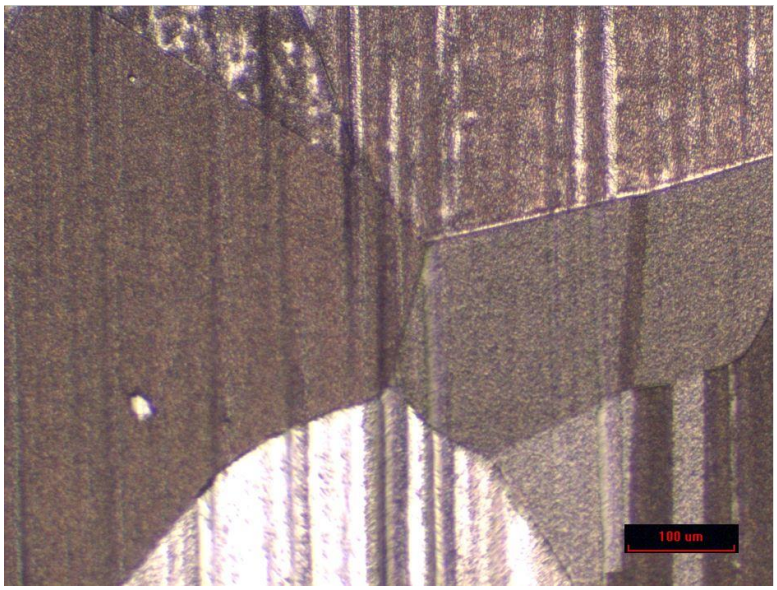

Figure 6.4: Etching in the surface kinetics controlled region revealed the larger grains that were obtained by high temperature annealing of copper.

Electropolishing in the mass transport controlled (second) region was carried out with a current density of 0.19 A/cm^2 using a constant current source for typically 10 minutes. We were eventually able to reduce the RMS roughness from 800 *nm* to 12 *nm*. The surface feature heights were reduced from 800 *nm* to no more than 30 *nm*. The rolling lines were completely gone. This is shown in figure 6.5. A note should be mentioned that the AFM images in figure 6.5 are not to the same scale so the electro polished image might seem rough when it is much smoother. Surface imperfections such as pitting and even spurious contaminations from the manufacturer were reduced as well. The resulting copper foils showed a very smooth texture that can be observed visibly.

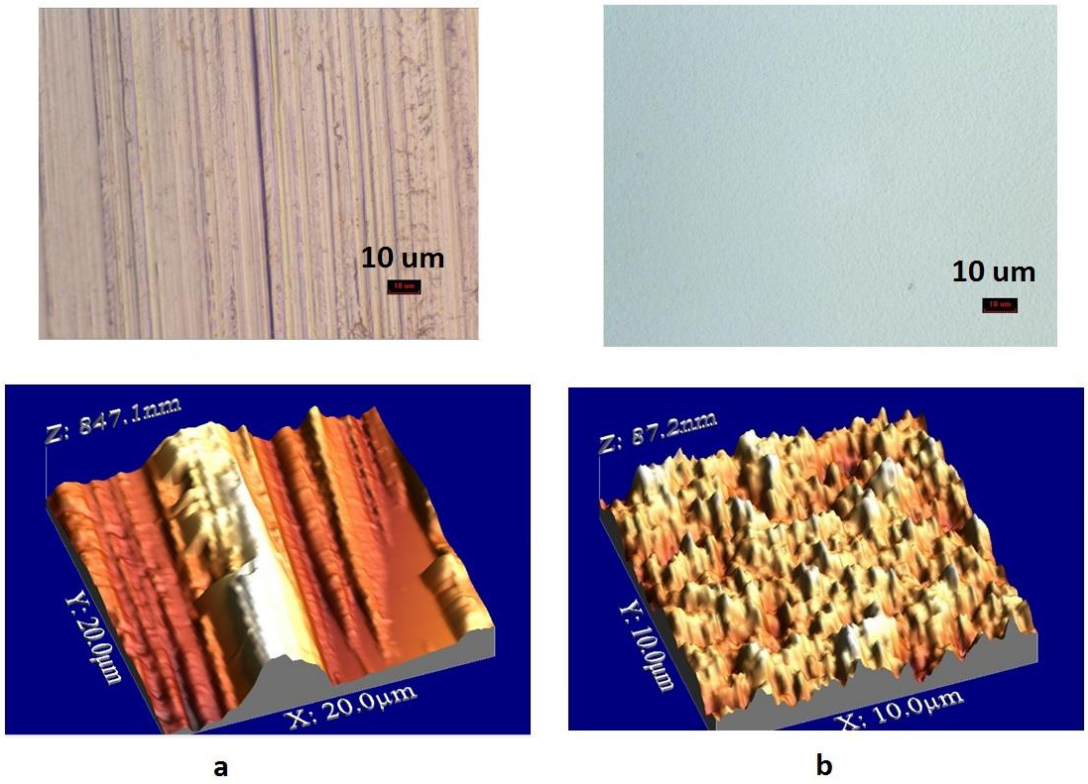

Figure 6.5: a. Microscope and AFM images of copper foil before electropolishing. b. After electropolishing.

These electropolished copper foils were tested for h-BN CVD nucleation growth. We achieved significant initial improvements in quality. Figure 6.6 shows nucleation triangles evident of high quality growth. None of the growth imperfections observed in non-electropolished copper were later observed. This is an ongoing project and coalesced films are currently being studied using the electropolished coper foils. Currently we are finding that electropolishing the copper foils before growth is a necessary step and the electropolishing setup is repeatable and reliable.

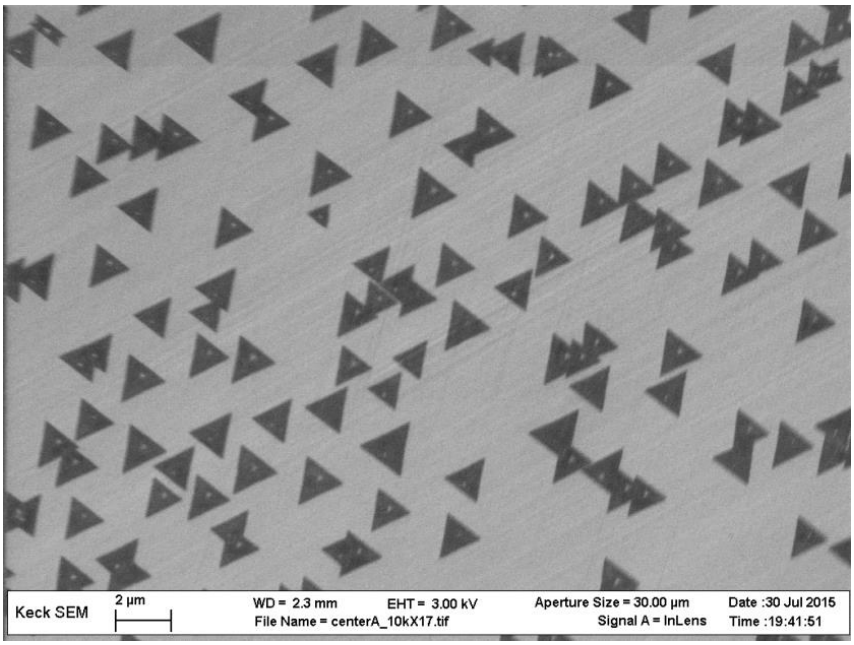

Figure 6.6: CVD h-BN nucleation triangles on electropolished copper foils.

6.3 CVD Graphene on CVD Boron Nitride Electric Transport

Graphene on h-BN as previously explained in chapter 1, exhibits high mobility due to h-BN having an atomically smooth surface, a lattice constant close to graphene, and high energy optical phonon modes that cause less scattering at room temperature. Ultimately, fabricating large scale 2D devices from 2D materials would yield the high performance excepted from 2D materials. One candidate for this large scale fabrication of 2D devices is CVD graphene on CVD h-BN where, ideally both growths are done in the same furnace to eliminate contamination issues. There have been early research efforts towards this goal [159]. But CVD h-BN is still an ongoing research topic as explained in the previous section and therefore, we have conducted a few experiments in the whole theme of CVD graphene on CVD h-BN.

We initially started out with some preliminary studies on the CVD growth of graphene

on exfoliated flakes of h-BN. We were successfully able to etch mesas and lay metal contacts on the CVD grown graphene which is on top of h-BN flakes as shown in figure 6.7. These were preliminary results and the graphene quality was not high. We were ultimately vying to use CVD h-BN as well so this project was not pursued any further.

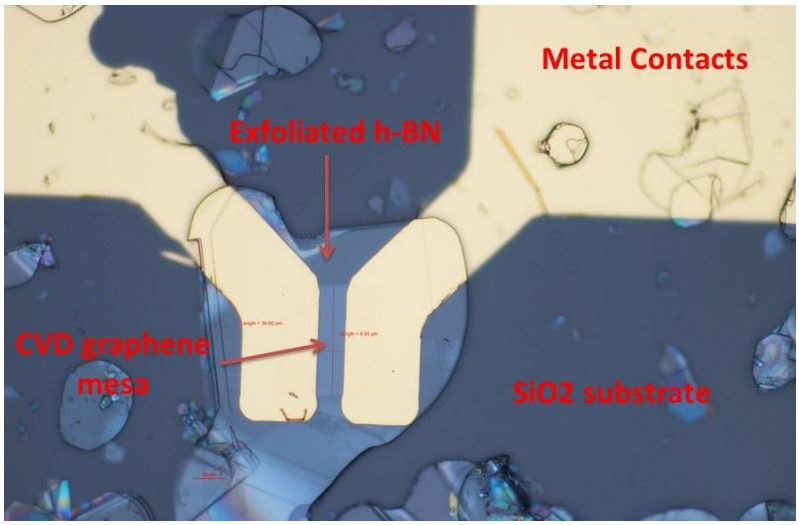

Figure 6.7: Early attempts of fabricating CVD graphene devices grown on top of exfoliated h-BN flakes.

We tested the CVD graphene on CVD h-BN concept by growing CVD h-BN on sapphire substrates. These films were of the thick variety. But they were uniform across the substrate, and therefore large area, unlike exfoliated h-BN. Thicknesses varied by growth conditions and we generally had three different thicknesses of 5, 20, and 60 monolayers.

CVD graphene was transferred using a PMMA copper etching procedure. Regular PMMA is spun on top of graphene and the copper is dissolved in copper etchant. The PMMA/Graphene stack is scoped out and placed in several DI rinse baths before finally being scoped out with the BN/Sapphire substrates. The procedure is illustrated in figure 6.8. CVD graphene was also transferred using the same procedure to a standard SiO_2/Si substrate for reference.

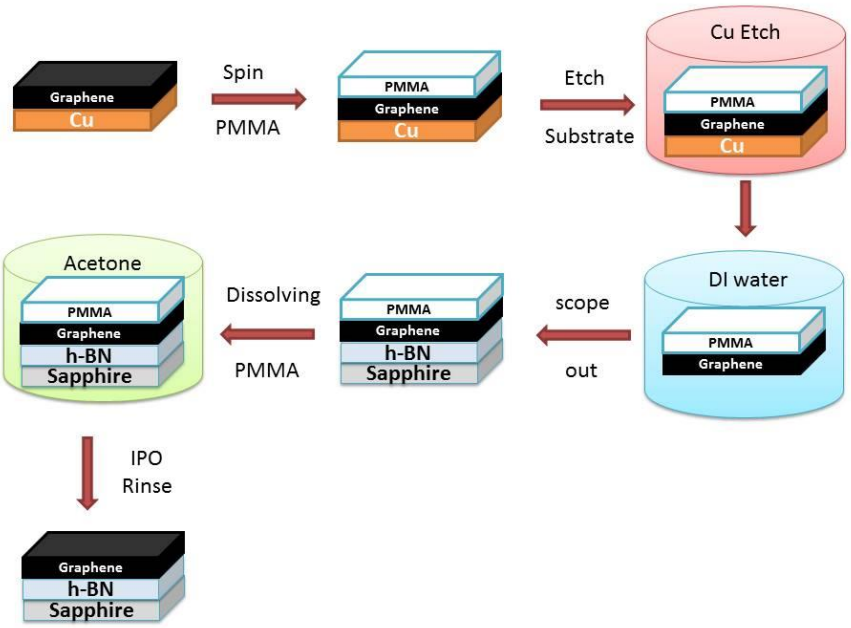

Figure 6.8: Transfer procedure for CVD graphene on CVD h-BN.

Unfortunately for the two thicker hBN substrates (20 and 60 monolayers), the h-BN layers mostly delaminated in the DI water step of the transfer procedure as shown in figure 6.9 and none of the devices survived further processing.

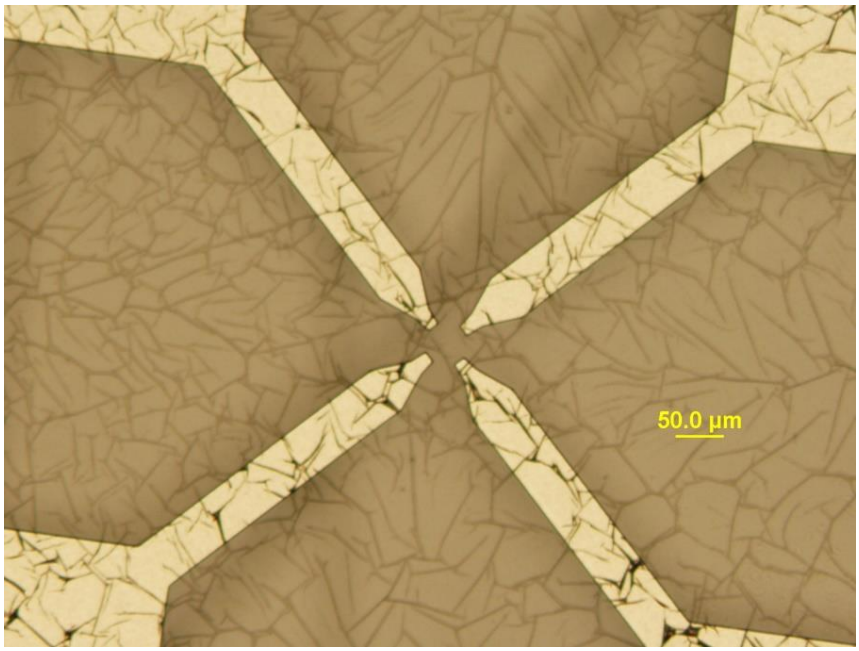

Figure 6.9: Thick CVD h-BN wrinkling badly from DI water and subsequently delaminating.

The thinner h-BN samples did not delaminate in DI water. We successfully fabricated Van der Paw devices, as shown in figure 6.10, using the same recipe used in chapter 5. We were successfully in obtaining Hall measurements for a few of these working devices. Unfortunately, the CVD graphene quality from the starting material was poor as evident by Raman after transfer and mobilities were very low. Nevertheless, there was a very clear trend showing that even with this poor quality CVD graphene, the mobilities were enhanced in the case of graphene on top of h-BN compared to the same CVD graphene on SiO_2/Si as can be seen in figure 6.11. This is still an ongoing project and experiments will be repeated with better quality CVD graphene on better quality h-BN.

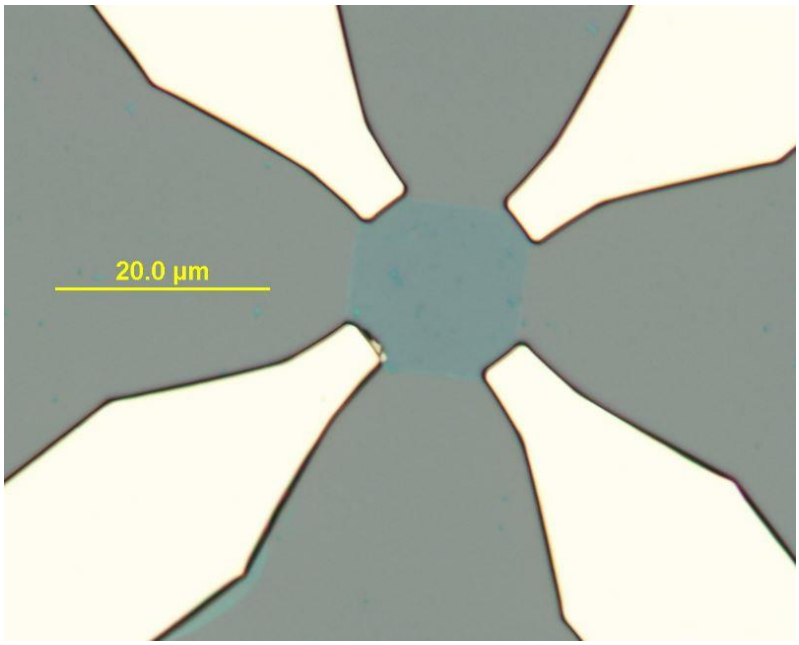

Figure 6.10: Van der Paw structures formed from CVD graphene on CVD h-BN.

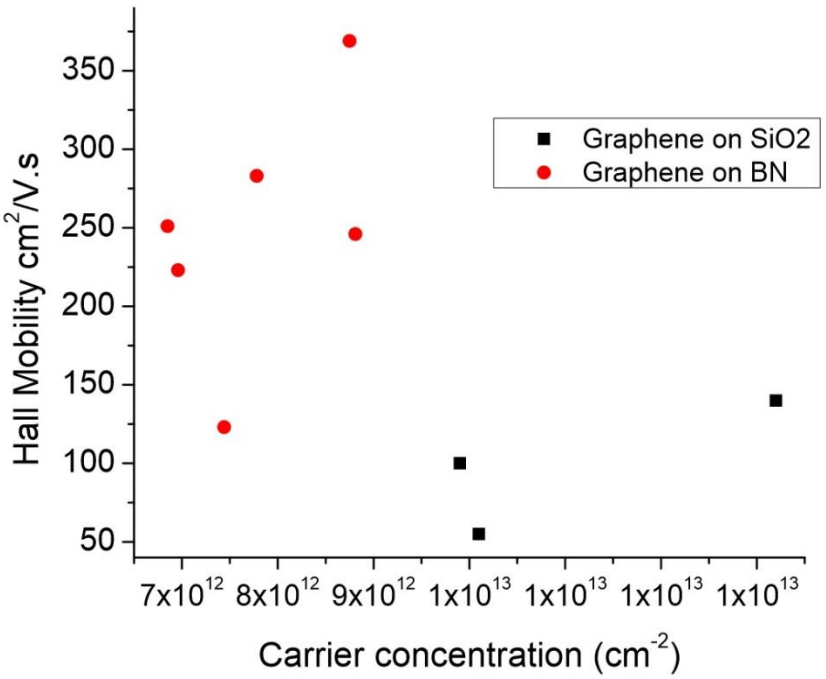

Figure 6.11: Hall mobility Vs. carrier concentration for CVD graphene on CVD h-BN and SiO_2 substrates.

CHAPTER 7

SUMMARY AND FUTURE PROSPECTIVE

We successfully transferred both monolayer and AB stacked bilayer Epitaxial Graphene off **(0001)** SiC and characterize the materials using Raman methods as well as TEM methods conclusively showing number and quality of layers as well as the orientation in the case of bilayers. We fabricated devices to measure the field effect mobility of monolayers and bilayers. We report mobility gains higher than two times before transfer for the case of monolayers. We also report bilayer field effect mobility characteristics that are exclusive to bilayers. In the high temperature annealing studies, we show the distinct ability of bilayer transferred epitaxial graphene in absorbing ambient moisture, opening a potential window for application in humidity sensors.

Future work should go into investigating the correlation between the quality of starting SiC wafer in terms of defects and the end transferred graphene. For the case of transferred monolayers, the demonstrated gain in mobility performance is already competitive with current large scale synthesis methods. The issue of SiC expensive substrate will be alleviated with time as reports from industry leading SiC manufacturers [160][161] are predicting rapid scale up in production and therefore lower costs.

Also, the BTEG is at a stage where more advanced device fabrication can be investigated and the determination of the possibility of scaled up AB stacked bilayer graphene device fabrication is now possible. The technological areas to pursue for BTEG are bolometers and gas sensors.

REFERENCES

[1] R. F. C. and R. E. S. H.W. Kroto, J.R. Heath, S.C. O'Brien, "H.W.Kroto:C60-Buckminsterfullerene:1985.pdf," *Nature*, vol. 318, no. 14. pp. 162–163, 1985.

[2] S. Iijima, "helical microtubules of graphitic carbon," *Nature*, vol. 354, pp. 56–58, 1991.

[3] S. Iijima and T. Ichihashi, "Single-shell carbon nanotubes of 1-nm diameter," *Nature*, vol. 363, no. 6430, pp. 603–605, 1993.

[4] a K. Geim and K. S. Novoselov, "The rise of graphene.," *Nat. Mater.*, vol. 6, no. 3, pp. 183–91, Mar. 2007.

[5] E. Fradkin, "Critical behavior of disordered degenerate semiconductors. II. Spectrum and transport properties in mean-field theory," *Phys. Rev. B*, vol. 33, no. 5, pp. 3263–3268, 1986.

[6] K. S. Novoselov, a K. Geim, S. V Morozov, D. Jiang, Y. Zhang, S. V Dubonos, I. V Grigorieva, and a a Firsov, "Electric field effect in atomically thin carbon films.," *Science*, vol. 306, no. 5696, pp. 666–9, Oct. 2004.

[7] K. S. Novoselov, a K. Geim, S. V Morozov, D. Jiang, M. I. Katsnelson, I. V Grigorieva, S. V Dubonos, and a a Firsov, "Two-dimensional gas of massless Dirac fermions in graphene.," *Nature*, vol. 438, no. 7065, pp. 197–200, Nov. 2005.

[8] B. Anasori, Y. Xie, M. Beidaghi, J. Lu, B. C. Hosler, L. Hultman, P. R. C. Kent, Y. Gogotsi, and M. W. Barsoum, "Two-Dimensional, Ordered, DoubleTransition Metals Carbides (MXenes)," 2015.

[9] D. L. Chandler and Y. Liang, "New 2D Materials Exhibit Exotic Quantum Properties," *Sci tech Daily*, 2014. [Online]. Available: http://scitechdaily.com/new-2d-materials-exhibit-exotic-quantum-properties.

[10] J. Coraux, "johann coraux RESEARCH ACTIVITIES," 2008. [Online]. Available: http://perso.neel.cnrs.fr/johann.coraux/index_en.htm. [Accessed: 01-Jan-2015].

[11] PhysOrg, "Study into two-dimensional materials shows great potential for battery life-span improvement," *Drexel University*, 2015. [Online]. Available: http://phys.org/news/2015-03-two-dimensional-materials-great-potential-battery.html. [Accessed: 01-Jan-2015].

[12] R. van Noorden, B. Maher, and R. Nuzzo, "The top 100 papers," *Nature*, no. 4, pp. 4–7, 2014.

[13] R. Saito, M. Fujita, G. Dresselhaus, and M. S. Dresselhaus, "Electronic structure of chiral graphene tubules," *Appl. Phys. Lett.*, vol. 60, no. 18, pp. 2204–2206, 1992.

[14] K. Nakada, M. Fujita, G. Dresselhaus, and M. Dresselhaus, “Edge state in graphene ribbons: Nanometer size effect and edge shape dependence,” *Phys. Rev. B*, vol. 54, no. 24, pp. 17954–17961, 1996.

[15] H. P. Bonuu, “surface properties of extremely thin graphite lamellae,” *fifth carbon Conf.*, vol. 12, pp. 73–80, 1961.

[16] a Clauss, “Das Adsorptionsverhalten sehr dunner,” vol. 316, pp. 119–127, 1962.

[17] Y. Zhang, Y.-W. Tan, H. L. Stormer, and P. Kim, “Experimental observation of the quantum Hall effect and Berry’s phase in graphene.,” *Nature*, vol. 438, no. 7065, pp. 201–4, Nov. 2005.

[18] G. Nanoelectronics, C. Berger, Z. Song, T. Li, X. Li, A. Y. Ogbazghi, R. Feng, Z. Dai, A. N. Marchenkov, E. H. Conrad, P. N. First, and W. A. De Heer, “Ultrathin Epitaxial Graphite : 2D Electron Gas Properties and a Route toward,” pp. 19912–19916, 2004.

[19] A. S. Mayorov, R. V Gorbachev, S. V Morozov, L. Britnell, R. Jalil, L. A. Ponomarenko, P. Blake, K. S. Novoselov, K. Watanabe, T. Taniguchi, and A. K. Geim, “Micrometer-Scale Ballistic Transport in Encapsulated Graphene at Room Temperature,” pp. 2396–2399, 2011.

[20] J. Baringhaus, M. Ruan, F. Edler, A. Tejeda, M. Sicot, A. Taleb-Ibrahimi, A.-P. Li, Z. Jiang, E. H. Conrad, C. Berger, C. Tegenkamp, and W. a de Heer, “Exceptional ballistic transport in epitaxial graphene nanoribbons.,” *Nature*, vol. 506, no. 7488, pp. 349–54, Feb. 2014.

[21] D.-K. Ki and A. F. Morpurgo, “High-quality multiterminal suspended graphene devices.,” *Nano Lett.*, vol. 13, no. 11, pp. 5165–70, Nov. 2013.

[22] Graphene@ICFO, “Suspended Graphene,” *The Institute of Photonic Sciences*, 2015. [Online]. Available: http://graphene.icfo.eu/media/upload/gif/cache/slider5editora761910.jpg. [Accessed: 01-Jan-2015].

[23] F. Bonaccorso, Z. Sun, T. Hasan, and a. C. Ferrari, “Graphene photonics and optoelectronics,” *Nat. Photonics*, vol. 4, no. 9, pp. 611–622, Aug. 2010.

[24] J. Wu, H. a. Becerril, Z. Bao, Z. Liu, Y. Chen, and P. Peumans, “Organic solar cells with solution-processed graphene transparent electrodes,” *Appl. Phys. Lett.*, vol. 92, no. 26, pp. 2008–2010, 2008.

[25] X. Wang, L. Zhi, and K. Müllen, “Transparent, conductive graphene electrodes for dye-sensitized solar cells,” *Nano Lett.*, vol. 8, pp. 323–327, 2008.

[26] B. M. Ludbrook, G. Levy, M. Zonno, M. Schneider, D. J. Dvorak, C. N. Veenstra, S. Zhdanovich, D. Wong, P. Dosanjh, S. Forti, U. Starke, and A. Damascelli, “Evidence for superconductivity in Li-decorated graphene,” *Arxiv*, vol. 1508.05925, pp. 1–6, 2015.

[27] T. Zhang, H. Chang, Y. Wu, P. Xiao, N. Yi, Y. Lu, Y. Ma, Y. Huang, K. Zhao, X.-Q. Yan, Z.-B. Liu, J.-G. Tian, and Y. Chen, "Macroscopic and direct light propulsion of bulk graphene material," *Nat. Photonics*, vol. 9, no. June, 2015.

[28] H. K. Avetissian, G. F. Mkrtchian, K. G. Batrakov, S. a. Maksimenko, and a. Hoffmann, "Multiphoton resonant excitations and high-harmonic generation in bilayer graphene," *Phys. Rev. B*, vol. 88, no. 16, p. 165411, Oct. 2013.

[29] B. Butz, C. Dolle, F. Niekiel, K. Weber, D. Waldmann, H. B. Weber, B. Meyer, and E. Spiecker, "Dislocations in bilayer graphene.," *Nature*, vol. 505, no. 7484, pp. 533–7, Jan. 2014.

[30] F. W. Chen, H. Ilatikhameneh, G. Klimeck, Z. Chen, and R. Rahman, "Configurable Electrostatically Doped High Performance Bilayer Graphene Tunnel FET," pp. 2–5.

[31] K. W. Clark, X.-G. Zhang, G. Gu, J. Park, G. He, R. M. Feenstra, and A.-P. Li, "Energy Gap Induced by Friedel Oscillations Manifested as Transport Asymmetry at Monolayer-Bilayer Graphene Boundaries," *Phys. Rev. X*, vol. 4, no. 1, p. 011021, Feb. 2014.

[32] C. Cobaleda, S. Pezzini, E. Diez, and V. Bellani, "Temperature- and density-dependent transport regimes in a <math><mi>h</mi></math>-BN/bilayer graphene/<math><mi>h</mi></math>-BN heterostructure," *Phys. Rev. B*, vol. 89, no. 12, p. 121404, Mar. 2014.

[33] a. Daboussi, L. Mandhour, J. N. Fuchs, and S. Jaziri, "Tunable zero-energy transmission resonances in shifted graphene bilayer," *Phys. Rev. B*, vol. 89, no. 8, p. 085426, Feb. 2014.

[34] G. Fiori, D. Neumaier, B. N. Szafranek, G. Iannaccone, and S. Member, "Bilayer Graphene Transistors for Analog Electronics," vol. 61, no. 3, pp. 729–733, 2014.

[35] M. S. Fuhrer, C. N. Lau, and A. H. MacDonald, "Graphene: Materially Better Carbon," *MRS Bull.*, vol. 35, no. 04, pp. 289–295, 2010.

[36] Y. Zhang, T.-T. Tang, C. Girit, Z. Hao, M. C. Martin, A. Zettl, M. F. Crommie, Y. R. Shen, and F. Wang, "Direct observation of a widely tunable bandgap in bilayer graphene.," *Nature*, vol. 459, no. 7248, pp. 820–3, Jun. 2009.

[37] J. Yan, M.-H. Kim, J. a Elle, a B. Sushkov, G. S. Jenkins, H. M. Milchberg, M. S. Fuhrer, and H. D. Drew, "Dual-gated bilayer graphene hot-electron bolometer.," *Nat. Nanotechnol.*, vol. 7, no. 7, pp. 472–8, Jul. 2012.

[38] M.-H. Kim, J. Yan, R. J. Suess, T. E. Murphy, M. S. Fuhrer, and H. D. Drew, "Photothermal Response in Dual-Gated Bilayer Graphene," *Phys. Rev. Lett.*, vol. 110, no. 24, p. 247402, Jun. 2013.

[39] C. R. Dean, A. F. Young, I. Meric, C. Lee, L. Wang, S. Sorgenfrei, K.

Watanabe, T. Taniguchi, P. Kim, K. L. Shepard, and J. Hone, "Boron nitride substrates for high-quality graphene electronics.," *Nat. Nanotechnol.*, vol. 5, no. 10, pp. 722–6, Oct. 2010.

[40] A. V Kretinin, Y. Cao, J. S. Tu, G. L. Yu, R. Jalil, K. S. Novoselov, S. J. Haigh, and A. Gholinia, "Electronic quality of graphene on different atomically flat substrates," pp. 9–11.

[41] A. S. Mayorov, R. V Gorbachev, S. V Morozov, L. Britnell, R. Jalil, L. a Ponomarenko, P. Blake, K. S. Novoselov, K. Watanabe, T. Taniguchi, and a K. Geim, "Micrometer-scale ballistic transport in encapsulated graphene at room temperature.," *Nano Lett.*, vol. 11, no. 6, pp. 2396–9, Jun. 2011.

[42] P. Vogt, P. De Padova, C. Quaresima, J. Avila, E. Frantzeskakis, M. C. Asensio, A. Resta, B. Ealet, and G. Le Lay, "Silicene: Compelling Experimental Evidence for Graphenelike Two-Dimensional Silicon," *Phys. Rev. Lett.*, vol. 108, no. 15, p. 155501, Apr. 2012.

[43] C. C. Liu, W. Feng, and Y. Yao, "Quantum spin Hall effect in silicene and two-dimensional germanium," *Phys. Rev. Lett.*, vol. 107, no. 7, pp. 1–4, 2011.

[44] A. Fleurence, R. Friedlein, T. Ozaki, H. Kawai, Y. Wang, and Y. Yamada-Takamura, "Experimental evidence for epitaxial silicene on diboride thin films," *Phys. Rev. Lett.*, vol. 108, no. 24, pp. 1–5, 2012.

[45] B. Lalmi, H. Oughaddou, H. Enriquez, A. Kara, Ś. Vizzini, B. Ealet, and B. Aufray, "Epitaxial growth of a silicene sheet," *Appl. Phys. Lett.*, vol. 97, no. 22, pp. 18–20, 2010.

[46] S. P. Koenig, R. a. Doganov, H. Schmidt, a. H. Castro Neto, and B. Özyilmaz, "Electric field effect in ultrathin black phosphorus," *Appl. Phys. Lett.*, vol. 104, no. 10, 2014.

[47] V. Tran, R. Soklaski, Y. Liang, and L. Yang, "Layer-controlled band gap and anisotropic excitons in few-layer black phosphorus," *Phys. Rev. B - Condens. Matter Mater. Phys.*, vol. 89, no. 23, pp. 1–6, 2014.

[48] F. Xia, H. Wang, and Y. Jia, "Rediscovering black phosphorus as an anisotropic layered material for optoelectronics and electronics.," *Nat. Commun.*, vol. 5, p. 4458, 2014.

[49] S. Z. Butler, S. M. Hollen, L. Cao, Y. Cui, J. A. Gupta, H. R. Gutie, T. F. Heinz, S. S. Hong, J. Huang, A. F. Ismach, E. Johnston-halperin, M. Kuno, V. V Plashnitsa, R. D. Robinson, R. S. Ruoff, S. Salahuddin, J. Shan, L. Shi, O. M. G. Spencer, M. Terrones, W. Windl, and J. E. Goldberger, "Prgoress, Challenges Opportunities in Two-Dimensional Materials Beyond Graphene," no. 4, pp. 2898–2926, 2013.

[50] P. Blake, E. W. Hill, A. H. C. Neto, K. S. Novoselov, D. Jiang, R. Yang, T. J. Booth, A. K. Geim, P. Blake, and E. W. Hill, "Making graphene visible," vol. 91, no. 063124, pp. 25–28, 2007.

[51] C. Wang, L. Zhan, W. Qiao, and L. Ling, “Preparation of graphene nanosheets through detonation,” *New Carbon Mater.*, vol. 26, no. 1, pp. 21–25, Jan. 2011.

[52] G. Ruan, Z. Sun, Z. Peng, and J. M. Tour, “Growth of graphene from food, insects, and waste,” *ACS Nano*, vol. 5, no. 9, pp. 7601–7607, 2011.

[53] H. Cao, Q. Yu, R. Colby, D. Pandey, C. S. Park, J. Lian, D. Zemlyanov, I. Childres, V. Drachev, E. a. Stach, M. Hussain, H. Li, S. S. Pei, and Y. P. Chen, “Large-scale graphitic thin films synthesized on Ni and transferred to insulators: Structural and electronic properties,” *J. Appl. Phys.*, vol. 107, no. 4, 2010.

[54] K. S. K. S. Kim, Y. Zhao, H. Jang, S. Y. Lee, J. M. Kim, K. S. K. S. Kim, J. Ahn, P. Kim, J.-Y. Choi, and B. H. Hong, “Large-scale pattern growth of graphene films for stretchable transparent electrodes.,” *Nature*, vol. 457, no. 7230, pp. 706–10, Feb. 2009.

[55] A. Reina, X. Jia, J. Ho, D. Nezich, H. Son, V. Bulovic, M. S. Dresselhaus, and J. Kong, “LETTERS Large Area , Few-Layer Graphene Films on Arbitrary Substrates by Chemical Vapor Deposition,” vol. xx, no. x, pp. 30–35, 2009.

[56] S. Bae, H. Kim, Y. Lee, X. Xu, J. Park, Y. Zheng, J. Balakrishnan, T. Lei, H. R. Kim, Y. Il Song, Y. Kim, and K. S. Kim, “Roll-to-roll production of 30-inch graphene films for transparent electrodes,” vol. 5, no. August, pp. 1–5, 2010.

[57] P. Y. Huang, C. S. Ruiz-Vargas, A. M. van der Zande, W. S. Whitney, M. P. Levendorf, J. W. Kevek, S. Garg, J. S. Alden, C. J. Hustedt, Y. Zhu, J. Park, P. L. McEuen, and D. a Muller, “Grains and grain boundaries in single-layer graphene atomic patchwork quilts.,” *Nature*, vol. 469, no. 7330, pp. 389–392, 2011.

[58] H. Zhang, G. Lee, C. Gong, L. Colombo, and K. Cho, “Grain Boundary E ff ect on Electrical Transport Properties of Graphene,” 2014.

[59] N. Petrone, C. R. Dean, I. Meric, A. M. Van Der Zande, P. Y. Huang, L. Wang, D. Muller, K. L. Shepard, and J. Hone, “Chemical vapor deposition-derived graphene with electrical performance of exfoliated graphene.,” *Nano Lett.*, vol. 12, no. 6, pp. 2751–6, Jun. 2012.

[60] Y. Hao, M. S. Bharathi, L. Wang, Y. Liu, H. Chen, S. Nie, X. Wang, H. Chou, C. Tan, B. Fallahazad, H. Ramanarayan, C. W. Magnuson, E. Tutuc, B. I. Yakobson, K. F. McCarty, Y. Zhang, P. Kim, J. Hone, L. Colombo, and R. S. Ruoff, “The role of surface oxygen in the growth of large single-crystal graphene on copper.,” *Science*, vol. 342, no. 6159, pp. 720–3, Nov. 2013.

[61] W. Regan, N. Alem, B. Alemán, B. Geng, Ç. Girit, L. Maserati, F. Wang, M. Crommie, and a. Zettl, “A direct transfer of layer-area graphene,” *Appl. Phys. Lett.*, vol. 96, no. 11, pp. 17–20, 2010.

[62] J. Song, F.-Y. Kam, R.-Q. Png, W.-L. Seah, J.-M. Zhuo, G.-K. Lim, P. K. H. Ho, and L.-L. Chua, “A general method for transferring graphene onto soft

surfaces.," *Nat. Nanotechnol.*, vol. 8, no. 5, pp. 356–62, May 2013.

[63] J. Kang, D. Shin, S. Bae, and B. H. Hong, "Graphene transfer: key for applications," *Nanoscale*, vol. 4, no. 18, p. 5527, 2012.

[64] X. Liang, B. a. Sperling, I. Calizo, G. Cheng, C. A. Hacker, Q. Zhang, Y. Obeng, K. Yan, H. Peng, Q. Li, X. Zhu, H. Yuan, A. R. Hight Walker, Z. Liu, L.-M. M. Peng, C. a. Richter, A. R. H. Walker, Z. Liu, L.-M. M. Peng, and C. a. Richter, "Toward clean and crackless transfer of graphene.," *ACS Nano*, vol. 5, no. 11, pp. 9144–9153, Nov. 2011.

[65] U. of Groningen, "Epitaxial graphene," *university of groningen*, 2015. [Online]. Available: http://www.rug.nl/research/zernike/physics-of-nanodevices/research/graphene/epitaxial-graphene?lang=en.

[66] K. W. Clark, X. Zhang, I. V Vlassiouk, G. He, R. M. Feenstra, A. Li, and C. E. T. Al, "Spatially Resolved Mapping of Electrical Conductivity across Individual Domain (Grain) Boundaries in Graphene," *ACS Nano*, vol. 7, no. 9, pp. 7956–7966, 2013.

[67] G. Wang, M. Zhang, Y. Zhu, G. Ding, D. Jiang, Q. Guo, S. Liu, X. Xie, P. K. Chu, Z. Di, and X. Wang, "Direct Growth of Graphene Film on Germanium Substrate," *Sci. Rep.*, vol. 3, pp. 1–6, 2013.

[68] J.-H. Lee, E. K. Lee, W.-J. Joo, Y. Jang, B.-S. Kim, J. Y. Lim, S.-H. Choi, S. J. Ahn, J. R. Ahn, M.-H. Park, C.-W. Yang, B. L. Choi, S.-W. Hwang, and D. Whang, "Wafer-scale growth of single-crystal monolayer graphene on reusable hydrogen-terminated germanium.," *Science*, vol. 344, no. 6181, pp. 286–9, Apr. 2014.

[69] B. Kiraly, R. M. Jacobberger, A. J. Mannix, G. P. Campbell, M. J. Bedzyk, M. S. Arnold, M. C. Hersam, and N. P. Guisinger, "Electronic and Mechanical Properties of Graphene–Germanium Interfaces Grown by Chemical Vapor Deposition," *Nano Lett.*, p. acs.nanolett.5b02833, 2015.

[70] N. Wataru and K. Michiko, "Epitaxial graphene on SiC{0001}: advances and perspectives," *PCCP*, vol. 16, pp. 3501–3511, 2014.

[71] M. H. Rümmeli, C. G. Rocha, F. Ortmann, I. Ibrahim, H. Sevincli, F. Börrnert, J. Kunstmann, A. Bachmatiuk, M. Pötschke, M. Shiraishi, M. Meyyappan, B. Büchner, S. Roche, and G. Cuniberti, "Graphene : Piecing it Together," pp. 4471–4490, 2011.

[72] C. Virojanadara, M. Syväjarvi, R. Yakimova, L. Johansson, a. Zakharov, and T. Balasubramanian, "Homogeneous large-area graphene layer growth on 6H-SiC(0001)," *Phys. Rev. B*, vol. 78, no. 24, p. 245403, Dec. 2008.

[73] K. V Emtsev, A. Bostwick, K. Horn, J. Jobst, G. L. Kellogg, L. Ley, J. L. Mcchesney, T. Ohta, S. a Reshanov, J. Röhrl, E. Rotenberg, A. K. Schmid, D. Waldmann, H. B. Weber, and T. Seyller, "Towards wafer-size graphene layers by atmospheric pressure graphitization of silicon carbide.," *Nat. Mater.*, vol. 8,

no. 3, pp. 203–7, Mar. 2009.

[74] C. Virojanadara, R. Yakimova, J. R. Osiecki, M. Syväjärvi, R. I. G. Uhrberg, L. I. Johansson, and A. A. Zakharov, "Surface Science Substrate orientation : A way towards higher quality monolayer graphene growth," *Surf. Sci.*, vol. 603, no. 15, pp. L87–L90, 2009.

[75] J. Robinson, X. Weng, K. Trumbull, R. Cavalero, M. Wetherington, E. Frantz, M. Labella, Z. Hughes, M. Fanton, and D. Snyder, "Nucleation of Epitaxial Graphene on SiC(0001)," vol. 4, no. 1, pp. 153–158, 2010.

[76] T. Kimoto, A. Itoh, H. Matsunami, and T. Okano, "Step bunching mechanism in chemical vapor deposition of 6H– and 4H–SiC{0001}," *J. Appl. Phys.*, vol. 81, no. 8, p. 3494, 1997.

[77] W. Norimatsu and M. Kusunoki, "Formation process of graphene on SiC (0 0 0 1)," *Phys. E Low-dimensional Syst. Nanostructures*, vol. 42, no. 4, pp. 691–694, 2010.

[78] A. C. Ferrari and D. M. Basko, "Raman spectroscopy as a versatile tool for studying the properties of graphene.," *Nat. Nanotechnol.*, vol. 8, no. 4, pp. 235–46, Apr. 2013.

[79] A. C. Ferrari, J. C. Meyer, V. Scardaci, C. Casiraghi, M. Lazzeri, F. Mauri, S. Piscanec, D. Jiang, K. S. Novoselov, S. Roth, and A. K. Geim, "Raman Spectrum of Graphene and Graphene Layers," *Phys. Rev. Lett.*, vol. 187401, no. NOVEMBER, pp. 1–4, 2006.

[80] A. Eckmann, A. Felten, A. Mishchenko, L. Britnell, R. Krupke, K. S. Novoselov, and C. Casiraghi, "Probing the Nature of Defects in Graphene by Raman Spectroscopy," 2012.

[81] A. Eckmann, A. Felten, I. Verzhbitskiy, R. Davey, and C. Casiraghi, "Raman study on defective graphene: Effect of the excitation energy, type, and amount of defects," *Phys. Rev. B*, vol. 88, no. 3, p. 035426, Jul. 2013.

[82] H. Shioya, M. F. Craciun, S. Russo, M. Yamamoto, and S. Tarucha, "Straining graphene using thin film shrinkage methods.," *Nano Lett.*, vol. 14, no. 3, pp. 1158–63, Mar. 2014.

[83] T. Mohiuddin, a. Lombardo, R. Nair, a. Bonetti, G. Savini, R. Jalil, N. Bonini, D. Basko, C. Galiotis, N. Marzari, K. Novoselov, a. Geim, and a. Ferrari, "Uniaxial strain in graphene by Raman spectroscopy: G peak splitting, Grüneisen parameters, and sample orientation," *Phys. Rev. B*, vol. 79, no. 20, p. 205433, May 2009.

[84] C. Virojanadara, a. a. Zakharov, R. Yakimova, and L. I. Johansson, "Buffer layer free large area bi-layer graphene on SiC(0001)," *Surf. Sci.*, vol. 604, no. 2, pp. L4–L7, Jan. 2010.

[85] J. A. Robinson, C. P. Puls, N. E. Staley, J. P. Stitt, M. A. Fanton, K. V Emtsev,

T. Seyller, and Y. Liu, “Raman Topography and Strain Uniformity of Large-Area Epitaxial Graphene,” *Nano Lett.*, vol. 9, no. 3, pp. 964–968, 2009.

[86] S. Forti, K. V. Emtsev, C. Coletti, a. a. Zakharov, C. Riedl, and U. Starke, “Large-area homogeneous quasifree standing epitaxial graphene on SiC(0001): Electronic and structural characterization,” *Phys. Rev. B*, vol. 84, no. 12, p. 125449, Sep. 2011.

[87] C. Riedl, C. Coletti, T. Iwasaki, A. A. Zakharov, and U. Starke, “Quasi-Free-Standing Epitaxial Graphene on SiC Obtained by Hydrogen Intercalation,” vol. 246804, no. DECEMBER, pp. 1–4, 2009.

[88] F. Speck, J. Jobst, F. Fromm, M. Ostler, D. Waldmann, M. Hundhausen, and H. B. Weber, “The quasi-free-standing nature of graphene on H-saturated SiC (0001),” no. 0001, pp. 1–3, 2011.

[89] M. H. Oliveira, T. Schumann, F. Fromm, R. Koch, M. Ostler, M. Ramsteiner, T. Seyller, J. M. J. Lopes, and H. Riechert, “Formation of high-quality quasi-free-standing bilayer graphene on SiC(0 0 0 1) by oxygen intercalation upon annealing in air,” *Carbon N. Y.*, vol. 52, pp. 83–89, 2013.

[90] E. Pallecchi, A. Locatelli, S. Latil, R. Belkhou, and A. Ouerghi, “Effect of oxygen adsorption on the local properties of epitaxial graphene on SiC (0001),” vol. 035435, pp. 1–5, 2012.

[91] I. Gierz, T. Suzuki, R. T. Weitz, D. S. Lee, B. Krauss, C. Riedl, U. Starke, H. Höchst, J. H. Smet, C. R. Ast, and K. Kern, “Electronic decoupling of an epitaxial graphene monolayer by gold intercalation,” *Phys. Rev. B*, vol. 81, no. 23, p. 235408, Jun. 2010.

[92] A. L. Walter, K. J. Jeon, A. Bostwick, F. Speck, M. Ostler, T. Seyller, L. Moreschini, Y. S. Kim, Y. J. Chang, K. Horn, and E. Rotenberg, “Highly p - doped epitaxial graphene obtained by fluorine intercalation,” *Appl. Phys. Lett.*, vol. 98, no. 18, pp. 4–7, 2011.

[93] G. Lee, R. C. Cooper, S. J. An, S. Lee, A. Van Der Zande, N. Petrone, A. G. Hammerberg, C. Lee, B. Crawford, W. Oliver, J. W. Kysar, and J. Hone, “High strength CVD Grapheen and Grain Boundaries,” vol. 1073, 2013.

[94] A. Castellanos-Gomez, M. Buscema, R. Molenaar, V. Singh, L. Janssen, H. S. J. van der Zant, and G. a Steele, “Deterministic transfer of two-dimensional materials by all-dry viscoelastic stamping,” *2D Mater.*, vol. 1, no. 1, p. 011002, Apr. 2014.

[95] L. I. N. E. T. Al, “A Direct and Polymer-Free Method for Transferring Graphene Grown by Chemical Vapor Deposition to Any,” no. Xx, 2014.

[96] L. Banszerus, M. Schmitz, S. Engels, J. Dauber, M. Oellers, F. Haupt, K. Watanabe, T. Taniguchi, B. Beschoten, and C. Stampfer, “Ultrahigh-mobility graphene devices from chemical vapor deposition on reusable copper,” *Sci. Adv.*, vol. 1, no. July, pp. 1–6, 2015.

[97] D. Waldmann, B. Butz, S. Bauer, J. M. Englert, J. Jobst, K. Ullmann, F. Fromm, M. Ammon, M. Enzelberger, A. Hirsch, S. Maier, P. Schmuki, T. Seyller, E. Spiecker, and H. B. Weber, "Robust graphene membranes in a silicon carbide frame," *ACS Nano*, vol. 7, no. 5, pp. 4441–4448, May 2013.

[98] K. Ryu, A. Badmaev, C. Wang, A. Lin, N. Patil, L. Gomez, A. Kumar, S. Mitra, H. P. Wong, and C. Zhou, "Nanotube-on-Insulator Approach for Submicrometer Devices and Integrated Circuits Using Aligned Nanotubes," vol. 9, no. 1, pp. 189–97, 2009.

[99] C. Wang, K. Ryu, A. Badmaev, N. Patil, A. Lin, S. Mitra, H.-S. P. Wong, and C. Zhou, "Device study, chemical doping, and logic circuits based on transferred aligned single-walled carbon nanotubes," *Appl. Phys. Lett.*, vol. 93, no. 3, p. 033101, 2008.

[100] J. D. Caldwell, T. J. Anderson, J. C. Culbertson, G. G. Jernigan, K. D. Hobart, F. J. Kub, M. J. Tadjer, J. L. Tedesco, J. K. Hite, M. a Mastro, R. L. Myers-Ward, C. R. Eddy, P. M. Campbell, and D. K. Gaskill, "Technique for the dry transfer of epitaxial graphene onto arbitrary substrates.," *ACS Nano*, vol. 4, no. 2, pp. 1108–14, Feb. 2010.

[101] D. S. Lee, C. Riedl, B. Krauss, K. von Klitzing, U. Starke, and J. H. Smet, "Raman spectra of epitaxial graphene on SiC and of epitaxial graphene transferred to SiO2.," *Nano Lett.*, vol. 8, no. 12, pp. 4320–5, Dec. 2008.

[102] S. Unarunotai, J. C. Koepke, Ḱ. C. Tsai, F. Du, C. E. Chialvo, Y. Murata, R. Haasch, I. Petrov, N. Mason, M. Shim, J. Lyding, and J. A. Rogers, "Layer-by-Layer Transfer of Multiple , Large Area Sheets of Graphene Grown in Multilayer Stacks on a Single SiC Wafer," vol. 4, no. 10, pp. 5591–5598, 2010.

[103] S. Unarunotai, Y. Murata, C. E. Chialvo, H. Kim, S. MacLaren, N. Mason, I. Petrov, and J. a. Rogers, "Transfer of graphene layers grown on SiC wafers to other substrates and their integration into field effect transistors," *Appl. Phys. Lett.*, vol. 95, no. 20, p. 202101, 2009.

[104] W. Gao and R. Huang, "Effect of surface roughness on adhesion of graphene membranes," *J. Phys. D. Appl. Phys.*, vol. 44, no. 45, p. 452001, 2011.

[105] S. Gorantla, A. Bachmatiuk, J. Hwang, H. a Alsalman, J. Y. Kwak, T. Seyller, J. Eckert, M. G. Spencer, and M. H. Rümmeli, "A universal transfer route for graphene.," *Nanoscale*, vol. 6, no. 2, pp. 889–96, Jan. 2014.

[106] J. Kim, H. Park, J. B. Hannon, S. W. Bedell, K. Fogel, D. K. Sadana, and C. Dimitrakopoulos, "Layer-resolved graphene transfer via engineered strain layers.," *Science*, vol. 342, no. 6160, pp. 833–6, Nov. 2013.

[107] O. Neill and M. R. C. Hunt, "pleat defects Determination of the adhesion energy of graphene on SiC (0001) via measurement of pleat defects," vol. 193109, no. May 2015, 2014.

[108] S. Scharfenberg, N. Mansukhani, C. Chialvo, R. L. Weaver, and N. Mason,

"Observation of a snap-through instability in graphene," *Appl. Phys. Lett.*, vol. 100, no. 2, pp. 10–13, 2012.

[109] I. Hamada and M. Otani, "Comparative van der Waals density-functional study of graphene on metal surfaces," *Phys. Rev. B*, vol. 82, no. 15, p. 153412, 2010.

[110] T. Yoon, W. C. Shin, T. Y. Kim, J. H. Mun, T. S. Kim, and B. J. Cho, "Direct measurement of adhesion energy of monolayer graphene as-grown on copper and its application to renewable transfer process," *Nano Lett.*, vol. 12, no. 3, pp. 1448–1452, 2012.

[111] D. J. Henry, C. A. Lukey, E. Evans, and I. Yarovsky, "Theoretical study of adhesion between graphite, polyester and silica surfaces," *Mol. Simul.*, vol. 31, no. 6–7, pp. 449–455, 2005.

[112] S. Das, D. Lahiri, D. Y. Lee, A. Agarwal, and W. Choi, "Measurements of the adhesion energy of graphene to metallic substrates," *Carbon N. Y.*, vol. 59, pp. 121–129, 2013.

[113] S. Scharfenberg, D. Z. Rocklin, C. Chialvo, R. L. Weaver, P. M. Goldbart, and N. Mason, "Probing the mechanical properties of graphene using a corrugated elastic substrate," *Appl. Phys. Lett.*, vol. 98, no. 9, p. 091908, 2011.

[114] J. Lahiri, T. S. Miller, A. J. Ross, L. Adamska, I. I. Oleynik, and M. Batzill, "Graphene growth and stability at nickel surfaces," *New J. Phys.*, vol. 13, 2011.

[115] P. Blake, E. W. Hill, A. H. C. Neto, K. S. Novoselov, D. Jiang, R. Yang, T. J. Booth, and A. K. Geim, "Making graphene visible Making graphene visible," vol. 063124, 2007.

[116] W. Liu, S. Kraemer, D. Sarkar, H. Li, P. M. Ajayan, and K. Banerjee, "Controllable and Rapid Synthesis of High-Quality and Large-Area Bernal Stacked Bilayer Graphene Using Chemical Vapor Deposition," *Chem. Mater.*, vol. 26, no. 2, pp. 907–915, Jan. 2014.

[117] R. W. Havener, H. Zhuang, L. Brown, R. G. Hennig, and J. Park, "Angle-resolved Raman imaging of interlayer rotations and interactions in twisted bilayer graphene.," *Nano Lett.*, vol. 12, no. 6, pp. 3162–7, Jun. 2012.

[118] K. Kim, S. Coh, L. Z. Tan, W. Regan, J. M. Yuk, E. Chatterjee, M. F. Crommie, M. L. Cohen, S. G. Louie, and a. Zettl, "Raman Spectroscopy Study of Rotated Double-Layer Graphene: Misorientation-Angle Dependence of Electronic Structure," *Phys. Rev. Lett.*, vol. 108, no. 24, p. 246103, Jun. 2012.

[119] J. C. Meyer, a. K. Geim, M. I. Katsnelson, K. S. Novoselov, D. Obergfell, S. Roth, C. Girit, and a. Zettl, "On the roughness of single- and bi-layer graphene membranes," *Solid State Commun.*, vol. 143, no. 1–2, pp. 101–109, Jul. 2007.

[120] W. Pong and C. Durkan, "A review and outlook for an anomaly of scanning tunnelling microscopy (STM) : superlattices on graphite," *J. Phys. D Appl. Physics2*, vol. 38, pp. 329–355, 2005.

[121] J. H. Warner, M. H. Ru, T. Gemming, B. Bu, and G. A. D. Briggs, “Direct Imaging of Rotational Stacking Faults in Few Layer Graphene 2009,” 2009.

[122] Z. Y. R. and P. Kuiper, “Electronic efFects in scanning tunneling microscopy: Moire pattern on a graphite surface,” vol. 48, no. 23, 1993.

[123] R. Bistritzer and A. H. Macdonald, “Moiré bands in twisted double-layer graphene,” vol. 108, no. 30, pp. 12233–12237, 2011.

[124] L. Wang, I. Meric, P. Y. Huang, Q. Gao, Y. Gao, H. Tran, T. Taniguchi, K. Watanabe, L. M. Campos, D. a Muller, J. Guo, P. Kim, J. Hone, K. L. Shepard, and C. R. Dean, “One-dimensional electrical contact to a two-dimensional material.,” *Science*, vol. 342, no. 6158, pp. 614–7, Nov. 2013.

[125] W. S. Leong, H. Gong, J. T. L. Thong, C. Engineering, and M. Science, “Low Contact Resistance Graphene,” *ACS Nano*, vol. 8, no. 1, pp. 994–1001, 2014.

[126] J. T. Smith, A. D. Franklin, D. B. Farmer, and C. D. Dimitrakopoulos, “Reducing contact resistance in graphene devices through contact area patterning.,” *ACS Nano*, vol. 7, no. 4, pp. 3661–7, Apr. 2013.

[127] B.-C. Huang, M. Zhang, Y. Wang, and J. Woo, “Contact resistance in top-gated graphene field-effect transistors,” *Appl. Phys. Lett.*, vol. 99, no. 3, p. 032107, 2011.

[128] F. Xia, V. Perebeinos, Y. Lin, Y. Wu, and P. Avouris, “The origins and limits of metal-graphene junction resistance.,” *Nat. Nanotechnol.*, vol. 6, no. 3, pp. 179–184, 2011.

[129] H. B. G.K., Reeves Harrison, “Obtaining the Specific Contact Resistance from Transmission Line Model Measurments,” no. May, pp. 111–113, 1982.

[130] G. M. Rutter, S. Jung, N. N. Klimov, D. B. Newell, N. B. Zhitenev, and J. a. Stroscio, “Microscopic Polarization in Bilayer Graphene,” *Nat. Phys.*, vol. 7, no. 8, pp. 649–655, 2011.

[131] P. Blake, R. Yang, S. V. Morozov, F. Schedin, L. a. Ponomarenko, a. a. Zhukov, R. R. Nair, I. V. Grigorieva, K. S. Novoselov, and a. K. Geim, “Influence of metal contacts and charge inhomogeneity on transport properties of graphene near the neutrality point,” *Solid State Commun.*, vol. 149, no. 27–28, pp. 1068–1071, Jul. 2009.

[132] T. Mueller, F. Xia, and P. Avouris, “Graphene photodetectors for high-speed optical communications,” vol. 4, no. March, pp. 297–301, 2010.

[133] J. H. Chen, W. G. Cullen, C. Jang, M. S. Fuhrer, and E. D. Williams, “Defect scattering in graphene,” *Phys. Rev. Lett.*, vol. 102, no. 23, pp. 1–4, 2009.

[134] T. Oznuluer, E. Pince, E. O. Polat, O. Balci, O. Salihoglu, and C. Kocabas, “Synthesis of graphene on gold,” *Appl. Phys. Lett.*, vol. 98, no. 18, p. 183101, 2011.

[135] W. Zhu, V. Perebeinos, M. Freitag, and P. Avouris, “Carrier scattering, mobilities, and electrostatic potential in monolayer, bilayer, and trilayer graphene,” *Phys. Rev. B*, vol. 80, no. 23, p. 235402, 2009.

[136] J. M. Tirado, D. Nezich, X. Zhao, J. W. Chung, J. Kong, and T. Palacios, “Study of transport properties in graphene monolayer flakes on SiO2 substrates,” *J. Vac. Sci. Technol. B Microelectron. Nanom. Struct.*, vol. 28, no. 6, p. C6D11, 2010.

[137] J.-H. Chen, C. Jang, S. Xiao, M. Ishigami, and M. S. Fuhrer, “Intrinsic and extrinsic performance limits of graphene devices on SiO2.,” *Nat. Nanotechnol.*, vol. 3, no. 4, pp. 206–9, Apr. 2008.

[138] Y. Taur and T. Ning, “Effective Mobility and Effective Normal Field,” pp. 132–134.

[139] S. Graphene, C. Foils, Z. Yan, J. Lin, Z. Peng, Z. Sun, Y. Zhu, L. Li, C. Xiang, E. Loı, C. Kittrell, and J. M. Tour, “Toward the Synthesis of Wafer-Scale Single-Crystal Graphene on Copper Foils,” no. 10, pp. 9110–9117, 2012.

[140] “Graphenea.” [Online]. Available: http://www.graphenea.com/.

[141] J. L. Tedesco, B. L. Vanmil, R. L. Myers-Ward, J. M. McCrate, S. a. Kitt, P. M. Campbell, G. G. Jernigan, J. C. Culbertson, C. R. Eddy, and D. K. Gaskill, “Hall effect mobility of epitaxial graphene grown on silicon carbide,” *Appl. Phys. Lett.*, vol. 95, no. 12, 2009.

[142] F. Speck, J. Jobst, F. Fromm, M. Ostler, D. Waldmann, M. Hundhausen, H. B. Weber, and T. Seyller, “The quasi-free-standing nature of graphene on H-saturated SiC(0001),” *Appl. Phys. Lett.*, vol. 99, no. 12, pp. 1–4, 2011.

[143] J. a Robinson, M. Hollander, M. Labella, K. a Trumbull, R. Cavalero, and D. W. Snyder, “Epitaxial graphene transistors: enhancing performance via hydrogen intercalation.,” *Nano Lett.*, vol. 11, no. 9, pp. 3875–80, Sep. 2011.

[144] J. Jobst, “Quantum Transport in Epitaxial Graphene on Silicon Carbide (0001),” 2013.

[145] S. Ji, J. B. Hannon, R. M. Tromp, V. Perebeinos, J. Tersoff, and F. M. Ross, “Atomic-scale transport in epitaxial graphene,” *Nat. Mater.*, vol. 11, no. 2, pp. 114–119, 2011.

[146] H. Kuramochi, S. Odaka, K. Morita, S. Tanaka, H. Miyazaki, M. V. Lee, S. L. Li, H. Hiura, and K. Tsukagoshi, “Role of atomic terraces and steps in the electron transport properties of epitaxial graphene grown on SiC,” *AIP Adv.*, vol. 2, no. 1, pp. 0–10, 2012.

[147] C. Dimitrakopoulos, A. Grill, T. J. Mcardle, Z. Liu, R. Wisnieff, A. Dimitri, C. Dimitrakopoulos, A. Grill, T. J. Mcardle, Z. Liu, R. Wisnieff, and D. A. Antoniadis, “Effect of SiC wafer miscut angle on the morphology and Hall mobility of epitaxially grown graphene Effect of SiC wafer miscut angle on the

morphology and Hall mobility of epitaxially grown graphene," vol. 222105, no. 2011, pp. 96–99, 2014.

[148] T. M. Radchenko, A. A. Shylau, and I. V Zozoulenko, "Conductivity of epitaxial and CVD graphene with correlated line defects," *Solid State Commun.*, vol. 195, pp. 88–94, 2014.

[149] E. Hwang, S. Adam, and S. Sarma, "Carrier Transport in Two-Dimensional Graphene Layers," *Phys. Rev. Lett.*, vol. 98, no. 18, p. 186806, May 2007.

[150] S. Xiao, J. H. Chen, S. Adam, E. D. Williams, and M. S. Fuhrer, "Charged impurity scattering in bilayer graphene," *Phys. Rev. B - Condens. Matter Mater. Phys.*, vol. 82, no. 4, pp. 2–5, 2010.

[151] F. Schedin, a K. Geim, S. V Morozov, E. W. Hill, P. Blake, M. I. Katsnelson, and K. S. Novoselov, "Detection of individual gas molecules adsorbed on graphene.," *Nat. Mater.*, vol. 6, no. 9, pp. 652–5, Sep. 2007.

[152] Y. Hajati, T. Blom, S. H. M. Jafri, S. Haldar, S. Bhandary, M. Z. Shoushtari, O. Eriksson, B. Sanyal, and K. Leifer, "Improved gas sensing activity in structurally defected bilayer graphene," *Nanotechnology*, vol. 23, no. 50, p. 505501, 2012.

[153] L. Song, L. Ci, H. Lu, P. B. Sorokin, C. Jin, J. Ni, A. G. Kvashnin, D. G. Kvashnin, J. Lou, B. I. Yakobson, and P. M. Ajayan, "Large scale growth and characterization of atomic hexagonal boron nitride layers," *Nano Lett.*, vol. 10, no. 8, pp. 3209–3215, Aug. 2010.

[154] K. K. Kim, a Hsu, X. Jia, S. M. Kim, Y. Shi, M. Hofmann, D. Nezich, J. F. Rodriguez-Nieva, M. Dresselhaus, T. Palacios, and J. Kong, "Synthesis of Monolayer Boron Nitride on Cu Foil Using Chemical Vapor Deposition," *Nano Lett.*, vol. xx, p. xx, 2011.

[155] S. M. Kim, A. Hsu, M. H. Park, S. H. Chae, S. J. Yun, J. S. Lee, D.-H. Cho, W. Fang, C. Lee, T. Palacios, M. Dresselhaus, K. K. Kim, Y. H. Lee, and J. Kong, "Synthesis of large-area multilayer hexagonal boron nitride for high material performance," *Nat. Commun.*, vol. 6, p. 8662, 2015.

[156] R. Y. Tay, M. H. Griep, G. Mallick, S. H. Tsang, R. S. Singh, T. Tumlin, E. H. T. Teo, and S. P. Karna, "Growth of large single-crystalline two-dimensional boron nitride hexagons on electropolished copper," *Nano Lett.*, vol. 14, no. 2, pp. 839–846, 2014.

[157] H. Wang, X. Zhang, H. Liu, Z. Yin, J. Meng, J. Xia, X.-M. Meng, J. Wu, and J. You, "Synthesis of Large-Sized Single-Crystal Hexagonal Boron Nitride Domains on Nickel Foils by Ion Beam Sputtering Deposition," *Adv. Mater.*, p. n/a–n/a, 2015.

[158] G. D. Kwon, Y. W. Kim, E. Moyen, D. H. Keum, Y. H. Lee, S. Baik, and D. Pribat, "Controlled electropolishing of copper foils at elevated temperature," *Appl. Surf. Sci.*, vol. 307, pp. 731–735, 2014.

[159] K. H. Lee, H. J. Shin, J. Lee, I. Y. Lee, G. H. Kim, J. Y. Choi, and S. W. Kim, "Large-scale synthesis of high-quality hexagonal boron nitride nanosheets for large-area graphene electronics," *Nano Lett.*, vol. 12, pp. 714–718, 2012.

[160] "Monolith Semiconductor Inc." [Online]. Available: http://www.nist.gov/pml/high_megawatt/upload/Banerjee-APPROVED.pdf.

[161] "USA Department of Energy." [Online]. Available: http://energy.gov/sites/prod/files/2015/02/f19/QTR Ch8 - Wide Bandgap TA Feb-13-2015.pdf.